

Immunoregulatory capacity of human skeletal muscle cells during a *Trypanosoma cruzi* infection

Dissertation with the aim of achieving a doctoral degree
at the Faculty of Mathematics, Informatics and Natural Sciences

Department of Biology

University of Hamburg

submitted by

Cari Lehmann

Hamburg, September 2023

Gutachter:

Prof. Dr. Tim-Wolf Gilberger

Zentrum für strukturelle Systembiologie CSSB

c/o Deutsches Elektronen-Synchrotron DESY

PD Dr. Thomas Jacobs

Bernhard-Nocht-Institut für Tropenmedizin

Protozoen-Immunologie

Tag der Disputation: 8.12.2023

Vorsitzende der Prüfungskommission: Prof. Dr. Tim-Wolf Gilberger

Mitglieder der Prüfungskommission: Prof. Dr. Tim-Wolf Gilberger

PD Dr. Thomas Jacobs

Prof. Dr. Minka Breloer

Prof. Dr. Esther Schnettle

Eidesstattliche Versicherung/ Statuary declaration

Hiermit versichere ich an Eides statt, dass ich die vorliegende Dissertation selbst verfasst und keine anderen als die angegebenen Quellen und Hilfsmittel benutzt habe.

I hereby declare upon oath that I have written the present dissertation independently and have not used further resources and aids than those stated in the dissertation.



Hamburg, 20.9.2023

Nachweis über die Korrektheit der Sprache

Hiermit bestätige ich, Madeleine Hamley, geb. 02.10.1991 in London, dass die vorliegende Dissertation „Immunoregulatory capacity of human skeletal muscle cells during a *Trypanosoma cruzi* infection“ sprachlich korrekt ist.

Hamburg, den 20.09.2023



A handwritten signature in black ink, appearing to read 'Madeleine Hamley', written over a horizontal line.

(Ort, Datum und Unterschrift)

Danksagung

Zuallererst möchte ich mich bei PD Dr. Thomas Jacobs für das spannende Projekt und für die wunderbare Betreuung bedanken. Sowie für die anregenden Diskussionen und die Möglichkeit das Projekt durch meine eigenen Ideen und Hypothesen zu gestalten und meine Fähigkeiten stets weiter entwickeln zu dürfen.

Prof. Dr. Tim-Wolf Gilberger danke ich herzlich für die Bereitschaft diese Arbeit zu begutachten.

Prof. Dr. Minka Breloer, Dr. Jessica Rauch und Dr. Imke Liebold danke ich für die Betreuung, die wissenschaftlichen und nicht wissenschaftlichen Diskussionen und die Unterstützung. Ein ganz besonderer Dank geht an Imke, für die hilfreichen Korrekturen und Kommentare und für die vielen weisen Ratschläge.

Bei Dr. Mathias Riehn und Dr. Rosa Isela Gálvez möchte ich mich für die Unterstützung und wissenschaftlichen Diskussionen vor allem an Anfang meiner Doktorandenzeit bedanken.

Ein großer Dank geht auch an die ganze AG Jacobs, insbesondere Ullricke Richardt und Christiane Steeg, an meine Labormädels, Amirah Al jawazneh, Clarissa Lanzloth, Jana Hey, Jessica Barton, Lea Kaminski, Marie-Therese Thieme und Stephanie Leyk. Und natürlich an meine Herzis! Danke, dass ihr so eine tolle Atmosphäre geschaffen habt! Es war wirklich eine unvergessliche, tolle und lustige Zeit!

Auch an alle meine Freunde, die während der ganzen Doktorarbeitszeit an meiner Seite standen, vielen lieben Dank! Vor allem an Jacqueline Jürgens, die mir immer eine Inspiration und unermüdliche Editorin war.

Zuletzt möchte ich mich bei meiner Familie bedanken, insbesondere bei meiner Schwester Mara, ohne euch wäre das alles nicht möglich gewesen.

Abbreviations

ADAM	a disintegrin and metalloproteinase
AHR	Aryl hydrocarbon receptor
APCs	Antigen-presenting cells
BTLA	B and T lymphocyte attenuator
CAECAM1	Carcinoembryonic antigen-related cell adhesion molecule 1
CCL	CC-chemokine ligand
CD40L	CD40 ligand
CD56	Neural cell adhesion molecule 1
CTLA-4	Cytotoxic T-lymphocyte-associated protein 4
CXCL	C-X-C motif chemokine ligand
DAMPs	Damage-associated molecular patterns
DAPI	4',6-diamidino-2-phenylindole
DC	Dendritic cells
DNA	Deoxyribonucleic acid
dsRNA	Double-stranded RNA
ELISA	Enzyme-linked immunosorbent assay
eNOS	Endothelial NOS
FAP	Fibro-adipogenic progenitor
FATAL	Fluorometric assessment of T lymphocyte antigen-specific lysis
FCS	Fetal calf serum
FDR	False discovery rate
FMO	Fluorescence minus one
FSC	Forward scatter
GO-term	Gene ontology term
GPI-anchors	Glycosylphosphatidylinositol-anchors
h	Hours
hcRPMI	human complete RPMI
HEPES	4-(2-hydroxyethyl)-1-piperazineethanesulfonic acid
HIV	Human immunodeficiency virus
HLA	Human leukocyte antigen
hpi	Hours post infection
HRP	Horseradish peroxidase
HVEM	Herpesvirus entry mediator
ICAM-1	Intercellular adhesion molecule 1
IDO1	Indoleamine 2, 3-dioxygenase 1
IDO2	Indolamin-2,3-Dioxygenase 2
IFITs	interferon-induced proteins with tetratricopeptide repeats
IFN- γ	Interferon- γ
IL	Interleukin
IL-411	Interleukin-4 induced 1
iNOS	Induced nitric oxide synthases
IRF9	IFN regulatory factor 9

Abbreviations

ISG	Interferon-regulated gene family
KO	Knock-out
	Homologous to Lymphotoxin, exhibits Inducible expression and competes for HSV Glycoprotein D for binding to Herpesvirus entry mediator
LIGHT	homologous to lymphotoxin, exhibits inducible expression and competes for HSV Glycoprotein D for binding to herpesvirus entry mediator
L-Nil	N6-(1-iminoethyl)-L-lysine
MACS	Magnetic cell sorting
MCL1	Induced myeloid leukemia cell differentiation protein
MMP	Matrix metalloprotease
MOI	Multiplicities of infection
MX1	Interferon-induced GTP-binding protein MX1
NF- κ B	Nuclear factor kappa-light-chain-enhancer of activated B cells
NK cells	Natural killer cells
nNOS	Neuronal nitric oxide synthases
NO	Nitrogen oxide
OD	Optical density
PAMPs	Pathogen-associated molecular patterns
PC	Principle components
PCA	Principal component analysis
PCR	Polymerase chain reaction tests
PD-1	Programmed cell death receptor 1
PD-L1	PD-1 ligand 1
PD-L2	PD-1 ligand 2
PFA	Paraformaldehyde
PtdSer	Phosphatidyl serine
RGMb	Repulsive guidance molecule b
RIG-1	RNA helicase retinoic acid-inducible gene I
RNA	Ribonucleic acid
RPMI-1640	Roswell Park Memorial Institute Medium 1640
RT	Room temperature
siRNA	Silencing RNA
sPD-L1	Soluble PD-L1
SSC	Sideward scatter
<i>T. cruzi</i>	<i>Trypanosoma cruzi</i>
TCR	T cell receptor
TGF- β	Transforming growth factor β
T _H cells	T helper cells
TIGIT	T cell immunoreceptor with immunoglobulin and ITIM domains
TIM-3	T cell immunoglobulin and mucin domain-containing protein 3
TLR	Toll-like receptor
TMB	3,3',5,5'-Tetramethylbenzidine
TNF- α	Tumour necrosis factor- α

Abbreviations

TRIM	Tripartite motif family
TSA	Trypomastigote surface antigen
US	United States

Table of content

Eidesstattliche Versicherung/ Statuary declaration.....	1
Nachweis über die Korrektheit der Sprache	2
Danksagung	3
Abbreviations	4
Table of content	7
List of figures	10
List of tables	12
Abstract	13
Zusammenfassung.....	15
1. Introduction	1
1.1 Chagas disease	1
1.2 <i>Trypanosoma cruzi</i>	1
1.3 Disease progression and chronicity	3
1.4 Vaccination, therapy and prevention.....	4
1.5 Overview of the immune system	5
1.6 Immune response against <i>T. cruzi</i>	7
1.7 Immune evasion strategies of <i>T. cruzi</i>	8
1.8 Co-inhibitory receptors	10
1.9 Immune homeostasis and T cell exhaustion	13
1.10 Muscle cell immunology.....	15
1.11 Aim of study	17
2. Materials	18
2.1 Laboratory equipment	18
2.2 Glass and consumables	19
2.3 Chemicals and reagents	20
2.4 Kits	21
2.5 Buffers, solutions and media.....	22
2.6 Antibodies	23
2.7 Software	24
2.8 Cells, Parasites and human donors	25

3. Methods.....	28
3.1 General remarks.....	28
3.2 Cell line LHCN-M2.....	28
3.3 Storage of cells	28
3.4 Determination of cell counts.....	29
3.5 Isolation of muscle stem cells from human tissue.....	29
3.6 Magnetic cell sorting (MACS) using CD56 Micro Beads (Miltenyi)	30
3.7 Cell culture of primary muscle stem cells	30
3.8 Differentiation of primary muscle cells and the cell line LHCN-M2.....	30
3.9 Cultivation of <i>T. cruzi</i> parasites in vitro.....	31
3.10 Isolation of <i>T. cruzi</i> parasites.....	31
3.11 Infection and stimulation of muscle cells.....	31
3.12 Immunofluorescence	32
3.13 Transcriptomic analysis	33
3.14 RNA Isolation.....	33
3.15 Determination of RNA Integrity Number (RIN).....	34
3.16 RNA sequencing library preparation and next-generation sequencing (NGS)	34
3.17 Bioinformatical analysis of the samples.....	34
3.18 Visualization of NGS Data.....	35
3.19 Flow cytometric analysis of skeletal muscle cells	36
3.20 High throughput immunofluorescence analysis using the OperaPhenix™	37
3.21 Flow cytometric bead-based immunoassay LEGENDplex™	38
3.22 Co-culture of T cells with the muscle cell line LHCN-M2	39
3.23 ELISA (enzyme-linked immunosorbent assay)	40
3.24 Statistical analysis.....	41
4. Results.....	42
4.1 Establishment of the muscle cell culture and infection with <i>T. cruzi</i>	42
4.2 Transcriptomic analysis of muscle cells revealed the upregulation of genes involved in the inhibition of parasite growth and immune cell modulation.....	46
4.3 Anti-parasitic mechanisms are induced in muscle cells.....	56
4.4 Cytokines responsible for immune cell recruitment are secreted by muscle cells	62
4.5 Muscle cells could present <i>T. cruzi</i> antigen via HLA-I and HLA-II.....	65

Table of content

4.6 Immunoregulatory mechanisms are induced in muscle cells.....	69
4.7 Immunoregulatory mechanisms of the muscle cells reduce T cell proliferation <i>in vitro</i>	76
5. Discussion.....	84
5.1 Sensing of <i>T. cruzi</i> infection and induction of an anti-parasitic response in muscle cells	84
5.2 Reduced parasite replication in muscle cells by pro-inflammatory cytokines is due to the induction of anti-parasitic mechanisms	87
5.3 <i>T. cruzi</i> infection leads to downregulation of genes in skeletal muscle cells	88
5.4 Immune cell recruitment and modulation by secretion of chemokines and cytokines	90
5.5 Presentation of <i>T. cruzi</i> antigens by HLA-I and HLA-II.....	91
5.6 Muscle cells downregulate the immune response by providing co-inhibitory signals to T cells via PD-L1 and PD-L2.....	93
5.7 Involvement of soluble co-inhibitory ligands.....	94
5.8 Role of galectin-9 in immune suppression during <i>T. cruzi</i> infection.....	95
5.9 Potential new immune regulatory pathway in <i>T. cruzi</i> -infected muscle cells	97
6. Future Perspectives.....	100
Literature.....	102

List of figures

Figure 1: Life cycle of <i>Trypanosoma cruzi</i>	3
Figure 2: T cell response can be modulated by antigen-presenting cells via the expression of ligands of co-inhibitory and co-stimulatory receptors.....	12
Figure 3: Isolation of muscle stem cells (satellite cells) from tissue samples of the gluteus maximus of human donors.	43
Figure 4: Infection of primary human muscle cells with <i>T. cruzi</i> Brazil at 48 hpi reveals susceptibility to low multiplicities of infection (MOIs)..	44
Figure 5: <i>T. cruzi</i> infection in primary human muscle cells and the cell line LHCN-M2 and its replication within the cells over time.	45
Figure 6: Principal component analysis (PCA) of the expressed genes of human primary muscle cells and the cell line LHCN-M2 after infection and/or stimulation with IFN- γ reveals comparable transcriptional changes within the treatments.	47
Figure 7: Heatmap and k-means diagram of 2000 highly expressed genes in human primary muscle cells and the cell line LHCN-M2 after infection (MOI 5:1) and/or stimulation with IFN- γ (100 IU/ml).....	48
Figure 8: Venn diagram visualising the number of differentially expressed genes in primary muscle cell donors across different treatments compared to the mock control reveals the highest amount of differentially expressed genes in <i>T. cruzi</i> -infected and IFN- γ stimulated muscle cells.	49
Figure 9: GO term analysis and heatmap of the 50 most highly differentially expressed genes in primary human muscle cells infected with <i>T. cruzi</i> and/or stimulated with IFN- γ , revealing upregulation of genes involved in the defence response.....	52
Figure 10: Volcano plot of the differentially expressed genes of the primary muscle cell donors under different conditions reveals the induction of anti-parasitic and immune-regulatory mechanisms.....	54
Figure 11: Heatmap of the six differentially expressed genes upregulated by IFN- γ and downregulated during <i>T. cruzi</i> infection.	55
Figure 12: Percent of <i>T. cruzi</i> -positive muscle cells declines upon stimulation with pro-inflammatory cytokines after 24 h, 48 h and 72 h post-infection.	57
Figure 13: The amount of <i>T. cruzi</i> per muscle cell nucleus decreases after stimulation with pro-inflammatory cytokines at 72 h post infection..	58

Figure 14: iNOS increase in *T. cruzi*-positive muscle cells..... 60

Figure 15: Inhibition of iNOS by L-Nil increases the parasitic load of *T. cruzi* in muscle cells..61

Figure 16: Immune cell-recruiting cytokines and chemokines are secreted by muscle cells infected with *T. cruzi* and/or stimulated with pro-inflammatory cytokines..... 64

Figure 17: Human primary muscle cells express HLA-I and upregulate the receptor expression upon infection and stimulation with pro-inflammatory cytokines..... 66

Figure 18: Human primary muscle cells express HLA-DR and CD40 and upregulate these receptors upon infection and stimulation with pro-inflammatory cytokines.. 68

Figure 19: Highly expressed *T. cruzi* genes in muscle cells represent potential targets for HLA class I and II antigen presentation. 69

Figure 20: Muscle cells secrete IL-4/1 after infection with *T. cruzi* and simultaneous stimulation with IFN- γ 70

Figure 21: Human primary muscle cells express the co-inhibitory receptor ligands PD-L1, PD-L2, and galectin-9 and upregulate these receptors upon infection and stimulation with pro-inflammatory cytokines..... 72

Figure 22: PD-L1, PD-L2 and galectin-9 are present in the supernatant after infection with *T. cruzi* and stimulation with IFN- γ and TNF- α 74

Figure 23: Patients with Chagas disease have soluble galectin-9 in their serum. 75

Figure 24: Co-culture of human donor CD4⁺ and CD8⁺ T cells with differently treated muscle cells..... 77

Figure 25: Proliferation of CD8⁺ and CD4⁺ T cells from human donors is reduced after co-incubation with differently treated muscle cells. 81

Figure 26: Human primary muscle cells express the co-inhibitory receptor ligands CD155, CD122, and HVEM and upregulate these receptors upon infection and infection and stimulation with pro-inflammatory cytokines.. 83

Figure 27: Histogram of iNOS expression in *T. cruzi*-infected, IFN- γ and TNF- α stimulated muscle cells. 128

Figure 28: Lower amounts of *T. cruzi* trypomastigotes are released from muscle cells after stimulation with pro-inflammatory cytokines at 96 hpi. 128

Figure 29: Negative correlation between serum galectin-9 concentration and age in female Chagas patients. 129

List of tables

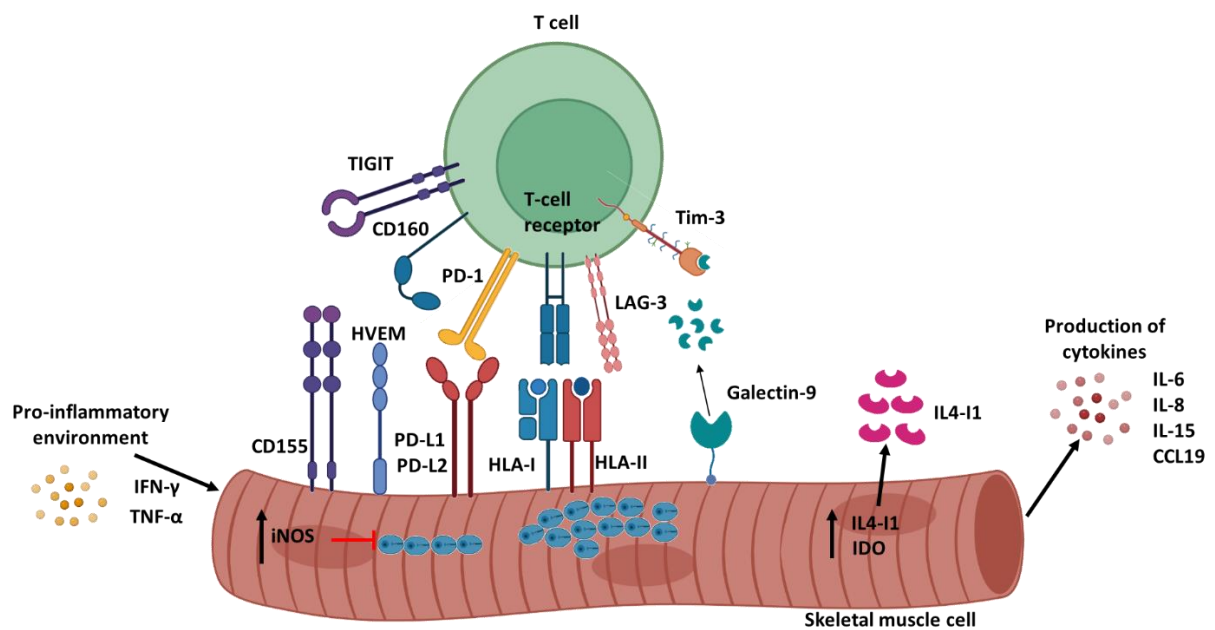
Table 1: Laboratory equipment.....	18
Table 2: Glass and consumables	19
Table 3: Chemicals and reagents.....	20
Table 4: Kits	21
Table 5: Buffers and solutions.....	22
Table 6: Media.....	22
Table 7: Antibodies.....	23
Table 8: Software	24
Table 9: Cell lines.....	25
Table 10: Parasites	25
Table 11: Human muscle cell donors	25
Table 12: Human blood cell donors	25
Table 13: Human Chagas Patients from Columbia.....	26

Abstract

The protozoan parasite *Trypanosoma cruzi* (*T. cruzi*) is the causative agent of the potentially life-threatening Chagas disease and leads to lifelong infection. During the infection, *T. cruzi*-specific cytotoxic CD8⁺ T cells are necessary for long-term reduction of parasite burden and inflammation ¹. However, in humans with Chagas disease, CD8⁺ T cells progressively lose function, characterised by decreased cytokine production, advanced differentiation, and increased expression of co-inhibitory receptors ². Nevertheless, high levels of pro-inflammatory cytokines, such as IFN- γ and TNF- α , are present throughout the infection, which are mainly secreted by T cells and NK cells ³⁻⁵. One of the key features of *T. cruzi* is a chronic infection over the whole lifespan of the host. Especially skeletal muscle cells, were shown to be persistently infected in mice models ⁶.

Here, strong evidence is presented that skeletal muscle cells provide a unique niche for *T. cruzi* by inhibiting clearance of the parasite by CD8⁺ T cells, thereby allowing the parasite to persist in the body. It could be shown that muscle cells actively shape the immune response. Infected primary human skeletal muscle cells produce immune-recruiting chemokines and cytokines, such as IL-6, IL-8, IL-15 and CCL-19. Furthermore, co-inhibitory receptor ligands, such as PD-L1, PD-L2, galectin-9, HVEM, CD155 and CD122 were expressed by the muscle cells upon stimulation with pro-inflammatory cytokines and infection with *T. cruzi*. While, the soluble forms of the ligands PD-L1, PD-L2 and galectin-9 are simultaneously found in the supernatant of muscle cell cultures. Proliferation-analysis of CD8⁺ and CD4⁺ T cells revealed suppressive capacity of *T. cruzi*-infected muscle cells in a PD-1 and TIM-3-dependent manner. In line, stimulation of the muscle cells with IFN- γ prior to the co-culture resulted in even higher suppression capacity. High levels of galectin-9 are present in the serum of Chagas patients, indicating a potential systemic inhibition of T cell function. Moreover, the secretion of the IL4-I1 enzyme by muscle cells could be demonstrated. This molecule can upregulate co-inhibitory receptor ligands on T cells, reduce T cell proliferation and induce apoptosis ⁷. Thus, IL4-I1 might represent a promising new candidate whose immunoregulatory role during *T. cruzi* infection needs to be further investigated. In conclusion, multiple mechanisms by which muscle cells can regulate the immune cell response are presented here and indicate that blocking only one of those mechanisms might not be sufficient to augment T cell activity.

Moreover, it was revealed that muscle cells sense the infection with *T. cruzi* and induce anti-parasitic mechanisms, like the induction of iNOS. This mechanism is capable of significantly reducing the parasite load in muscle cells. The pro-inflammatory environment plays an ambiguous role in the muscle during *T. cruzi* infection by inducing anti-parasitic mechanisms, thereby reducing parasite burden and at the same time inducing immune regulatory mechanisms, which down-regulate the T cell response. Together, these mechanisms might be essential to ensure limited tissue damage and parasite persistence. Thus, muscle cells prove to be crucial modulators of immune cells during *T. cruzi* infection.



Zusammenfassung

Der protozoische Parasit *Trypanosoma cruzi* (*T. cruzi*) ist der Erreger der potenziell lebensbedrohlichen Chagas-Krankheit und führt zu einer lebenslangen Infektion. Während der Infektion sind *T. cruzi*-spezifische zytotoxische CD8⁺ T-Zellen notwendig, um die Parasitenlast und die Entzündung langfristig zu reduzieren ¹. Bei Chagas-Patienten verlieren CD8⁺ T-Zellen jedoch ihre Multifunktionalität, was sich in einer verminderten Zytokin Produktion, einer fortgeschrittenen Differenzierung und einer verstärkten Expression von Ko-inhibitorischen Rezeptoren äußert ². Dennoch sind während der gesamten Infektion hohe Mengen an proinflammatorischen Zytokinen wie IFN- γ und TNF- α vorhanden, die vorallem von T-Zellen und NK-Zellen sekretiert werden ³⁻⁵. Eines der Hauptmerkmale von *T. cruzi* ist eine chronische Infektion über die gesamte Lebensspanne des Wirts. In Mausmodellen wurde gezeigt, dass vorallem Skelettmuskelzellen persistent infiziert sind ⁶.

In der vorliegenden Arbeit konnte gezeigt werden, dass Skelettmuskelzellen eine einzigartige Nische für *T. cruzi* darstellen, indem sie die Beseitigung des Parasiten durch CD8⁺ T-Zellen hemmen und es dem Parasiten dadurch ermöglichen, im Körper zu persistieren. Die erhaltenen Daten zeigen, dass Muskelzellen die Immunantwort beeinflussen können. Primäre menschliche Skelettmuskelzellen produzierten immunrekutierende Chemokine und Zytokine, wie IL-6, IL-8, IL-15 und CCL-19. Darüber hinaus wurden von den Muskelzellen nach Stimulation mit pro-inflammatorischen Zytokinen und nach Infektion mit *T. cruzi* Ko-inhibitorische Rezeptorliganden wie PD-L1, PD-L2, Galectin-9, HVEM, CD155 und CD122 exprimiert. Die löslichen Formen der Liganden PD-L1, PD-L2 und Galectin-9 wurden gleichzeitig im Überstand von Muskelzellkulturen gefunden. Es konnte mittels der Analyse der Proliferationskapazität von CD8⁺ und CD4⁺ T-Zellen gezeigt werden, dass *T. cruzi*-infizierte Muskelzellen über PD-1 und TIM-3 eine suppressive Wirkung ausüben. Die Stimulation der Muskelzellen mit IFN- γ vor der Ko-Kultur führte zu einer erhöhten Suppressionskapazität. Im Serum von Chagas-Patienten waren hohe Konzentrationen von Galektin-9 vorhanden, was auf eine mögliche systemische Hemmung der T-Zell-Funktion hinweist. Außerdem konnte die Sekretion des Enzyms IL-4I1 durch Muskelzellen nachgewiesen werden. Dieses Molekül kann Ko-inhibitorische Rezeptorliganden auf T-Zellen hochregulieren, die T-Zellproliferation reduzieren und Apoptose induzieren ⁷.

Somit könnte IL-4I1 ein vielversprechender neuer Kandidat sein, dessen immunregulatorische Rolle während einer *T. cruzi*-Infektion weiter untersucht werden muss. Zusammenfassend lässt sich sagen, dass mehrere Mechanismen beschrieben wurden, durch die Muskelzellen Immunzellen regulieren können, und dass die Blockierung nur eines dieser Mechanismen möglicherweise nicht in der Lage ist, die Aktivität der T-Zellen zu erhöhen.

Darüber hinaus wurde gezeigt, dass Muskelzellen die Infektion mit *T. cruzi* erkennen und antiparasitäre Mechanismen, wie die Expression von iNOS, einleiten. Dieser Mechanismus ist in der Lage, die Parasitenlast in den Muskelzellen erheblich zu reduzieren. Das pro-inflammatorische Umfeld spielt während einer *T. cruzi*-Infektion im Muskel eine zwiespältige Rolle, indem es antiparasitäre Mechanismen auslöst und dadurch die Parasitenlast reduziert, aber auch immunregulatorische Mechanismen auslöst, die die Funktion von T-Zellen herunterregulieren. Zusammengenommen könnten diese Mechanismen wichtig sein, um eine Gewebeschädigung zu begrenzen und zugleich die Parasitenpersistenz ermöglichen. Somit stellen Muskelzellen entscheidende Modulatoren von Immunzellen während einer *T. cruzi*-Infektion dar.

1. Introduction

1.1 Chagas disease

The protozoan parasite *Trypanosoma cruzi* (*T. cruzi*) causes the potentially life-threatening Chagas disease⁸. While 6-7 million people are afflicted worldwide, approximately 30,000 are newly infected every year, and the disease causes 12,000 deaths annually. The disease is endemic in 21 countries in Latin America and is highly associated with low socioeconomic factors⁹. Through migration, the parasites spread to other countries, and it is estimated that currently, 300,000 people are infected in the United States (US). At the same time, seroprevalence studies among Latin American immigrants in Germany and Europe could find a seroprevalence of 1.8 % and 4.2 %, respectively^{10,11}. Moreover, autochthonous infections with *T. cruzi* parasites from local bugs such as the *Triatoma protracta* species have been reported in multiple southern states of the US, like California and Louisiana^{12,13}. Since its discovery in 1909 by Dr. Carlos Chagas, no significant breakthroughs in combating the disease have been achieved¹⁴. It remains one of the leading public health problems for most Latin American countries and was classified as a neglected tropical disease by the WHO⁸. It is a vector-borne disease, as the parasite's main transmission route is by triatomine bugs. These bugs can be found in the houses of the rural population, and it has been shown that it is mainly children who are infected at a young age^{11,14}. However, the parasite can also be transmitted by food contaminated with triatomine bugs or their faeces, and this form of transmission was shown to lead to a more severe disease¹⁵. Furthermore, it can be transmitted congenitally from mother to child, by blood transfusions or by transfer of organs of chronically infected patients¹⁵. If the infection with *T. cruzi* is not treated early on, the disease becomes chronic, leading to a life-long infection with the parasite.

1.2 *Trypanosoma cruzi*

The obligate intracellular protozoan parasite *T. cruzi* is part of the genus *Kinetoplastida*¹⁶. The kinetoplast, which gave the name to this class, is a single large mitochondrion containing fibrillar DNA, which is often closely related to the base of the flagellum. The flagellum is used for the locomotion of the parasite but can also facilitate the interplay between the parasite and host cells¹⁷.

The parasite's life cycle alternates between arthropod vectors and vertebrate hosts (Figure 1). *T. cruzi* can infect a wide range of vertebrates. Still, mammals such as humans, dogs, rodents and opossums are the most common hosts¹⁸. Mammalian hosts, like humans, are primarily infected by triatomine bugs. When the bug takes a blood meal from an infected individual, parasites can be ingested by the bug. Inside the bug, *T. cruzi* infects the epithelial cells of the midgut and develops from an amastigote to an epimastigote form¹⁹. Epimastigotes, present only in the arthropod phase, replicate via binary fission. They transform into infectious metacyclic trypomastigotes and are secreted with the faeces of the vector.

During a subsequent feeding, the infectious metacyclic trypomastigotes of the parasite can enter the human body through the bite mark, scratching under the skin or accidental rubbing into the eyes or mouth. Here, the parasites can infect cells at the site of infection, like fibroblasts or macrophages, or enter the bloodstream and disseminate throughout the body, potentially infecting any nucleated cell. Depending on the strain and the mouse model used, it could be shown that the parasite prefers different cell types²⁰. The *T. cruzi* Brazil strain is a myotropic strain that prefers muscle tissues, like the skeletal muscle, the heart or the smooth muscle cells in the colon²¹. The parasites can attach to the cell surface of the host cells by surface proteins like mucins²². Different methods of cell invasion have been discussed²³. Cells like macrophages, capable of phagocytosis, were shown to ingest *T. cruzi* in a phagocytic-like process²⁴. In contrast, nonphagocytic cells are infected in a process involving lysosome recruitment to the cell membrane to engulf the parasite²⁵. Independent of the cell type, a parasitophorous vacuole is formed around the parasite. Upon acidification of the parasitophorous vacuole, the parasite escapes into the cytoplasm using a pore-forming protein active in an acidic environment²². Here, the parasite differentiates from the trypomastigote form into the amastigote form and undergoes several replication cycles of binary division. The parasites then differentiate back into the motile, infectious trypomastigote form and cause the rupture of the host cells' plasma membrane. The released trypomastigotes can infect surrounding cells, enter the bloodstream, infect cells in other tissues, or be ingested by a triatomine bug taking a blood meal.

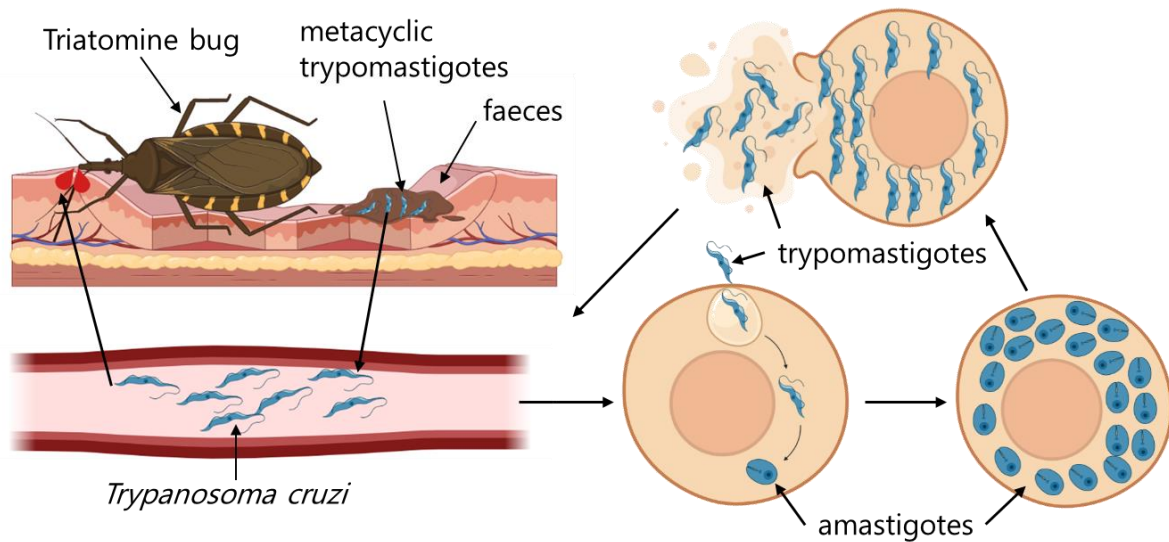


Figure 1: Life cycle of *Trypanosoma cruzi*. Triatomine bugs take a blood meal and excrete metacyclic trypomastigotes with their faeces. These parasites typically enter the mammalian host through the bite wound. Once they enter the host, the parasites infect resident cells, are incorporated by a parasitophorous vacuole, escape from the vacuole to the cytosol and transform into the intracellular amastigote form, multiplying by longitudinal division. They later revert to the motile trypomastigote form and burst the host cell to infect other cells or be consumed by another arthropod. Inside the bug, these trypomastigotes penetrate the midgut epithelial cells, changing into and replicating as amastigotes and epimastigotes. They ultimately differentiate into infective metacyclic trypomastigotes, ready for the next transmission cycle. Created with *biorender*.

1.3 Disease progression and chronicity

The Chagas disease can be categorised into the acute phase and chronic phase, while the chronic phase is further divided into the indetermined phase and symptomatic phase²⁶. The acute phase is characterised by high parasitaemia, and in most cases, only mild symptoms occur. Mainly, children are infected in endemic areas, and symptoms typically start one to two weeks post-infection. Symptoms that occur are often unspecific and result from the general inflammation induced by the infection, like fever, myalgia or tachycardia. However, swelling at the side of infection, called a Chagom or Romaña-sign on the eyelid, can also be found in some cases²⁷. The infection with *T. cruzi* is frequently undetected due to its non-specific symptoms, lack of awareness by patients, and inadequate medical resources in regions where the disease is prevalent²⁸. If the disease is not treated in the acute phase, encephalomyelitis or severe cardiac failure, leading to death, can occur in about 5-10 % of symptomatic patients. Nevertheless, the symptoms subside after 2-4 months, and the patients develop an indetermined form of the disease. This phase is characterised by a low parasitaemia in the

blood, and 70 % of infected people will remain in this stage. However, no sterile immunity is achieved, and the parasite will reside in tissues of persistence like the muscle or the adipose tissue^{6,29–31}. Moreover, parasites will reappear in the bloodstream and can still be infectious. Patients in this phase are often diagnosed via polymerase chain reaction tests (PCR) or serology screening during a blood donation³². After decades of infections, some patients develop the symptomatic chronic phase of the disease with 30 % of patients showing cardiac manifestations like heart failure, syncope, sudden death from heart block, ventricular arrhythmias or thromboembolism³³. In contrast, about 10 % develop gastrointestinal symptoms such as megaesophagus or megacolon³⁴. Mixed manifestations are also possible. Most cases are identified at this stage, and the disease can ultimately be fatal for the patients.

The factors leading to the disease progression and pathogenesis are not yet determined. It is believed that a combination of the host and parasite's genetic characteristics, like the *T. cruzi* strain, host defence strategies, the infection dose, and the route of infection, play a role³⁵. The proposed clonal-histotropic hypothesis postulates that *T. cruzi* populations in the host present different forms of blood trypomastigotes (slender, intermediate, and broad), which showed different tissue tropisms. Moreover, genetic profiling revealed the presence of distinct *T. cruzi* clones in different tissues in the host. Furthermore, it is hypothesised that parasite persistence in the tissue and the constant immune response against the parasites leads to tissue destruction and fibrosis²⁹. This hypothesis is supported by the presence of pathology in the organs of persistence and evidence that anti-parasitic treatments reduce parasite burden and disease severity. Furthermore, an auto-immune hypothesis postulates that the auto-reactive antibodies against the adrenergic or cholinergic receptor found in patients contribute to physiopathology³⁶.

1.4 Vaccination, therapy and prevention

Despite multiple attempts, no approved vaccine for the Chagas disease exists³⁷. Any such efforts have only resulted in partial immunity, with lower mortality but persistent parasitaemia. Additionally, current treatment options for *T. cruzi* infections are limited to the drugs benznidazole and nifurtimox. These drugs target and kill the parasites but must be activated by the type I nitroreductase³⁸. Both drugs rely on the formation of free radicals and reactive oxygen species. For example, benznidazole depends on the formation of free radicals

and electrophilic metabolites to induce breakage in the deoxyribonucleic acid (DNA) of the parasite ³⁹. However, the drugs can cause serious side effects, including anorexia, allergic dermatitis, and peripheral neuropathy ⁴⁰. They also require a prolonged treatment period of at least two months ⁴¹. In addition, drug resistance has been described for a long time in different *T. cruzi* strains by downregulating the enzyme type I nitroreductase ³⁸. Moreover, these drugs are only potent during the acute phase, marked by a significant presence of the parasite in the blood. In contrast, the efficacy of the treatment is inconsistent during the chronic phase ⁴². It can reduce the parasite load, but the treatment cannot slow or reverse the progression of fibrotic heart disease in symptomatic chronic patients ⁴².

Therefore, efforts have been made to reduce the disease's spread by eradicating the arthropod vector using insecticides or insecticide-treated nets to prevent the infection ^{43,44}. This strategy has achieved commendable results in Latin America, but areas without continuous efforts have seen resurgences ⁴⁵. Furthermore, systemic blood tests are implemented to minimise the risk of transmission via blood transfusions and organ transplants. However, promising effects could be found in a therapeutic vaccine trial with infected rhesus macaques. A DNA vaccine encoding for trypomastigote surface antigen (TSA-1) and the flagellar calcium-binding Tc24 parasite antigens prevented cardiac alterations ³⁷. Similarly, a breakthrough was recently achieved by describing a cyanotriazole compound that could kill trypanosomes ⁴⁶. It could be shown that this compound selectively inhibited the parasite topoisomerase II enzyme, which caused irreversible and lethal DNA damage. Moreover, this compound rapidly cleared the parasite *T. cruzi* and the related parasites of the sleeping disease *T. brucei* in *in vitro* and *in vivo* experiments in mice. Therefore, this compound emerges as a promising new treatment option for Chagas patients.

1.5 Overview of the immune system

The immune system is our body's defence against infections caused by parasites, viruses, bacteria and fungi ⁴⁷. It comprises different cells and molecules that work together in complex ways to eradicate pathogens while ensuring that the host remains unharmed. One of its primary functions is to distinguish between the body's cells (self) and foreign cells (non-self) and between healthy and damaged or infected cells using the human leukocyte antigen

system (HLA). The immune response is divided into innate and adaptive immune responses, which work together to fight pathogens effectively.

The innate immune response acts quickly after the onset of infection and provides a general defence. On the other hand, the adaptive immune system has B and T cells that provide a precise defence against specific invaders but take longer to be established.

For any pathogen to cause infection, it must bypass the immune system's first line of defence, which includes physical barriers such as the skin and innate immune cells such as dendritic cells (DCs), natural killer (NK) cells and macrophages. DCs, which exist in various forms, are particularly important as they present antigens to naive T cells, initiating the adaptive immune response. Meanwhile, NK cells act quickly to produce toxins that eliminate pathogen-infected cells. In addition, they can either suppress or enhance the immune responses of several other immune cells. Macrophages are phagocytic cells that aid in the immune response by the uptake and digestion of pathogens and presenting antigens to immune cells, bridging the innate and adaptive immune systems.

T cells mature in the thymus and come in two main types: cytotoxic CD8⁺ T cells and CD4⁺ T helper cells (T_H cells). After recognising signals from T cell receptors on antigen-presenting cells (APCs), naive T cells activate, expand, and modify their expression and cytokine production. This leads to the creation of effector T cells and long-lasting, self-renewing memory T cells. CD8⁺ T cells aim to suppress or eliminate target cells, while CD4⁺ T cells, also known as T helper cells, help other immune cells by producing activating cytokines. These helper cells can further specialise into T_H1, T_H2 and T_H17 types. T_H1 cells are characterised by producing the pro-inflammatory cytokine interferon- γ (IFN- γ), which stimulates macrophages and cytotoxic CD8⁺ T cells. They are associated with a pro-inflammatory response that releases cytokines such as tumour necrosis factor- α (TNF- α) and interleukin-2 (IL-2). Conversely, T_H2 cells, which produce IL-4, IL-5 and IL-13, help to eliminate parasites and activate B-cells. T_H17 cells, known for producing IL-17 and IL-22, play a key role in fighting bacteria and fungi.

1.6 Immune response against *T. cruzi*

Innate immune system

The immune response against the parasite is initiated as soon as the parasite enters the host through the skin. Cells of the innate immune system, like tissue-resident macrophages, neutrophils and dendritic cells, encounter the parasite first ⁴⁸. These cells express receptors recognising pathogen-associated molecular patterns (PAMPs) and damage-associated molecular patterns (DAMPs), enabling the detection of the pathogen and cell debris caused by cell rupture. Toll-like receptors (TLR) have been shown to recognise different parts of *T. cruzi*. TLR-2 can recognise glycosylphosphatidylinositol-anchors (GPI-anchors) derived from *T. cruzi* mucin-like glycoproteins, and TLR-4 recognises glycoinositolphospholipids ^{49,50}. In contrast, TLR-9 and -7 can recognise *T. cruzi* DNA, which is rich in unmethylated CpG motif ⁵¹. Once macrophages recognise the presence of *T. cruzi*, they shape the immune response by producing proinflammatory cytokines like IL-1, IL-12, TNF- α and IL-10 ^{52,53}. IL-12 can stimulate NK cells to produce the pro-inflammatory cytokine IFN- γ ⁵⁴. NK cells were shown to be the main producers of IFN- γ and TNF- α during the acute phase, and IFN- γ was demonstrated to be crucial for parasite control ^{3,4}. This cytokine can activate macrophages and lead to the production of induced nitric oxide synthases (iNOS), which is an enzyme involved in the formation of reactive oxygen species using L-arginine as a substrate, which have a trypanocidal activity ⁵⁵⁻⁵⁷. However, NK cells themselves play a crucial role in eliminating the parasite during the early phase of the infection. They can detect infected cells and kill them in a granulysin, granzyme and perforin-dependent manner ⁴. Moreover, NK cells were shown to bind to extracellular trypomastigotes and lyse them ⁵⁸. At the same time, neutrophils are rapidly recruited to the site of infection by IL-8, which can be produced by epithelial cells ⁵⁹. Even though their involvement during the Chagas disease is not well studied, they could be shown to phagocyte and kill amastigote *T. cruzi* parasites ⁶⁰. Additionally, neutrophils were shown to release neutrophil extracellular traps, consisting of DNA and histones, which can trap the parasite and induce differentiation to the amastigote form, thereby limiting infectivity ⁶¹. The complement system was shown to aid the phagocytic cells via the lectin and alternative complement pathway by opsonising the parasites and initiating phagocytosis ⁶².

Adaptive Immune system

B cells were shown to be essential during the *T. cruzi* infection and display multiple functions. They are part of the humoral immune response, produce antibodies against the parasite, secrete immune stimulatory cytokines, and can bridge the innate to the adaptive immune system by antigen presentation^{63,64}. Mature B cells are essential for IFN- γ and IL-12 production. Moreover, B cells were shown to activate T cells towards a T_H1 response, which is favourable for parasite control, and are involved in the induction of effector CD8⁺ T cells⁶³. CD8⁺ T cells are essential for fighting and controlling the parasite during the lifelong infection. However, it has been shown that the T cell response, with the induction of *T. cruzi*-specific CD8⁺ T cells, is delayed in the host. *T. cruzi*-specific CD8⁺ T cells can be found only 8-9 days post-infection in mice⁶⁵. The initial *T. cruzi* infection is believed to fail to trigger a systemic recognition of the parasite. Therefore, a complete replication cycle of *T. cruzi* of 4-5 days can occur before T cells are activated. The subsequent release of trypanosomes, PAMPS from the parasites and DAMPS from the destroyed host cells enables the induction of a robust CD8⁺ T cell response. Especially peptides of trans sialidases and amastigote proteins 1 and 2 are presented by APCs via HLA-I to the CD8⁺ T cells and are capable of inducing a protective response^{66,67}. CD8⁺ T cells are essential in controlling the parasites during the acute and chronic stages of the disease. Mice depleted of CD8⁺ T cells do not survive the acute phase, while the depletion during the chronic stage results in increased parasitaemia and parasitic load in muscle and adipose tissue⁶⁸. CD8⁺ T cells kill infected host cells and intracellular parasites via the secretion of granulysin, perforin and granzymes⁴. Together with CD4⁺ T cells, they contribute to the pro-inflammatory environment by secreting IFN- γ and TNF- α ⁶⁸⁻⁷⁰. Moreover, it was shown that cytotoxic CD4⁺ T cells are induced during *T. cruzi* infection, which mediated cytotoxicity against cells presenting pathogen-derived antigens and particularly infiltrated the heart in mice⁷¹.

1.7 Immune evasion strategies of *T. cruzi*

T. cruzi can activate both the innate and adaptive immune response, including the induction of *T. cruzi*-specific antibodies and *T. cruzi*-specific CD8⁺ T cells capable of reducing the parasite burden and keeping the infection under control. However, no sterile eradication of the parasites can be achieved⁷². Very evidently, in chronic Chagas patients undergoing

immunosuppression due to organ transplantation or by a human immunodeficiency virus (HIV) infection, a reactivation of the acute phase can be induced with increased parasitaemia, potentially leading to neurological complications like meningitis ⁷³.

It could already be demonstrated that *T. cruzi* parasites can induce different immune evasion strategies to prevent eradication. Macrophage function is directly down-regulated by *T. cruzi*. Phagocytosed *T. cruzi* parasites can avoid destruction in the phagolysosome by escaping using a pore-forming protein Tc-TOX ⁷⁴. At the same time, infected macrophages were also shown to secrete the anti-inflammatory cytokines IL-10 and transforming growth factor β (TGF- β), which induces susceptibility to the parasite ⁷⁵. Both cytokines are potent regulators of T cells, capable of down-regulating the response of T_H1 cells ⁷⁰. Furthermore, membrane-bound GPI-anchored mucin of *T. cruzi* can bind to macrophages and induce the secretion of IL-1 β while inhibiting the secretion of the protective IL-12 ⁷⁶. Additionally, apoptosis of macrophages with increased release of viable, infective trypomastigotes in the presence of IFN- γ could be induced by glycoinositolphospholipids of *T. cruzi* ⁷⁷.

Moreover, *T. cruzi* exposes a high variability of antigens, like trans-sialidases and mucins, hampering the production of effective antibodies. Trans-sialidases cover the parasites in sialic acid and protect the parasites against antibody-mediated killing and advert the complement system by inhibiting the binding of complement factor B ^{78,79}. Besides the delayed response of T cells, it has also been shown that even though B cells secrete antibodies early on, these are not specific against the pathogen and do not control the parasitaemia ⁸⁰. Antigen-specific antibodies capable of reducing the parasitaemia in mice are only present three weeks post-infection. Trans-sialidases of *T. cruzi* were shown to activate B cells *in vitro* and induce abnormal polyclonal B cell activation and *T. cruzi*-unspecific antibody secretion and enhanced virulence *in vitro* ⁸¹. Moreover, *T. cruzi* was shown to cause a regulatory B cell type, which could down-regulate the CD4⁺ T cell response *in vitro* by reducing proliferation and IFN- γ production ⁸². Additionally, T cell responses can be down-regulated by binding of CD33 to *T. cruzi* mucins, inhibiting mitogenic response in CD4⁺ T cells, resulting in increased susceptibility to the parasite ^{83,84}.

1.8 Co-inhibitory receptors

Different co-inhibitory and co-stimulatory receptors can influence the T cell response upon encountering an antigen-presenting cell (Figure 2). During T cell activation, the T cell receptor (TCR) complex binds its specific antigen, which are short peptide fragments of a pathogen protein, presented by APCs via the HLA complex⁸⁵. The T cell receptor complex comprises of a ligand-binding subunit, the α - and β -chains, the signalling subunits CD3, and the TCR ζ -chain. The eponymous receptors CD4 or CD8 have to additionally bind to form an immune synapse, which is essential for T cell activation. Upon activation of the TCR, the lymphocyte-specific protein tyrosine kinase in the cytosol becomes active. It phosphorylates CD3, initiating a signalling cascade leading to the induction of the transcription factor nuclear factor kappa-light-chain-enhancer of activated B cells (NF- κ B). Furthermore, co-stimulatory signals are received by binding of CD28 to CD80/CD86. Additionally, for CD4⁺ T cells, CD40 ligand (CD40L) can bind to CD40. The interaction of the TCR and the co-stimulatory receptors, as well as the stimulation with IL-2, are necessary to lead to T cell activation and induce proliferation⁴⁷.

Nevertheless, the activation of T cells can also be downregulated by co-inhibitory receptors. The co-inhibitory receptor cytotoxic T-lymphocyte-associated protein 4 (CTLA-4) has a high sequence similarity to CD28 and competes with this co-stimulatory receptor for the binding of CD80/CD86. It has a higher binding affinity and can, in contrast to CD28, induce a negative signalling cascade leading to the down-regulation of a T cell response^{86,87}.

While programmed cell death receptor 1 (PD-1) also belongs to the CD28 family and can be found within 24 h on activated T cells, it is also used as a marker for exhausted and dysfunctional T cells⁸⁸⁻⁹⁰. In contrast, PD-1 binds to PD-1 ligand 1 (PD-L1), and PD-1 ligand 2 (PD-L2) and the interaction results in the negative regulation of T cell activity, inhibiting proliferation, IL-2 and IFN- γ production, and inducing apoptosis⁹¹⁻⁹³. It has been shown that the PD-1-associated SHP-tyrosine phosphatase 2 preferentially dephosphorylates CD28 over the TCR-associated ζ -chain, reducing the phosphorylation of CD28, thereby limiting activating signals⁹⁴. The ligands of PD-1 are expressed on APCs, can be upregulated by interferons and are induced in the context of auto-immunity as a protective mechanism^{95,96}. However, tumour cells also express PD-L1 and inhibiting the interaction with PD-1 using monoclonal blocking antibodies is an effective way to improve tumour clearance⁹⁷.

The T cell immunoglobulin and mucin domain-containing protein 3 (TIM-3), also called CD366, is part of the TIM-gene family and is expressed by many cell types, including differentiated T_H1 cells, regulatory T cells, and macrophages⁹⁸. This co-inhibitory receptor has been described in auto-immune diseases like lupus and viral infections like HIV and has been linked to immune regulation⁹⁹. It could be shown that TIM-3 is necessary for the induction of antigen-specific tolerance, and it inhibits T_H1-mediated auto- and alloimmune responses¹⁰⁰. Multiple ligands exist, like the membrane-bound receptor carcinoembryonic antigen-related cell adhesion molecule 1 (CAECAM1) found on epithelial cells and leukocytes¹⁰¹. Furthermore, soluble ligands have been described, like the C-lectin galectin-9¹⁰². The binding of galectin-9 can induce exhaustion and apoptosis in T_H1 cells, T_H17 cells and tumour-infiltrating CD8⁺ T cells^{103,104}. Another ligand is phosphatidyl serine (PtdSer), a molecule found on apoptotic cells. Since antigen-presenting cells can express TIM-3, the binding has been implicated in the uptake of apoptotic cells¹⁰⁵. It is not yet known how the different ligands change the intracellular signalling cascade. However, it has been shown that the cytoplasmic tail of TIM-3 has the potential to interact with multiple components of the TCR complex⁹⁹.

The co-inhibitory receptor T cell immunoreceptor with immunoglobulin and ITIM domains (TIGIT) is a member of the immunoglobulin superfamily and is induced on activated T cells, memory T cells and T_{regs}⁹⁹. It binds to CD155 or CD112 but with higher affinity to CD155 and competes with the CD226 co-stimulatory receptor on T cells. Moreover, TIGIT interaction with CD155 has another immune regulatory effect: the secretion of IL-10 by DCs and subsequent T cell suppression¹⁰⁶. Besides this DC-induced T cell suppression, TIGIT also targets molecules in the TCR signalling pathway, thereby blocking T cell activation, proliferation, and effector functions¹⁰⁷. Furthermore, engagement of TIGIT downregulates components of the TCR complex.

B and T lymphocyte attenuator (BTLA) is a co-inhibitory receptor, negatively regulating T cell responses by interacting with herpesvirus entry mediator (HVEM)¹⁰⁸. This ligand is part of the TNF-receptor superfamily, acting as a molecular switch by interacting with LIGHT (homologous to lymphotoxin, exhibits inducible expression and competes for HSV Glycoprotein D for binding to herpesvirus entry mediator) and producing stimulatory signals or binding to BTLA to induce inhibitory signals. HVEM can also bind to the membrane protein CD160¹⁰⁹. While the function of CD160 is diverse, an inhibiting effect in T cells could be shown¹¹⁰. In contrast,

in NK cells, in combination with type 1 interferons and IL-2, this receptor-ligand interaction can induce stimulatory signals ¹¹¹.

The expression of co-inhibitory receptors on T cells is crucial to ensure immune balance and to promote tolerance, for example, in auto-immune diseases ¹¹². However, this mechanism is also induced by cancers and viral infections ^{113,114}. During persistent antigen exposure, T cells express co-inhibitory receptors and lose essential T cell functions such as cytotoxicity, proliferation and the production of cytokines such as IFN- γ , TNF- α and IL-2 ¹¹⁵. In Chagas patients, CD8⁺ T cells exhibited higher expression of the co-inhibitory receptors CD244, CD160, PD-1, CTLA-4 and TIM-3 compared to healthy donors ¹¹⁶. Therefore, the expression of co-inhibitory receptors and the down-regulation of T cell function was proposed as a persistence mechanism by *T. cruzi* ¹¹⁷. Inhibition of co-inhibitory receptors with their ligands can improve T cell function. Monoclonal blocking antibodies against co-inhibitory receptors, also called checkpoint inhibitors, are already used in different cancer treatments and have shown great success in improving T cell function and patients' survival ¹¹⁸.

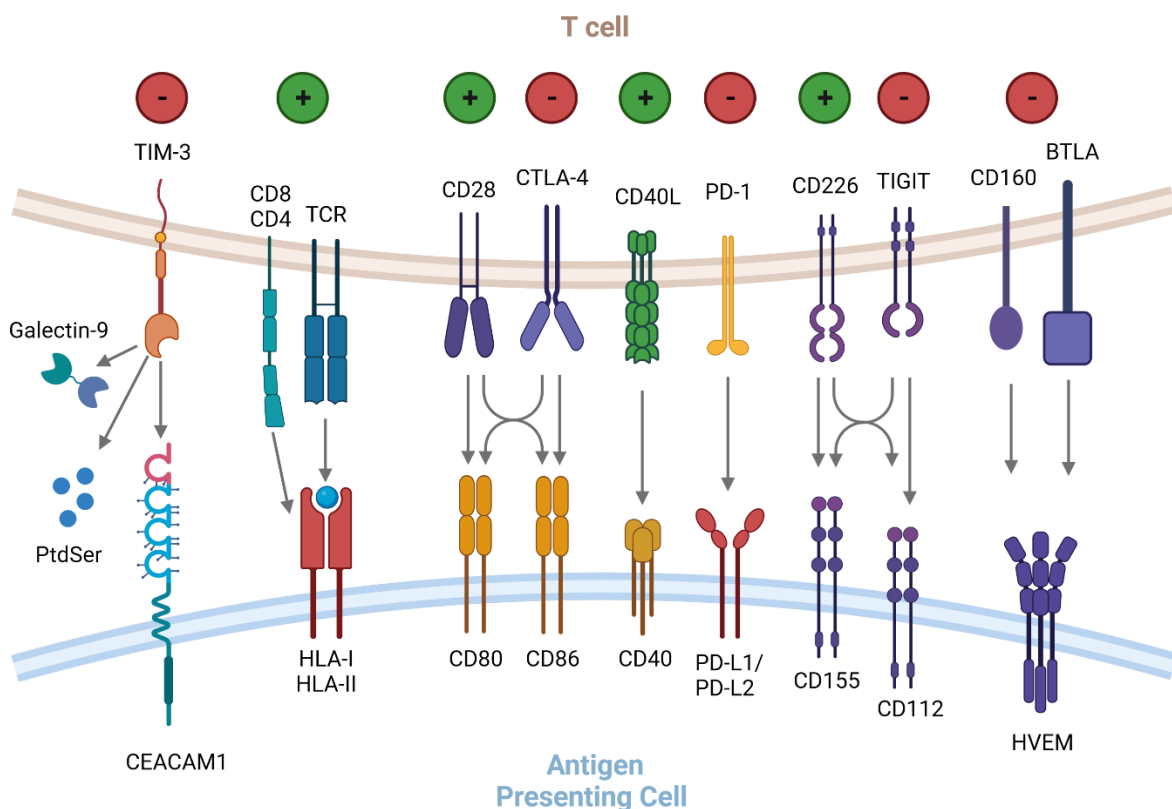


Figure 2: T cell response can be modulated by antigen-presenting cells via the expression of ligands of co-inhibitory and co-stimulatory receptors. Engagement of the T cell receptor with HLA-I or II and CD8 or CD4, respectively, is essential for T cell activation. Following this interaction, the engagement of different co-activating or co-inhibitory receptor ligands determines the T cell response. The

interaction of CD28 and CD80/CD86 creates an activating signal in T cells, while additionally, for CD4⁺ T cells, CD40L can interact with CD40 on the APC. Down-regulation of T cell activity can be achieved by the interaction of TIM-3 with the ligand CEACAM1 on the cell surface of the APC or via the soluble ligands galectin-9 and PtdSer. At the same time, CTLA-4 competes with CD28 for the binding of CD80/CD86. PD-1 binds to the ligands PD-L1 and PD-L2. In contrast, TIGIT and CD226 can bind to CD112 and CD155. Moreover, the co-inhibitory receptors CD160 and BTLA can bind to HVEM. Created with *biorenderer*.

1.9 Immune homeostasis and T cell exhaustion

During the life-long *T. cruzi* infection, it is necessary to keep an immune homeostasis. While an effective immune response elicited by CD8⁺ T cells is crucial to fight the parasite, the effector mechanisms are also causing tissue damage¹¹⁹. It is hypothesised that by the persistence of *T. cruzi* in tissues like the heart, a constant immune response is elicited in these organs, leading to pathological changes and ultimately leading to the loss of function. Therefore, it is necessary for the host to limit the immune response to protect the tissue from harm. One mechanism which has been described previously is the up-regulation of ligands of co-inhibitory receptors. Nevertheless, down-regulation of the immune response might also lead to parasite persistence, and the induction of co-inhibitory molecules on T cells was proposed as a mechanism of immune evasion by the parasite¹²⁰.

This hypothesis is supported by a transcriptomic study with Chagas patients¹²¹. They could demonstrate that higher expression of genes related to NK/CD8⁺ T cell cytotoxicity was beneficial. These patients exhibited reduced parasitaemia and less severe cardiomyopathy. Moreover, CD8⁺ T cells of Chagas patients showed a higher frequency of terminally differentiated CD8⁺ T cells at an advanced severe disease stage than patients at an early stage of the disease¹¹⁶. It could be demonstrated that CD8⁺ T cells exhibited higher expression of the co-inhibitory receptors CD244, CD160, PD-1, CTLA-4 and TIM-3 in comparison to healthy donors¹¹⁶. These receptors were more expressed in patients in the symptomatic phase of the disease in comparison to asymptomatic cases. In addition, it was shown that symptomatic patients had a higher frequency of monofunctional cytotoxic parasite-specific CD8⁺ T cells, only able to produce granzyme b and perforin in contrast to asymptomatic patients exhibiting more polyfunctional parasite-specific CD8⁺ T cells, producing additionally IFN- γ and TNF- α . The authors hypothesised that the monofunctional cytotoxic parasite-specific CD8⁺ T cells might contribute to the tissue damage. Furthermore, dysfunctional CD8⁺ T cells could be found explicitly in the muscle of mice, which is a location of persistence for the parasite⁶. They

exhibit a reduced IFN- γ production and cytotoxic effector function compared to the spleen's T cell counterparts. This effect was present during the acute and chronic phases of the disease in different mouse strains.

Therefore, blocking co-inhibitory receptors during the infection with *T. cruzi*, similar to the successes seen during viral infections or cancer, has emerged as a promising therapeutic approach to improve T cell function and parasite clearance. However, multiple attempts have been made in mouse models and could not show improved T cell function or parasite clearance. One study using PD-L1 knock-out (KO) mice and the monoclonal blocking antibodies against PD-1 and TIM-3 could find no improvement of T cell function and no decline in blood parasitaemia in *T. cruzi* Tulahuen infected mice ¹²². Although, T cell function and parasitaemia were only investigated systemically and not in locations of persistence, like the skeletal muscle. Nevertheless, another study found similar results using the *T. cruzi* Brazil strain. They could also not find improved T cell function in the skeletal muscle in PD-L1 KO mice or by blocking the anti-inflammatory cytokines IL-10 ⁶⁸. In another study using the *T. cruzi* Brazil strain, T cells expressing the co-inhibitory receptors PD-1, TIM-3, and LAG-3 could be observed systemically in the spleen early in the infection on days 15 and 30 ¹²³. Moreover, TIM-3-positive T cells were found in the skeletal muscle during the acute phase. However, exhausted T cells, characterised by the transcription factor TOX, could only be seen late during the infection on day 800 post-infection. A TIM-3 blockade was insufficient in significantly decreasing the parasitaemia in the muscle.

Furthermore, an attempt was made to improve the CD8⁺T cell response in the skeletal muscle ¹²⁴. The potential reduced presentation of *T. cruzi* antigens by muscle cells should be possible to overcome by the constitutional upregulation of the antigen-presenting molecule MHC-I, the mouse equivalent to HLA-I. While this up-regulation improved parasite clearance at the beginning of the infection, it ultimately led to T cell exhaustion and higher parasitic load in the chronic phase of the disease. These results illuminate the importance of an immune homeostasis during the infection.

1.10 Muscle cell immunology

While *T. cruzi* parasites show remarkable versatility in invading and reproducing within almost any nucleated cell type, in hosts with chronic infection, these parasites are commonly found in muscle tissue, such as the heart or in the muscle tissue of the gastrointestinal system and these tissues are also where pathophysiological changes occur^{30,125}. However, in a mouse model of *T. cruzi* Brazil infection, it was shown that specifically, the skeletal muscle is a reservoir for *T. cruzi* parasites¹²³. The skeletal muscle is the largest cellular compartment of the body, an immunologically unique tissue considered a nonclassical immunologically privileged site¹²⁶. Immune privilege is an evolutionarily conserved mechanism that protects vulnerable indispensable tissues with limited regeneration capacity, like the brain and the eye, from harmful uncontrolled inflammatory immune response¹²⁷.

Even though the skeletal muscle tissue is permeated with blood vessels, enabling quick recruitment of lymphocytes, without inflammation, muscle cells only express low amounts of the antigen-presenting molecules HLA class I and II^{126,128}. Moreover, regulatory T cells are present in the muscle and are additionally recruited upon injury¹²⁹. They are vital players in the immune response in the skeletal muscle and perform immunosuppressive function by secreting the anti-inflammatory cytokine IL-10¹³⁰. They thereby regulate other T cell responses and are involved in switching the pro-inflammatory response towards tissue regeneration. Additionally, they play a crucial role in activating satellite cells, the stem cells of the muscle, by secreting the epidermal growth factor amphiregulin¹²⁹. Skeletal muscle cells have a remarkable regenerative capacity. Satellite cells are localised on top of muscle cell fibres and leave their quiescent state upon tissue damage, proliferate, differentiate to myoblast and fuse to rebuild the muscle fibre¹³¹.

Macrophages play an essential role in orchestrating the immune response in the skeletal muscle. Upon injury or infection, tissue-resident macrophages are activated by DAMPS and recruit monocytes and neutrophils from the blood by secretion of the CXC-chemokine ligand 1 (CXCL1) and CC-chemokine ligand 2 (CCL2)¹³². The pro-inflammatory cytokines TNF- α and IFN- γ present in the muscle environment upon injury drive the newly recruited monocytes towards a pro-inflammatory phenotype¹³³. These cytokines are produced by a multitude of cells in the muscle, for example, by tissue-resident macrophages, neutrophils, and by the skeletal muscle cells themselves^{133–135}. Initially, macrophages exhibit a pro-inflammatory M1

phenotype and express T_H1 cytokines that regulate muscle stem cells' proliferation, migration and differentiation ¹³⁶. Furthermore, macrophages and neutrophils are crucial in phagocytosing cell debris and dead cells ¹³⁷. However, they also produce reactive oxygen species and can induce further tissue damage ¹³⁸. After a few days, the macrophages switch their phenotype towards an anti-inflammatory M2 phenotype to enable tissue repair and attenuate inflammation, driven by the IL-10 produced by regulatory T cells ¹³⁹. Moreover, phagocytosis of apoptotic leukocytes induces the production of arginase and other proteins essential for the M2 phenotype and tissue regeneration ¹²⁶. Tissue regenerative macrophages secrete growth factors such as the Insulin-like growth factor, promoting muscle cell growth and differentiation ¹⁴⁰. By secreting transforming growth factor β (TGF- β) and platelet-derived growth factors, they activate fibro-adipogenic progenitor (FAP) cells ¹⁴¹. These cells contribute to the secretion of extracellular matrix proteins such as collagen 1 and fibronectin and induce the differentiation of primary myogenic progenitors ^{142,143}.

However, if the inflammation cannot be resolved, as seen during chronic inflammation in autoimmune diseases, exacerbation of fibre damage or fibrosis can be observed ¹³³. Prolonged-activated neutrophils and macrophages can cause severe tissue damage by producing reactive oxygen species. Macrophages producing anti-inflammatory protein arginase 1 lead to high levels of polyamines, which further expand FAPS and lead to increased connective tissue production and fibrosis ¹³³.

Moreover, muscle cells themselves can actively shape the immune response. They do not express HLA-I in high amounts on their surface, thereby limiting immune responses against intracellular pathogens ¹²⁸. However, upon inflammation and stimulation with pro-inflammatory cytokines such as IFN- γ , they can upregulate HLA-I ¹⁴⁴. They balance the immune response by providing pro-inflammation and anti-inflammatory stimuli ¹⁴⁵. The pro-inflammatory cytokine IL-6 is constantly secreted but can be upregulated upon stimulation with pro-inflammatory cytokines ¹⁴⁶. Furthermore, they can secrete the pro-inflammatory cytokines IFN- γ and TNF- α , providing pro-stimulatory signals to T cells via CD40 and ICOS ^{147,148}. Nevertheless, they can also down-regulate an immune response by the production of IL-10 and TGF- β and upregulation of the T cell suppressing receptors PD-L1 and HLA-G ¹⁴⁹⁻¹⁵¹.

1.11 Aim of study

During the infection with the obligate, intracellular parasite *T. cruzi*, CD8⁺ T cells are crucial to control the parasite. Nevertheless, even though an effective immune response capable of controlling the disease is elicited, parasite eradication is not achieved, and the parasites persist in locations like the skeletal muscle. CD8⁺ T cells isolated from the skeletal muscle were shown to have reduced function, marked by a reduced cytotoxic capability and reduced IFN- γ expression¹⁵². It can be hypothesised that while a CD8⁺ T cell response against *T. cruzi* is initiated, this response cannot clear parasites from the host due to the anti-inflammatory environment present in locations of persistence, like the skeletal muscle. These organs are inducing immune tolerance and resulting in the persistence of parasites. Effector T cells might be suppressed by the upregulation of co-inhibitory receptor ligands, like PD-L1, which is upregulated in the muscle in muscle myopathies¹⁵³.

Therefore, using primary human skeletal muscle stem cells and the human muscle cell line LHCN-M2, in this study it should be investigated how skeletal muscle cells can influence the immune system. Particular emphasis should be put on their immune recruiting capabilities by the expression of chemokines and cytokines, their capability of activating T cells via the presentation of *T. cruzi* antigens and their capability of modulating the T cell response through the expression of co-inhibitory receptor ligands and other immune regulatory molecules.

Furthermore, it was of interest how the pro-inflammatory environment represented by the cytokines IFN- γ and TNF- α , present throughout an infection, can influence the immune modulating capacities of skeletal muscle cells and their capability to reduce intracellular parasites.

2. Materials

2.1 Laboratory equipment

Table 1: Laboratory equipment.

Name	Company
Analytical scale	Satorius AG, Göttingen, Germany
Autoclave 6464L	Schlumbohm Medizintechnik, Hamburg, Germany
Benchtop centrifuge 5810 R	Eppendorf, Hamburg, Germany
Bioanalyzer System Agilent 2100	Agilent Technologies, Santa Clara, USA
Centrifuge Heraeus Megafuge X3R	Thermo Fisher Scientific, Walham, USA
CO2 incubator Hera Cell 150	Heraeus instruments, Hanau, Germany
Flow cytometer Cytex® Aurora CS	Cytex Biosciences, Fremont, USA
Fluorescence microscope Axio Imager M.1	Carl Zeiss AG, Oberkochen, Germany
Freezer (-20°C/-70°C)	Liebherr, Biberach, Germany
Fridge (4°C)	Liebherr, Biberach, Germany
Laminar Flow FlowSafe B-(MaxPro)3-130	Berner, Elmshorn, Germany
Liquid nitrogen tank	Tec-Lab GmbH, Idstein, Germany
MidiMACS™ Separator	Miltenyi Biotec B.V. & Co. KG, Bergisch Gladbach, Germany
Microscope	Olympus, Hamburg, Germany
Milli-Q purification system	Merck Millipore, Burlington, USA
Mr. Frosty freezing device	Zefa Laborservice, Harthausen, Germany
Multichannel pipettes	Eppendorf, Hamburg, Germany
NanoDrop 2000 microvolume spectrophotometer	Thermo Fisher Scientific, Walham, USA
Opera Phenix™ high-content confocal imaging system	PerkinElmer, Inc., Waltham, USA
NextSeq 550 system	Illumina, San Diego, USA
pH meter	Hanna Instruments, Kehl am Rhein, Germany
Pipetboy accu-jet® pro	Brand, Wertheim, Germany
Pipettes (10µl, 20µl, 100µl, 200µl, 1000 µl)	Eppendorf, Hamburg, Germany
Vortex VF2	IKA-Werke GmbH & Co. KG, Staufen, Germany
Waterbath Thermomix® MM	B. Braun Melsungen AG, Melsungen

2.2 Glass and consumables

Table 2: Glass and consumables

Name	Company
Cell culture flasks (T25, T75, T175)	Sarstedt, Nümbrecht, Germany
Cell culture plates (6-well F-bottom, 12-well F-bottom, 24-well F-bottom, 96 well F-bottom, 96 well U-bottom)	Sarstedt, Nümbrecht, Germany
Cell strainer (30 µm, sterile)	Sysmex, Norderstedt, Germany
Cell strainer (40 µm, sterile)	Corning Inc., Corning, USA
Cell strainer (70 µm, sterile)	Corning Inc., Corning, USA
Chamber slides (16-well)	Nunc, Roskilde, Denmark
Cover slips	Paul Marienfeld GmbH & Co. KG, Lauda-Königshofen, Germany
CryoTube™ vials	Nunc, Roskilde, Denmark
Falcon tubes (15 ml, 50 ml)	Sarstedt, Nümbrecht, Germany
Filter tips (10 µl, 20 µl, 100 µl, 200 µl, 1000 µl)	Sarstedt, Nümbrecht, Germany
Glass bottles	Schott AG; Mainz, Germany
LS-MACS columns	Miltenyi Biotec, Bergish Gladbach, Germany
Microplate CellCarrier™-96 ultra	PerkinElmer, Inc., Waltham, USA
Neubauer chambers (0.1 mm x 0.0025 mm, 0.02 mm x 0.0025 mm)	Paul Marienfeld GmbH & Co. KG, Lauda-Königshofen, Germany
Nunc™ Lab-Tek™ II Chamber slides (16-well)	Thermo Fisher Scientific, Waltham, USA
Pipette tips (10 µl, 200 µl, 1000 µl)	Sarstedt, Nümbrecht, Germany
Reaction tubes (0.5 ml, 1.5 ml, 2 ml)	Sarstedt, Nümbrecht, Germany
Round-bottom flow cytometry tubes (5 ml)	Sarstedt, Nümbrecht, Germany
Safety-Multifly®-Needle	Sarstedt, Nümbrecht, Germany
SepMate™ PBMC isolation tubes (50 ml)	Stemcell, Vancouver, Canada
Serological pipettes (5 ml, 10 ml, 25 ml)	Sarstedt, Nümbrecht, Germany
S-Monovette 9 ml Heparin blood collection tubes	Sarstedt, Nümbrecht, Germany
Stericup® quick release vacuum driven filtration system	Merck KGaA, Darmstadt, Germany
Sterile filters 0.2 µm	Sarstedt, Nümbrecht, Germany
Strep-Tactin® TACS Agarose Column 0.3 ml	IBA Lifesciences GmbH, Göttingen Germany
Tubes (0.5 ml, 1.5 ml, 2 ml)	Eppendorf, Hamburg, Germany

2.3 Chemicals and reagents

Table 3: Chemicals and reagents

Name	Company
Ampuwa water	Fresenius, Graz, Austria
Basic Fibroblast growth factor	PeptoTech, Hamburg, Germany
BSA (Bovine serum albumin)	SERVA GmbH & Co. KG, Heidelberg, Germany
Collagenase D	Sigma-Aldrich, St. Luis, USA
DAPI (4',6-diamidino-2-phenylindole)	Thermo Fisher Scientific, Waltham, USA
Descosept	Dr. Schumacher, Malsfeld, Germany
Dexamethasone	Sigma-Aldrich, St. Luis, USA
Dimethylsulfoxide (DMSO)	Sigma-Aldrich, St. Luis, USA
Dispase II	Sigma-Aldrich, St. Luis, USA
DMEM (Dulbecco's Modified Eagle Medium) high glucose with stable glutamine, with 25 mM HEPES	Capricorn Scientific GmbH, Ebsdorfergrund, Germany
Dulbecco's Modified Eagle's Medium (DMEM)	PAN-Biotech, Aidenbach, Germany
Dulbecco's Phosphate-Buffered Saline (DPBS)	PAN-Biotech, Aidenbach, Germany
Ethylenediaminetetraacetic acid (EDTA)	Merck Millipore, Burlington, USA
Fetal calf serum (FCS)	Capricorn Scientific GmbH, Ebsdorfergrund, Germany
Ficoll-Paque™ Plus	GE Healthcare, Little Chalfont, England
Foxp3/Transcription Factor Staining Buffer Set	Thermo Fisher Scientific, Waltham, USA
Gentamycinsulfate	Lonza, Basel, Switzerland
Hepatocyte growth factor	PeptoTech, Hamburg, Germany
HEPES 4-(2-hydroxyethyl)-1-piperazineethanesulfonic acid	Sigma-Aldrich, St. Luis, USA
Human recombinant IFN- γ (hrIFN- γ)	PeptoTech, Hamburg, Germany
Human recombinant TNF- α (hrTNF- α)	PeptoTech, Hamburg, Germany
Human serum, Seraclot, Type AB	PAN-Biotech, Aidenbach, Germany
Iba CD4+ and CD8+ T cell isolation kit	IBA Lifesciences GmbH, Göttingen, Germany
Incidin liquid	Ecolab, Düsseldorf, Germany
L-glutamine	PAA Laboratories GmbH, Cölbe, Germany
live/dead fixable blue	Thermo Fisher Scientific, Waltham, USA
Medium-199	PAN-Biotech, Aidenbach, Germany
Paraformaldehyd(PFA)	Merck KGaA, Darmstadt, Germany

Materials

Penicillin/streptomycin solution	Capricorn Scientific GmbH, Ebsdorfergrund, Germany
Roti®-Mount FluorCare DAPI	Carl Roth GmbH & Co. KG, Karlsruhe
RPMI-1640 (Roswell Park Memorial Institute Medium 1640)	PAN-Biotech, Aidenbach, Germany
SpectroFlo® QC beads	Cytek Biosciences, Inc., Firemont, USA
Triton X-100	Sigma-Aldrich, St. Luis, USA
Trypan Blue	Sigma-Aldrich, St. Luis, USA
Trypsin-EDTA (0.05%)	PAA Laboratories GmbH, Cölbe, Germany
TrypsinLE™ Express	Thermo Fisher Scientific, Waltham, USA
UltraComp eBeads™	Thermo Fisher Scientific, Waltham, USA
Vitamin B12	Sigma-Aldrich, St. Luis, USA
Zinc sulfate	Sigma-Aldrich, St. Luis, USA
β-Mercapthoethanol	Invitrogen, Gibco, Auckland, New Zealand

2.4 Kits

Table 4: Kits

Name	Company
Agilent RNA 6000 Pico Kit	Agilent technologies, Santa Clara, USA
eBioscience™ Foxp3/Transcription Factor Staining Buffer Set	Thermo Fisher Scientific Inc., Waltham, USA
LEGENDplex™ Human (customized)	BioLegend, San Diego, USA
LEGENDplex™ Human (galectin-9)	BioLegend, San Diego, USA
Rneasy Maxi Kit	Qiagen, Hilden, Germany
IL-411 ELISA	R&D Systems, Inc., Minneapolis, USA
QIASeq Stranded mRNA selection kit (24)	Illumina, San Diego, USA
NextSeq 500/550 Mid output Kit v2.5 (150 cycles)	Illumina, San Diego, USA
QiaShredder	Qiagen, Hilden, Germany
CD4 Fab-TACS® Magnetic Microbead Starter Kit, human	IBA Lifesciences GmbH, Göttingen Germany
CD8 Fab-TACS® Magnetic Microbead Starter Kit, human	IBA Lifesciences GmbH, Göttingen Germany
Strep-Tactin® TACS Agarose Column 0.3 ml	IBA Lifesciences GmbH, Göttingen Germany

Materials

CD56 MicroBeads, human

Miltenyi Biotec, Bergish Gladbach,
Germany

2.5 Buffers, solutions and media

Table 5: Buffers and solutions

Name	Content
Fix/perm solution	1 part Fixation/Permeabilization concentrate 3 parts Fixation/Permeabilization diluent (Foxp3/Transcription Factor Staining Set)
Fixation solution	4% PFA in DPBS
Freezing medium	FCS (heat inactivated) 10 % DMSO
HCS blocking solution	DPBS 2 % BSA 0.1 % Triton-X-100
HCS permeabilization buffer	DPBS 0.1 %, Triton-X-100, 50 mM NH ₄ Cl
HCS wash buffer	DPBS 0.1 % Triton-X-100
PBS/FCS	DPBS, 2% (v/v) FCS, 2 mM EDTA
Perm/wash buffer	1 part 10 x Permeabilization buffer (Foxp3/Transcription Factor Staining Set) 9 parts ddH ₂ O
Permeabilisation buffer	0.1% Triton X-100 in DPBS

Table 6: Media

Name	Content
Differentiation medium (cell line LHCN-M2)	DMEM (high Glucose 25 mM HEPES)/M199 4:1, 2 % Horse Serum
Differentiation medium (primary muscle cells)	OptiMEM 20 % SMCGM
hcRPMI (human complete RPMI)	RPMI 1640 10 % Human AB serum 2 mM L-Glutamine 50 µg/ml Gentamicin 25 mM HEPES Buffer sterile filtered

Materials

Hg39 medium	RPMI 1640, 50 µg/ml Gentamicin, 2 mM L-Glutamine, 10 % FCS (heat inactivated)
Muscle cell culture medium	DMEM (high Glucose 25 mM HEPES)/M199 4:1, 15% FCS, 0.03 µg/ml Zinc sulfate, 1.4 µg/ml Vitamin B12, 0.055 µg/ml Dexamethasone 2.5 ng/ml HGF 10 ng/ml bFGF
Muscle cell medium	DMEM (high Glucose 25 mM HEPES), 10% FCS, 1% PenStrep
MyoUp ready-to use medium	Evercyte Cat: MHT-040
Skeletal muscle cell growth media (SMCGM)	Provitro Cat: 200 0602
Transport medium	DMEM (high Glucose 25 mM HEPES), 1% PenStrep

2.6 Antibodies

Table 7: Antibodies

Target	Fluorophore	Clone	Dilution	Company
PD-L1	BV421	29E.2A3	1:100	BioLegend, San Diego, USA
HVEM	PE	122	1:100	BioLegend, San Diego, USA
CD155	APC	SKIL4	1:200	BioLegend, San Diego, USA
HLA-DR	AF-700	L243	1:100	BioLegend, San Diego, USA
Galectin-9	PE-Cy7	9M1-3	1:100	BioLegend, San Diego, USA
PD-L2	AF-647	24F.10C12	1:100	BioLegend, San Diego, USA
CD40	Pacific blue	5C3	1:100	BioLegend, San Diego, USA
Nectin CD112	PerCP-Cy5.5	TX31	1:100	BioLegend, San Diego, USA
HLA a,b,c	APC-Cy7	W6/32	1:200	BioLegend, San Diego, USA
iNos	AlexaFluor488	CXNFT	1:100	Invitrogen/Thermo Fisher Scientific Inc., Waltham, USA
CD4	APC	OKT4	1:100	BioLegend, San Diego, USA
CD8	AF700	RPA-T8	1:200	BioLegend, San Diego, USA
CD45	FITC	HI30	1:1000	BioLegend, San Diego, USA
Rabbit α-Desmin serum	-	-	1:800	BNITM own production
Rabbit α- <i>T. cruzi</i> serum	-	-	1:1000	BNITM own production

Materials

Mouse α -Myosin Heavy Chain cell culture supernatant	-	MF-20	1:5	Developmental Studies Hybridoma Bank, Iowa City, USA
Goat α -Mouse IgG	AF488	-	1:200	Jackson ImmunoResearch Europe, Ely, UK
Goat α -Rabbit IgG	AF568	-	1:200, FACS 1:800	Invitrogen/Thermo Fisher Scientific Inc., Waltham, USA
Goat α -Mouse IgG	AF647	-	1:8000	Invitrogen/Thermo Fisher Scientific Inc., Waltham, USA

2.7 Software

Table 8: Software

Software	Purpose
Agilent 2100 Expert Software	RIN determination of RNA samples
AxioVision 4.7	Acquisition of fluorescence microscopic images
BD Accuri TM C6 Software	Acquisition of flow cytometry data
BioLegend LEGENplex Software (https://legendplex.qognit.com)	Analysis of LEGENDplex™ data
BioRender	Creation of figures
FlowJo V10.8	Analysis of flow cytometry data
Galaxy Server EU (https://usegalaxy.eu/)	Bioinformatical processing and visualisation of transcriptomic data
GraphPad Prism V10.0	Statistical analysis
Harmony® 4.6	Analysis of high throughput Immunofluorescence images
IDEP.96 (http://bioinformatics.sdstate.edu/idep96/)	Bioinformatical processing and visualisation of transcriptomic data
ImageJ with Fiji plugin	Composition of fluorescence microscopic images
Inkscape V1.1	Creation of figures
Mendeley Desktop V1.19.8	Citation
Microsoft Office 2019	Preparation of written documents, graphs and illustrations

Materials

Nanodrop 2000 Software	Determination of nucleic acid concentrations and purity
ShinyGO 0.77 (http://bioinformatics.sdstate.edu/go/)	GO-Term analysis of transcriptomic data
SpectralFlo® Software	Acquiring of flow cytometry data

2.8 Cells, Parasites and human donors

Table 9: Cell lines

Cell line	Description	Provider
LHCN-M2	human skeletal muscle stem cell line	Evercyte (CkHT-040-231-2)
86-HG-39	human glioblastoma cell line	BNITM, Hamburg, Germany

Table 10: Parasites

Parasites	Origin
<i>Trypanosoma cruzi</i> Brazil	Dr. Maria Fatala Chaben, Instituto Nacional de Parasitologia, Buenos Aires, Argentina

Table 11: Human muscle cell donors

Donor	Sex	Age
Donor D	female	55
Donor E	male	55
Donor F	male	57
Donor G	female	67
Donor H	female	68
Donor K	male	66
Donor L	female	58

Table 12: Human blood cell donors

Donor	Sex	Age
1	female	64
2	female	63
3	female	28
4	female	28

Table 13: Human Chagas Patients from Columbia

Donor Code	Sex	Age	AHA classification
W001	male	38	A
W005	female	45	B1
W008	female	23	A
W011	male	38	A
W012	female	31	B1
W016	female	14	A
W018	female	44	B1
W019	female	11	A
W021	male	20	A
W022	female	18	A
W024	male	22	A
W039	female	33	B1
W054	male	48	B1
W055	female	40	B1
W061	male	23	B1
W069	male	32	B2
W089	male	28	B1
W092	male	22	B1
W095	male	31	A
W096	female	50	B1
W098	female	56	C
W107	male	64	A
W108	female	60	B1
W113	male	29	B2
W143	female	32	A
W149	male	18	A
W156	female	24	A
W160	female	19	A
W178	male	25	A
W188	female	45	A
W195	male	22	A
W200	female	22	A

Materials

W202	female	43	A
W206	female	64	A
W216	female	45	A
W217	female	67	A
W227	male	50	B2
W230	female	35	A
W250	male	54	C
W251	female	59	B1
W289	male	24	A
W309	male	61	B2
W326	female	17	A
W327	female	19	A
W328	female	36	A
W331	female	25	A
W334	male	42	A
W336	male	15	A
W344	male	29	A
W347	male	13	A
W360	female	72	B2
W375	female	32	A
W388	male	68	B2
W389	female	69	B2
W405	male	32	A
W414	female	28	A
W418	female	35	A
W429	male	57	B2
W432	female	48	B1
W437	female	65	B1
W452	female	55	B1
W453	male	68	B2

3. Methods

3.1 General remarks

All cell culture procedures and tissue preparations were carried out under sterile conditions using a laminar airflow hood. Experiments involving the parasite *T. cruzi* were carried out in an S3 laboratory. Cells were cultivated at 37°C and 5% CO₂ in a Hera Cell 150 incubator. Muscle cells were centrifuged at 220 g at room temperature (RT) for 5 min unless otherwise stated. Washing of cells refers to the addition of medium or buffer, centrifugation and removal of the medium or buffer.

3.2 Cell line LHCN-M2

The muscle cell line LHCN-M2 was purchased from Evercyte GmbH and shipped frozen on dry ice. Upon arrival, the cells were thawed and resuspended in the company's muscle cell culture medium. The cells were centrifuged at 220 g for 10 min, and the supernatant was removed. T75 flasks were incubated for four hours (h) with 0.1 % gelatine in an incubator to allow better attachment of the muscle cells. The cells were resuspended in MyoUp ready-to-use medium provided by the company and seeded in a gelatine-coated T75 flask. After 2-3 days, the cells were detached using 20 µl/cm² trypsin solution and counted using a Neubauer cell chamber. To maintain a stem cell-like phenotype, the cells had to be seeded at a low cell density (210.000 cells per T175 flask) because a cell density of over 60 % would induce terminal differentiation of the cells.

3.3 Storage of cells

For long-term storage, cells were harvested, washed and resuspended in cold freezing medium at a concentration of $2 - 10 \times 10^5$ cells/ml. 1 ml of the obtained cell suspension was transferred into a pre-cooled cryotube and slowly chilled at -80°C for 24 h using a Mr Frosty™ freezing container. The tubes were transferred to liquid nitrogen and stored until needed. To restart the cell culture, the frozen cell suspension was thawed in a water bath at 37°C. The cells were transferred to 10 ml muscle cell medium, mixed gently washed once to remove the DMSO and seeded in the respective medium.

3.4 Determination of cell counts

An aliquot of the cell suspensions was diluted 1 to 1 in Trypan Blue solution (1:20 dilution in PBS) to assess the amount of human cells inside a cell suspension. Trypan Blue is a dye used to discriminate between living and dead cells. 10 μ l of the cell solution was pipetted on a Neubauer counting chamber with a height of 0.1 mm. Unstained, living cells in 4 large squares were counted, and the cell concentration of the solution was determined using the following formula:

$$\frac{\text{cell count}}{4} * \text{dilution factor} * 10^4 = \text{cells/ml}$$

To determine *T. cruzi* Brazil trypomastigotes inside of a solution, 5 μ l of the parasite solution was pipetted on a Neubauer chamber with a height of 0.02 mm. Motile trypomastigotes were counted in 4 large squares. The same formula was used to determine the cell count. However, a chamber factor of 5 had to be added to account for the different sizes of the chambers.

$$\frac{\text{cell count}}{4} * \text{dilution factor} * 10^4 * 5 = \text{cells/ml}$$

3.5 Isolation of muscle stem cells from human tissue

Muscle tissue samples from the *gluteus maximus* from patients undergoing hip replacement surgeries were obtained at the Elbe Clinique in Buxtehude. The samples were transported to the Bernhard Nocht Institute for Tropical Medicine (BNITM) in Hamburg at RT in a transport medium (see material section for specifications). Upon arrival, the medium was removed, the tissue was weighed and cut into small pieces using sterile scissors, and all visible connective tissue was removed. 3.5 ml of the Collagenase D solution (5 mg/ml) and Dispase II solution (1.2 U/ml) was added for each gram of muscle tissue, as well as 500 μ l of Trypsin/EDTA (0.05%) solution. The muscle tissue with the digestive enzymes was incubated for 45 min at 37°C in a water bath and shaken frequently. Afterwards, the mixture was pipetted through a Pasteur pipette to dismember the tissue further. This process was repeated until the cell mixture easily passed through the pipette and all tissue was visibly dissolved. The digestive enzymes were washed away by centrifugation at 234 g at RT for 5 min. The cells were suspended in 3 ml skeletal muscle cell growth media (SMCGM) from pro-vitro, transferred into a T-25 flask, and incubated for seven days in an incubator (37°C, 5% CO₂). After seven days, muscle stem cells

were attached to the surface of the flask, and 2 ml medium SMCGM was added. Unbound cells were detached by removal of the cell culture medium, washing with PBS and addition of SMCGM.

3.6 Magnetic cell sorting (MACS) using CD56 Micro Beads (Miltenyi)

To detach the muscle cells without losing the expression of CD56, TrypsinLE™ solution from Thermofisher was used ($20 \mu\text{l}/\text{cm}^2$) and subsequent incubation in the incubator for 10 min followed. The detached cells were suspended in medium and washed once. Afterwards, the cells were washed once with MACS buffer, and $20 \mu\text{l}$ CD56 microbeads were added for every 10 million cells and incubated at 4°C for 15 min. 2 ml cold buffer was added to the cell suspension. The cells were centrifuged, the supernatant discarded, and 2 ml fresh buffer was added. The LS MACS columns were placed into a magnet, equilibrated with 3 ml buffer, and the cell suspension was added. The supernatant contained the CD56 negative cells (contaminating fibroblasts) and the CD56 positive satellite cells bound to the column. The column was washed three times with 3 ml MACS buffer. The columns were removed from the magnet, and the CD56 positive cells were flushed out with a pistol in 5 ml MACS buffer. Cells were washed once, resuspended, and cultivated in SMCGM.

3.7 Cell culture of primary muscle stem cells

Once the primary cells were isolated, they could be kept in culture for several passages, depending on the donor. The cells were cultured in SMCGM and seeded at a cell density of $1800 \text{ cells}/\text{cm}^2$ of the cell flask to keep their stem cell character. The flasks were checked daily, and the cells were split every 2-3 days as necessary.

3.8 Differentiation of primary muscle cells and the cell line LHCN-M2

To differentiate the muscle cells, they were seeded at high densities and incubated until the cells reached confluency. Cells were cultured, detached using trypsin and counted. For primary skeletal muscle cells, cells were seeded at a density of approximately $52,000 \text{ cells}/\text{cm}^2$ and the cell line at approximately $46,875 \text{ cells}/\text{cm}^2$. The cells were cultivated for 1-3 days to

reach confluency. Consequently, a differentiation medium was added. OptiMem with 20 % SMCGM was added for primary muscle cells, and for the cell line, LHCN-M2 muscle cell differentiation medium was added. The medium was changed every 2-3 days, and the differentiation process was finished after 10 days.

3.9 Cultivation of *T. cruzi* parasites in vitro

To propagate the obligate, intracellular parasite *Trypanosoma cruzi* Brazil, host cells were needed. The human glioblastoma cell line 86-HG-39 was used. T175 flasks were used to culture the cells until 60 % confluency was reached. 2 to 6 ml of cell culture supernatant from a previous 7 days infected T175 flask was used to infect the new flask.

3.10 Isolation of *T. cruzi* parasites

The supernatant of T175 flasks of 86-HG-39 infected with *T. cruzi* Brazil for 7 days, containing the released trypomastigotes, was harvested and transferred to 50 ml falcon tubes. The falcon tubes were centrifuged at 300 g for 5 min to remove the remaining 86-HG-39 cells. The supernatant was transferred to a new 50 ml falcon tube and centrifuged at 2670 g for 15 min to pellet the *T. cruzi* trypomastigotes. The supernatant was removed, and the pellet was resuspended in 2-5 ml muscle cell medium. Alive parasites were counted using a Neubauer cell chamber. Trypanosomes were diluted as required in muscle cell medium.

3.11 Infection and stimulation of muscle cells

Muscle cells were seeded and differentiated in the cell culture plates required for the experiment. *T. cruzi* trypomastigotes were obtained as previously described and diluted in muscle cell medium at the required concentration. Muscle cells were infected at a multiplicity of infection (MOI) of 5:1 (trypomastigotes: muscle cells) unless otherwise stated. The differentiation medium was removed, and muscle cell medium with the trypomastigotes and/or with 100 IU/ml IFN- γ and/or 100 IU/ml TNF- α was added. After 24 h, the medium was removed, cells were washed three times with DPBS, and fresh muscle cell medium with or without cytokines was added.

3.12 Immunofluorescence

Immunofluorescence stainings were performed to determine the purity of the primary human muscle stem cells after the MACS isolation, to investigate their differentiation status and to determine the infection rate of *T. cruzi* Brazil. 16-well glass chamber slides were coated for 4 h with 0.1 % gelatine at 37°C, and 14,000 muscle stem cells were seeded per well. Cells were incubated for 24 h to let the cells get attached to the glass slides. Depending on the experiment, the cells were either used directly or differentiated for 10 days and infected with *T. cruzi* Brazil, as described before. The cell culture medium was removed, and the cells were washed once with DPBS, fixed with 4% PFA solution for 20 min and washed three times with DPBS. Consequently, the cells were permeabilised with 0.1% Triton X-100 solution for 5 min, blocked for 1 h in 3 % BSA solution, and incubated with the respective primary antibodies for 1.5 h at 37°C. Next, the cells were washed three times with DPBS and secondary antibodies diluted in 0.1 % BSA solution were added. The cells were washed again with DPBS, and Roti®-Mount FluorCare DAPI embedding medium was added. Glass slides were used to cover the cells. The cover slides were stored at 4°C until the microscopic analysis at the Axio Imager M.1 fluorescence microscope. Fluorescent images were taken using the DAPI channel to detect nuclei from muscle cells and *T. cruzi*, the TexasRed channel for visualisation of anti-*T. cruzi*-Alexa568-stained parasites and Desmin-Alexa568-stained muscle cell cytoplasm and the GFP channel for the AF488-stained myosin heavy stained cytoplasm of differentiated muscle cells.

Primary antibodies

Rabbit α -Desmin 1:800 in 1% BSA/DPBS

Rabbit α -*T. cruzi* Serum 1:1000 in 1% BSA/DPBS

Mouse α -Myosin Heavy Chain 1:5 in 1% BSA/DPBS

Secondary antibodies

α -Mouse AF488 1:200 in 1% BSA/DPBS

α -Rabbit AF568 1:200 in 1% BSA/DPBS

3.13 Transcriptomic analysis

A transcriptomic analysis should investigate the changes elicited by stimulation of primary human muscle cells with IFN- γ stimulation and infection with *T. cruzi* Brazil. While, the muscle cell line LHCN-M2 was analysed to compare the differences between the cell line and the primary cells. Therefore, 500,000 muscle cells were plated into a 6-well plate and differentiated for 10 days in their respective differentiation medium. The cells were either not infected and stimulated (mock control) stimulated with 100 IU/ml IFN- γ , infected with *T. cruzi* Brazil with a multiplicity of infection of 5:1 or infected with 100 IU/ml IFN- γ and infected with *T. cruzi* Brazil (MOI 5:1) in muscle cell medium. After 24 h, the medium was removed, the cells were washed three times to remove the remaining Trypanosomes and the IFN- γ , and new muscle medium was added. After 48 h, the cells were washed once with DPBS and the DPBS was carefully and thoroughly removed. 350 μ l RLT buffer with 1 % β -Mercaptoethanol was added, and the cells were detached by pipetting the solution up and down, and the cells were shredded using Qiagen Shredder columns. The cells were stored in the RLT buffer at -20°C until the RNA isolation.

3.14 RNA Isolation

The Qiagen's RNeasy Mini Kit was used to purify the RNA from the samples according to the manufacturer's instructions. In brief, the cells stored in RLT buffer were quickly thawed in a water bath and mixed with 350 μ l Ethanol. The suspension was transferred to silica membrane spin columns (RNeasy mini column) to purify the ribonucleic acid (RNA). The column was centrifuged for 20 s at 13000 rpm for every wash step. The RNA bound to the column and was washed with RW1 buffer. Next, a DNA digestion on the column with DNASE I (27 Kunitz units) for 15 min was performed. After a subsequent wash with buffer RW1, 500 μ l RPE2 buffer was used twice to wash the column. A centrifugation step for 2 min without adding a solution followed to remove all remaining buffer. The RNA was eluted in 25 μ l RNase-free water, and the concentration was measured at the Nanodrop 2000 microvolume spectrophotometer. The RNA was stored at -80°C until further use.

3.15 Determination of RNA Integrity Number (RIN)

To determine the quality of the isolated RNA, RIN values were determined using the Bioanalyzer System Agilent 2100. Using this method, it is possible to see how much the RNA has degraded. The RIN algorithm compares the 28S and 18S RNA of the sample by using capillary gel electrophoreses. RNA from the differently treated samples were prepared using the Agilent RNA 6000 Nano Kit according to the manufacturer's protocol. In short, the RNA samples were mixed with an interacting fluorescent dye, loaded onto an RNA Nano Chip and combined with a provided RNA ladder. The Agilent 2100 Expert Software evaluates the pictures of the gel electrophoreses and calculates RIN values between 1 and 10. The values correspond to the integrity of the RNA, with 10 being the highest, indicating no degradation of the RNA. All samples had a RIN Value of 9.2 or higher (a value of 8 indicates high quality of the RNA and was necessary to sequence the samples).

3.16 RNA sequencing library preparation and next-generation sequencing (NGS)

Dr. Dániel Cadar and Heike Baum performed the following steps at the BNITM NGS Core Facility. Briefly, the QIAseq Stranded mRNA Select Kit from Qiagen was used to enrich mRNA from the previously purified RNA based on its polyadenylation. The kit was also used to prepare the RNAseq library for NGS. Sequencing was performed using Illumina's NextSeq 500/550 Mid Output Kit and Illumina's NextSeq 550 system.

3.17 Bioinformatical analysis of the samples

The Galaxy EU server (<https://usegalaxy.eu/>) was used to perform bioinformatical analysis of the sequences obtained from the NGS. First, a quality analysis was performed using FastQC (version 0.11.9) ¹⁵⁴. This tool determines the quality of raw sequencing data by providing a quality score for each position of the reads. If degradation of the RNA or other problems occurs during the sequencing, poor quality scores can typically be found towards the ends of the read. However, the sequenced samples obtained here received all high scores (mean quality between 28 and 34). Next, the adapter sequences from the NGS were trimmed using the tool Trimmomatic (Galaxy Version 0.38.1) ¹⁵⁵. If a low quality of the samples is detected, the ends of the reads can be cut off to improve the quality of the reads and ensure correct

alignment. Illumina adapter sequences were cut using the additional IlluminaClip “TruSeq3 (pair-ended for MiSeq and HiSeq)” option. Next, HISAT2 aligned the reads to the genome of choice ¹⁵⁶. The “Human Dec. 2013 (GRCh38/hg38)” was used to map the reads from the skeletal muscle cells. For the reads of *T. cruzi* Brazil, the genome of *T. cruzi* Brenner was loaded into Galaxy and used as a reference genome ¹⁵⁷. The tool featureCounts was used to transform the aligned reads into a read count table ¹⁵⁸. The input data had read pairs, and these were counted as individual reads. Next, an annotation file was created using the tool AnnoateMyIDs. The table created by featureCounts only included ENTREZ IDs, and this program adds the ENSEMBL ID, the gene name and the gene symbol to the ENTREZ ID to allow the comparison of gene names from the aligned reads. To perform differential gene expression between the different treatment groups, (*T. cruzi* infected – mock control, IFN- γ stimulated – mock control, *T. cruzi* infected + IFN- γ stimulated – mock control and IFN- γ stimulated – *T. cruzi* infected + IFN- γ stimulated) the tool limma-voom was used ¹⁵⁹⁻¹⁶². A minimum of 1 count per million counts for the 5 replicates was selected to exclude potential bias from low expressed genes. The p-value was adjusted using the Benjamini and Hochberg method ¹⁶³.

3.18 Visualization of NGS Data

The online tool iDEP.96 (<http://bioinformatics.sdstate.edu/idep96/>) was used to calculate the heatmap, comparing the gene expression of genes of the donors and the cell line ¹⁶⁴. Here, the reads count table of all samples created with Galaxy were combined and uploaded. The 2000 highest expressed genes were plotted and clustered using a minimum CPM of 1 and the algorithm EdgeR. Moreover, a k-means diagram was calculated using the 2000 highest expressed genes. This diagram visually represents the clustering of gene expression patterns into 'k' distinct groups, in this case, three, based on their similarities and visualises the gene ontology term (GO-term) assigned to them. A principal component analysis (PCA) of the samples of the human donors and the cell line was performed. This analysis reduces the dimensionality of data by transforming it into a new set of orthogonal variables called principal components. A Venn diagram was calculated using a false discovery rate (FDR) cut-off of 0.1 and minimum log₂ fold change of 2. The FDR is a measurement of statistical significance, and the log₂ fold change indicates how highly a gene's expression is up or downregulated. A

logarithmic transformation is performed to compare the downregulation of genes. This means the gene expression has quadruplet for a log₂ fold change of 2. The Venn diagram visualises the identical and distinct genes upregulated between different treatment groups. GO-Term analysis was done using the online tool ShinyGO 0.77 (<http://bioinformatics.sdstate.edu/go/>). In Excel, differentially expressed genes were sorted for statistically significant upregulated genes (adjusted p-value < 0.05 and a minimum log fold change of 2). These genes were uploaded to the website. An FDR cut-off of 0.05 and a minimum of 2 genes per pathway were selected. The heatmap with the differentially expressed genes was created using GraphPad Prism V10. The 50 highest significantly different expressed genes for the condition of *T. cruzi* infected and IFN- γ treated muscle cells were selected and compared to the *T. cruzi* infected muscle cells and IFN- γ treated muscle cells.

3.19 Flow cytometric analysis of skeletal muscle cells

Flow cytometric analysis characterises cells by their granularity and size using a sideward scatter (SSC) and forward scatter (FSC). Additionally, cells can be stained with fluorescent-labelled antibodies to obtain information about the proteins they express on the cell surface or intracellularly. Different fluorochromes are used to investigate multiple targets simultaneously. Skeletal muscle cells were seeded in 12 well plates, differentiated for 10 days and infected and stimulated as described previously. Adherent muscle cells had to be detached from the cell culture plate using the enzyme TrypsinLE™, which allows the detachment of the cells and limited enzymatic digestion of extracellular receptors. Cells were washed once with DPBS, TrypsinLE™ was added and incubated for 15 min at 37°C in an incubator. Muscle cell medium was added, and the detached cells were mixed carefully and transferred into a 96-well round bottom plate for the staining. The cells were centrifuged at 220 g for 5 min at 4°C, the medium was removed, and DPBS was added. After another centrifugation step, DPBS was removed, and the live/dead dye fixable blue was added (1:1000 dilution in DPBS). After a 15 min incubation step at 4°C, PBS/FCS was added, and the cells were centrifuged. The master mix containing all extracellular antibodies diluted in PBS/FCS was added and incubated for 30 min at 4°C. The cells were washed 3 times with PBS/FCS and fixed and permeabilised using 150 μ l fix/perm solution of the Foxp3 staining kit (eBioscience™) per well for 20 min in the dark at 4°C. Afterwards, the cells were washed twice with fix/perm

solution. The cells were either resuspended in 200 μ l fix/perm solution, and the plate was stored at 4°C in the dark until needed or directly stained with the intracellular antibody mixture. The cells were stained for 30 min at 4°C and washed twice with 200 μ l perm/wash. If primary antibodies were used, another staining step was performed using the secondary antibody for 30 min at 4°C. The cells were washed twice with 200 μ l perm/wash and resuspended in 120 μ l perm/wash. The antibodies used for the cell staining are listed in Table 7. The samples were measured at the Cytex Aurora.

3.20 High throughput immunofluorescence analysis using the OperaPhenix™

The high-throughput immunofluorescence system Opera Phenix® was used to determine the infection rate of *T. cruzi*-infected muscle cells. Muscle cells were seeded and differentiated in black 96-well CellCarrier™ plates and infected with *T. cruzi* Brazil (MOI of 5:1) and stimulated with IFN- γ (100 IU/ml) and TNF- α (100 IU/ml) as previously described. After 24 h, 48 h and 72 h, the wells were carefully washed twice with DPBS and fixed for 20 min with 100 μ l of 4 % PFA at RT. Afterwards, the cells were washed with DPBS thrice and stored at 4°C in 200 μ l DPBS. To perform the immunofluorescence staining, 150 μ l HCS wash buffer was added to the cells and incubated for 5 min on a shaker (300 rpm). All subsequent washing and incubation steps were performed on a shaker. 150 μ l permeabilization buffer was added and incubated for 15 min to permeabilise the cells. Free binding sites were blocked with 150 μ l of HCS blocking solution for 30 min. Intracellular *T. cruzi* amastigotes were stained by adding 60 μ l mouse α -*T. cruzi* serum diluted 1:2000 in blocking solution for 90 min. Unbound antibodies were washed away by adding 150 μ l wash buffer and incubation for 5 min. This step was performed 3 times. Next, the secondary α -mouse IgG AF647 was diluted 1:8000 in blocking solution with 0.01 mg/ml DAPI, incubated for 45 min, and covered by an aluminium foil to protect the fluorochrome from light. The cells were washed twice with 150 μ l wash buffer and once with 150 μ l of DPBS. 200 μ l DPBS was added, and the plate was stored at 4°C until it was measured at the Opera Phenix® confocal high throughput microscope using a 10 \times water objective lens. The microscope Harmony® software divided each well into multiple fields; 15 fields were randomly selected, and an image was taken at the same spot for each well. Fluorescent images were recorded using the DAPI channel (excitation: 405 nm/emission 435–480 nm) for the detection of muscle cells and *T. cruzi* nuclei and the Alexa647 channel

(excitation: 640 nm/emission 650–760 nm) for the visualisation of α -*T. cruzi*-stained parasites and muscle cell cytoplasm. For every field in a well, a z-stack was setup. Image analysis was performed using the Harmony® software. The DAPI staining identified muscle cell nuclei, and *T. cruzi* parasites were identified by a high AF647 signal and a DAPI-stained nucleus spot. The ratio of muscle cell nuclei to *T. cruzi* amastigotes was calculated.

3.21 Flow cytometric bead-based immunoassay LEGENDplex™

LEGENDplex™ bead-based immunoassays (BioLegend) were used to analyse soluble factors released by skeletal muscle cells after infection with *T. cruzi* and stimulation with the pro-inflammatory cytokines IFN- γ and TNF- α as indicated, using a customised human 13-Plex including CCL19, IL-8, galectin-9, IFN- γ , IL-10, IL-15, IL-1 β , IL-4, IL-6, PD-L1, PD-L2, TGF- β 1, and TNF- α . Cell culture supernatants of the muscle cells were frozen at -20°C and thawed upon performance of the LEGENDplex™ assay. The supernatants were centrifuged thrice at 2670 g for 15 min and transferred into a new plate to eliminate cell debris and Trypanosomes.

Additionally, human serum samples from Chagas patients from a cohort in Columbia were analysed using a galectin-9 monoplex (BioLegend). The serum was stored at -80°C, thawed and diluted with assay diluent. For this assay, MatrixB was mixed to the standard to account for proteins present in the serum which might interfere with the assay.

Afterwards, the samples were processed according to the manufacturer's instructions, with the volume of reagents and samples being reduced to 1/3 of the original volume. In brief, the analytes of interest bound to beads coated with the appropriate antibodies. To distinguish between the different analytes, the beads differ in size and intensity of the bound fluorochrome for each cytokine. The beads are detected using a second antibody linked to biotin. The fluorescence intensity can determine the amount of analyte in the cell culture supernatant by adding a streptavidin-bound fluorochrome. The muscle cell supernatant samples were measured using the BD LSRFortessa™ and the serum samples from the Columbia cohort at the Accuri C6™. The concentration of the respective analytes was calculated using a standard dilution series for each analyte using the web-based LEGENDplex™ software.

3.22 Co-culture of T cells with the muscle cell line LHCN-M2

A high amount of muscle cells was needed for the co-culture with human T cells. Therefore, the muscle cell line LHCN-M2 was used to replace primary human skeletal muscle cells. This cell line is produced by the transduction of satellite cells (muscle stem cells) from a *pectoralis major* muscle tissue (male, 41 years) with retroviral vectors containing the *CDK-4* and *hTERT* gene produced by the company Evercyte.

For the assay, muscle cells were infected and stimulated with IFN- γ (100 IU/ml) for 24 h, as described previously. Blood was drawn from healthy donors using an S-Monovette[®] with Lithium Heparin, and peripheral blood mononuclear cells (PBMCs) were isolated using SepMate[™] PBMC Isolation Tubes. The blood was transferred to 50 ml falcon tubes and diluted 1:1 with DPBS. 15 ml Ficoll-Paque[™] Plus was added into the SepMate[™] tubes, and the diluted blood was added carefully. The tubes were centrifuged at 1200 g for 15 min at RT. Using density centrifugation, erythrocytes and granulocytes accumulated below the membrane and PBMCs and plasma could be transferred to a new 50 ml tube with a pipette. 15 ml human complete RPMI (hcRPMI) was added, and the PBMCs were pelleted at 650 g for 15 min at RT. 10 ml hcRPMI was added, and the PBMCs were filtered through a sterile 30 μ m filter and counted. PBMCs were diluted to a concentration of $1 - 5 \times 10^7$ cells per ml. A positive selection of CD4⁺ and CD8⁺ T cells followed using the human CD8 and CD4 Fab-TACS[™] Agarose Column Kit and the 0.3 ml Strep-Tactin[®] TACS Agarose Columns. The cells were purified following the manufacturer's protocol. The columns were prepared by a wash with 3 ml CL buffer and a subsequent incubation for 2 min with 400 μ l Fab-Strep solution (either coupled to CD8 or CD4 antibodies). The PBMCs were added to the columns, and specific cells were retained in the column by binding to antibodies coupled to a Strep-tag[®]II. The cells were washed three times with 3 ml buffer CL. A biotin solution was used to disrupt the binding of the cells, the strep tag and the column, resulting in the elution of cells without any antibodies bound to them. The cells were first purified for CD8⁺ T cells, and afterwards, the remaining cells in the flow-through were used to purify CD4⁺ T cells. Eluted cells were washed with 10 ml hcRPMI, centrifuged at 650 g for 10 min and counted. A staining of the cells was performed with the proliferation dye eFluor450. T cells were washed once with cold DPBS, centrifuged at 650 g for 10 min and resuspended in 750 μ l DPBS. A 20 μ M dilution of the dye eFluore450 was added to the cells while mixing. After a 10 min incubation at 37°C in an incubator, 10 ml ice-cold medium was added to stop the staining. The cells were centrifuged at 650 g for 10 min and counted.

Subsequently, the cells were resuspended in 5 ml medium containing α CD3/ α CD28-covered beads (ratio of 1:1 to the cells) and 30 IU/ml IL-2. The cells were transferred into a T25 flask and incubated for 18 h. To evaluate the efficacy of the purification process, an aliquot of the cells before and after the purification steps was taken with antibodies against CD4 and CD8 as previously described. The cells were analysed using the spectral flow cytometer Aurora. In all purifications performed for the assays, over 90 % of the cells were positive for either CD4 or CD8 after the respective isolation.

On the following day, the cells were transferred into a 15 ml falcon tube and mixed extensively with a pipette to disrupt the binding of beads to cells. Next, the magnetic α CD3/ α CD28-covered beads were removed using a Stemcell magnet. To remove the IL-2-containing medium, the cells were centrifuged at 650 g for 10 min. The cells were resuspended in fresh hRPMI and incubated with blocking antibodies, α -PD-1 (10 μ g/ml), α -TIM-3 (5 μ g/ml), or with an IgG control antibody (5 μ g/ml) and incubated for a minimum of 30 min. These antibodies prevent receptor activation by obstructing their ligand interactions without triggering them.

In the meantime, the differentiated and infected or IFN- γ stimulated LHCN-M2 muscle cells were washed thoroughly three times with DPBS to remove remaining trypomastigotes and IFN- γ . T cells with their respective antibodies were added. As a control, T cells were incubated without muscle cells but with the addition of α CD3/ α CD28-covered beads. After three days of co-culture, T cells were removed from the muscle cells using ice-cold DPBS, stained for alive cells using the live/dead dye fixable blue and stained for CD45, CD4 and CD8 as previously described. The proliferation was analysed by flow cytometry using the proliferation dye eFluore450. Proliferated cells divide the dye in each proliferation step, leading to a reduced fluorescent intensity in the fluochrome channel. The data was analysed using FLOWJo v10.9.

3.23 ELISA (enzyme-linked immunosorbent assay)

The DuoSet ELISA for human IL-4I1 from R&D Systems was used to determine the concentration of the enzyme Interleukin-4 induced 1 (IL-4I1) in the cell culture supernatant of infected and stimulated muscle cells. This ELISA worked on the principle of a sandwich ELISA, and it was performed according to the manufacturer's protocol. In brief, a capture antibody against IL-4I1 was coated to a high-binding 96-well plate overnight at RT. The antibody was

washed away, and free binding sites were blocked with assay diluent for 1 h at RT. Afterwards, the supernatants of the muscle cells and a serially diluted standard were added and incubated at RT for 2 h. The plate was washed again, and the detection antibody conjugated to biotin was added and incubated for 2 h at RT. Horseradish peroxidase (HRP) conjugated to streptavidin was added, and non-binding HRP was washed away after 20 min at RT. The substrate solution containing 3,3',5,5'-Tetramethylbenzidine (TMB) was added. After 20 min, the enzyme reaction of the HRP was stopped by the addition of 2M H₂SO₄. Optical density (OD) was measured at 450 nm in a microplate reader. A baseline correction was performed at 540 nm. The OD is proportional to the amount of IL-4I1. The IL-4I1 concentrations in the tested samples were calculated based on the standard series.

3.24 Statistical analysis

GraphPad Prism 10 software was used to perform all statistical analyses. The Shapiro-Wilk test was used to test for the normal distribution of the sample groups. If only two groups were compared to each other and were normally distributed, statistically significant differences were tested with a paired t-test and, for non-normal distributed samples, the Wilcoxon test. The RM one-way ANOVA was used to test for statistically significant differences for normal distributed, paired samples of more than two sample groups. The Friedman test was used for non-normal distributed, paired samples. P-values were indicated as * $p \leq 0.05$; ** $p \leq 0.01$; *** $p \leq 0.001$; **** $p \leq 0.0001$. Only statistically significant differences between groups were labelled.

4. Results

T. cruzi is an obligate intracellular parasite which needs host cells to reproduce. Although the parasite can infect all nucleated cells, muscle cells in particular have been shown to be infected throughout the chronic phase of the disease in mice⁶. This study aimed to determine why the muscle is a favourable site for *T. cruzi* persistence, particularly investigating the involvement of skeletal muscle cells, which are heavily targeted by the *T. cruzi* Brazil strain. In the chronic phase of the disease, CD8⁺ T cells play a major role in eliminating the parasites. Therefore, the potential influence of muscle cells on CD8⁺ T cells was investigated. To this end, a co-culture with muscle cells and allogenic donors was established. In addition, the impact of the pro-inflammatory environment, which is present during the chronic phase of the disease, was investigated using flow cytometry, high throughput immunofluorescence, ELISAs and bead-based immunoassays.

4.1 Establishment of the muscle cell culture and infection with *T. cruzi*

To study the involvement of muscle cells during *T. cruzi* infection *in vitro*, human muscle stem cells, known as satellite cells, were isolated from the *gluteus maximus* muscle. Different protocols, including fluorescent-activated cell sorting of muscle stem cells, were attempted until a protocol that yielded high quantities and purity of muscle stem cells was established¹⁶⁵. The procedure is presented in Figure 3A. The muscle tissue was digested and the stem cells were purified using positive selection of the neural cell adhesion molecule 1 (CD56). The culture was enriched for muscle stem cells until no contaminating fibroblasts could be found. Cells were identified by immunofluorescence staining using the staining of the nucleus with DAPI (in blue) and muscle cells were distinguished from fibroblasts with the intracellular muscle-specific cytoskeletal protein Desmin (red) in Figure 3B. In the beginning, a high number of contaminating fibroblasts were identified, so the purification steps were repeated until only Desmin-positive cells were visible in the immunofluorescence analysis. Once successful isolation was confirmed, the cells were seeded at a very high density and a differentiation medium which lacked the growth factors necessary for the stem cells was added. During this 10-day differentiation process, muscle cells fused to form large multinucleated cells and began expressing the muscle-specific cytoskeletal protein myosin heavy chain (shown in green).

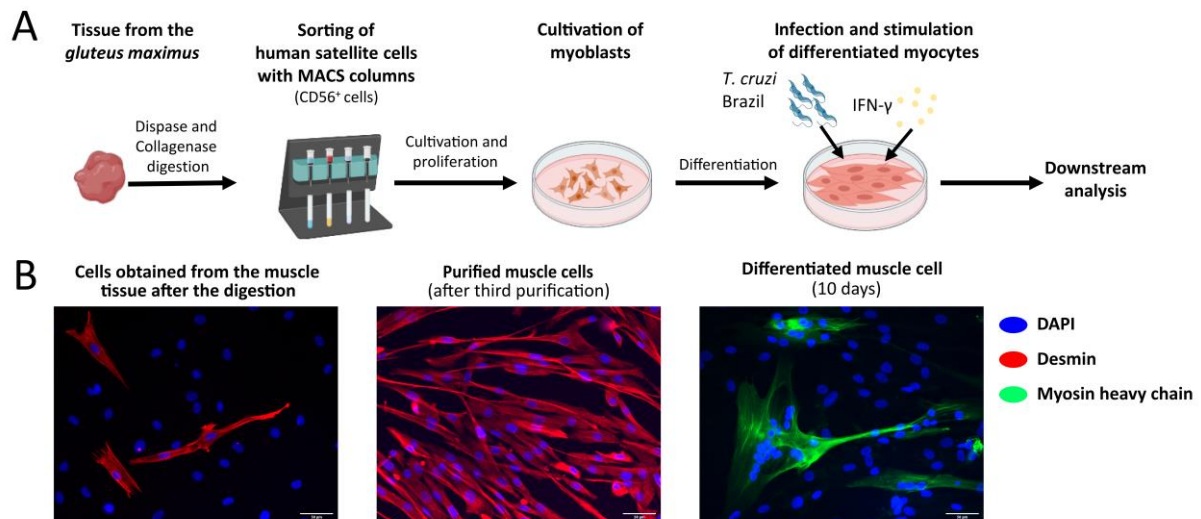


Figure 3: Isolation of muscle stem cells (satellite cells) from tissue samples of the *gluteus maximus* of human donors. A) The muscle tissue was digested. Subsequently, the muscle stem cells were purified by positive selection using the extracellular muscle stem cell marker CD56. B) The purification grade was assessed using immunofluorescence staining of the intracellular muscle marker Desmin (red) and the staining of the nucleus using DAPI (blue). The purification process was repeated until no contaminating fibroblasts were visible in the immunofluorescence. The purified muscle cells were seeded at a high density and differentiated for ten days using a differentiation medium. The differentiation state was assessed by immunofluorescence staining of myosin heavy chain (green), the marker for terminally differentiated muscle cells. Scale: 50 μ m.

Once the successful purification and differentiation process was established, the muscle cells were subjected to *T. cruzi* infection. Various multiplicities of infection (MOI) were tested to determine the infection potential of the parasite. The cells were infected with the parasites for 24 h, then the remaining extracellular parasites were washed away and the muscle cells were fixed 48 hours post-infection (hpi). Already a low MOI of 0.3:1 (*T. cruzi* to muscle cell ratio) resulted in infection (Figure 4). However, with higher MOIs, the amounts of *T. cruzi*-positive cells and the number of parasites inside the muscle cell increased. Higher infection rates of 3:1 and 5:1 resulted in better parasite development inside the muscle cell at 48 hpi, especially at a MOI of 5:1, which resulted in the whole cell being filled with parasites in some cases. A MOI of 5:1 was chosen for subsequent experiments as it yielded the most consistent infection rate.

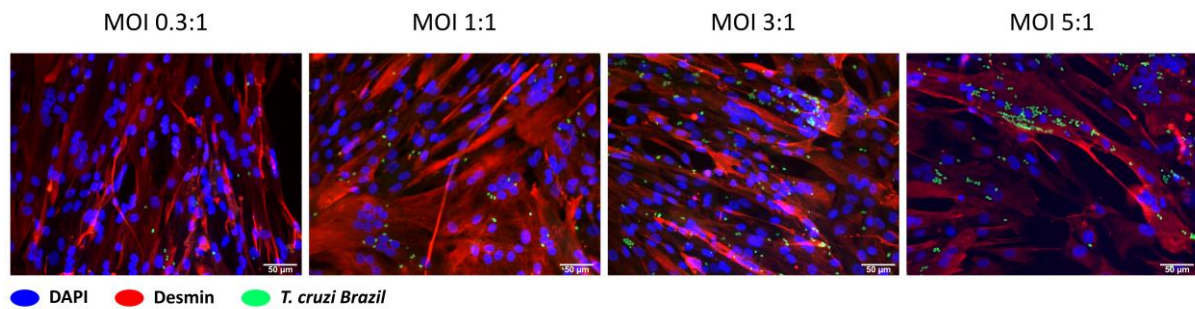


Figure 4: Infection of primary human muscle cells with *T. cruzi* Brazil at 48 hpi reveals susceptibility to low multiplicities of infection (MOIs). Primary human muscle cells were seeded and allowed to reach confluency prior to a 10-day differentiation process. Subsequently, the muscle cells were infected with *T. cruzi* at varying MOIs of 0.3:1, 1:1, 3:1 and 5:1. The infection rate was assessed through immunofluorescence staining using specific antibodies. The intracellular muscle marker Desmin was labelled using a rabbit anti-Desmin antibody, followed by staining with an AF568-labelled anti-rabbit antibody (red). The cell nuclei were stained with DAPI (blue), while *T. cruzi* parasites were specifically stained with murine anti-*T. cruzi* Brazil serum and a FITC-labelled anti-mouse IgG secondary antibody (green). Scale: 50 μ m.

Immunofluorescence staining and analysis using the Opera Phenix[®] high-throughput imaging system was employed to better characterise parasite development within muscle cells. Primary human muscle cells and the muscle cell line LHCN-M2 were seeded, differentiated for ten days and infected with *T. cruzi* for 24, 48 and 72 h (Figure 5A). The cell nucleus was stained with DAPI (blue) and staining with an anti-*T. cruzi* antibody (red) also resulted in faint, non-specific staining of the muscle cell cytoplasm, allowing estimation of cell dimensions (faint red).

After 24 hpi, muscle cells were infected at multiple sites and trypanosomes had differentiated from the flagellated infectious trypomastigote form to the round, proliferating amastigote form. At 48 hpi, parasite division was visible, often in a string-like distribution. This division continued, and by 72 hpi, the parasites filled the entire muscle cell in some cases.

The ratio of *T. cruzi* parasites to muscle cell nuclei was assessed (Figure 5B). There was an increase at 48 hpi and an even higher increase at 72 hpi in both primary cells and the cell line. These results highlight that *T. cruzi* can infect primary muscle cells and the LHCN-M2 cell line, and proliferate within both.

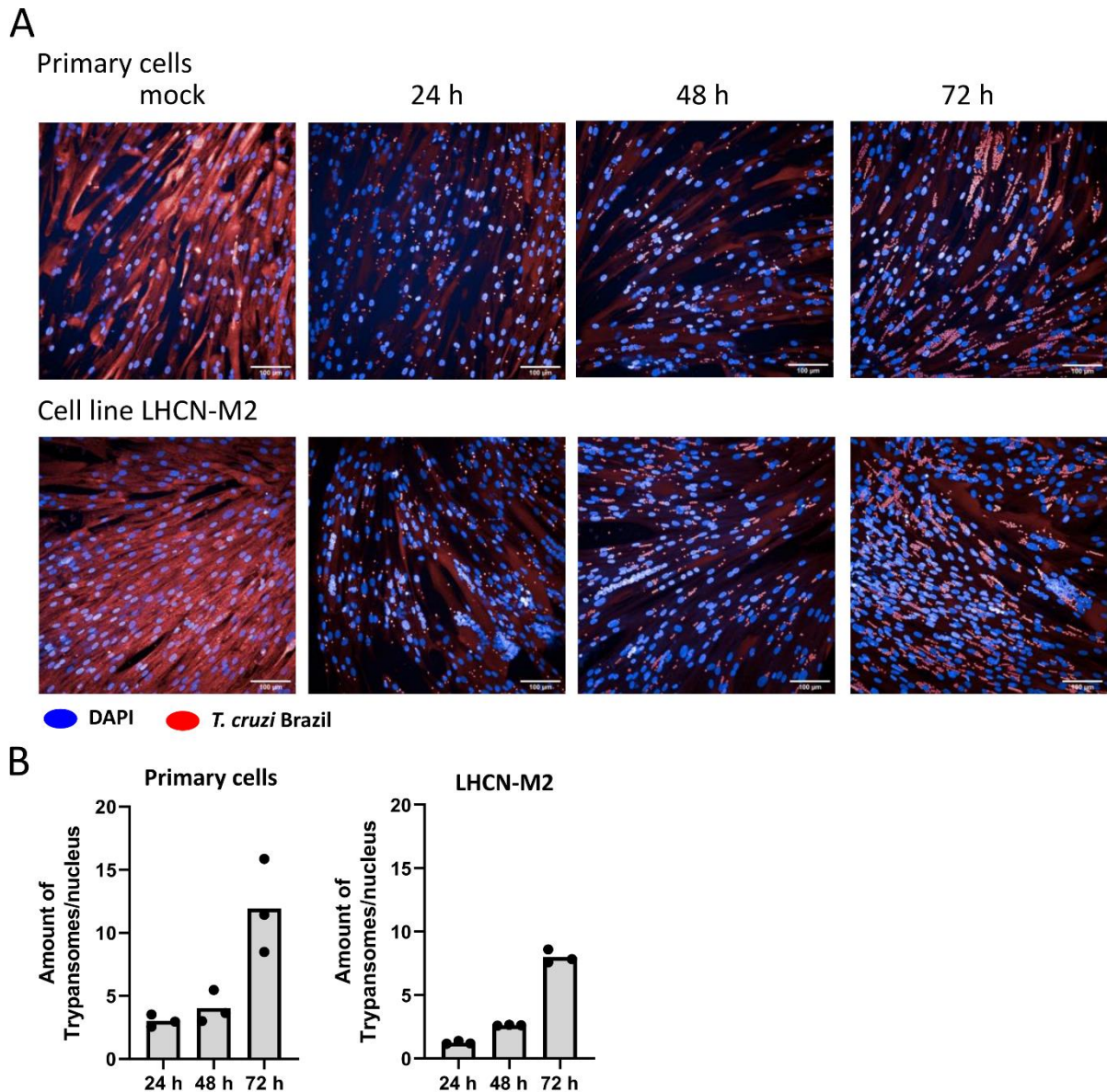


Figure 5: *T. cruzi* infection in primary human muscle cells and the cell line LHCN-M2 and its replication within the cells over time. Differentiated muscle cells were infected with *T. cruzi* at a MOI of 5:1 for 24, 48, and 72 h. The infection rate was assessed using immunofluorescence staining of the cell nucleus with DAPI (blue) and *T. cruzi* with a murine anti-*T. cruzi* serum and an AF647-conjugated anti-mouse IgG secondary antibody (red). B) Immunofluorescence analysis performed by the Opera Phenix®, plotting the quantity of trypanosomes to the number of muscle cell nuclei. Each dot represents one donor (analysis was performed in triplicate, 15 images were taken and analysed for each well) and the respective means are displayed by bars. Scale: 100 μ m.

4.2 Transcriptomic analysis of muscle cells revealed the upregulation of genes involved in the inhibition of parasite growth and immune cell modulation

It was hypothesised that *T. cruzi* parasites can alter the muscle cell function to avoid detection by immune cells. Therefore, determining how the infection with *T. cruzi* influences muscle cell biology is crucial, particularly in the context of expression of molecules that interact with immune cells and can alter their activation and function. As seen in mouse models and patients with Chagas disease in particular, T cells express co-inhibitory receptor molecules which can alter the T cell activation and may lead to the chronicity of the disease^{6,166}. Here, the potential of infected muscle cells expressing ligands of these receptors or other immune regulatory molecules was investigated. Additionally, high levels of the pro-inflammatory cytokine IFN- γ can be found in the plasma of chronically *T. cruzi*-infected patients¹⁶⁷. Stimulating muscle cells with a pro-inflammatory cytokine, such as IFN- γ , leads to the upregulation of many immune regulatory receptors¹⁶⁸.

Therefore, transcriptomic analysis was employed to acquire an overview of the changes in muscle cell function after *T. cruzi* infection and through stimulation with the pro-inflammatory cytokine IFN- γ . Additionally, the human muscle cell line LHCN-M2 was examined for differences compared to primary muscle cells according to their transcriptomic profile. The aim was to determine whether the cell line is a suitable model for primary muscle cells since high amounts of muscle cells would be needed for further analysis and functional assays.

To this end, RNA sequencing of mock and *T. cruzi*-infected, IFN- γ -stimulated, and *T. cruzi*-infected and IFN- γ -stimulated primary muscle cells of 5 donors at 48 hpi was performed and compared to the cell line LHCN-M2. Principal component analysis (PCA) was used to investigate the similarities of the donors within the treatment groups and compare those changes with the changes elicited in the cell line under the same conditions. The expressed genes are reduced in multiple principle components (PC), and PC1 and PC2 are plotted against each other (Figure 6). The greater the distance of one dot (representing one sample), the less similar those two are in their transcriptional profile. The primary human muscle cell donors cluster together according to the condition used for each group. The distance of the cell line sample under the same treatment as the primary cells is always the same distance in PC1 and PC2, except for the sample with IFN- γ treatment, which seems to cluster more closely to the sample of the cell line infected with *T. cruzi*.

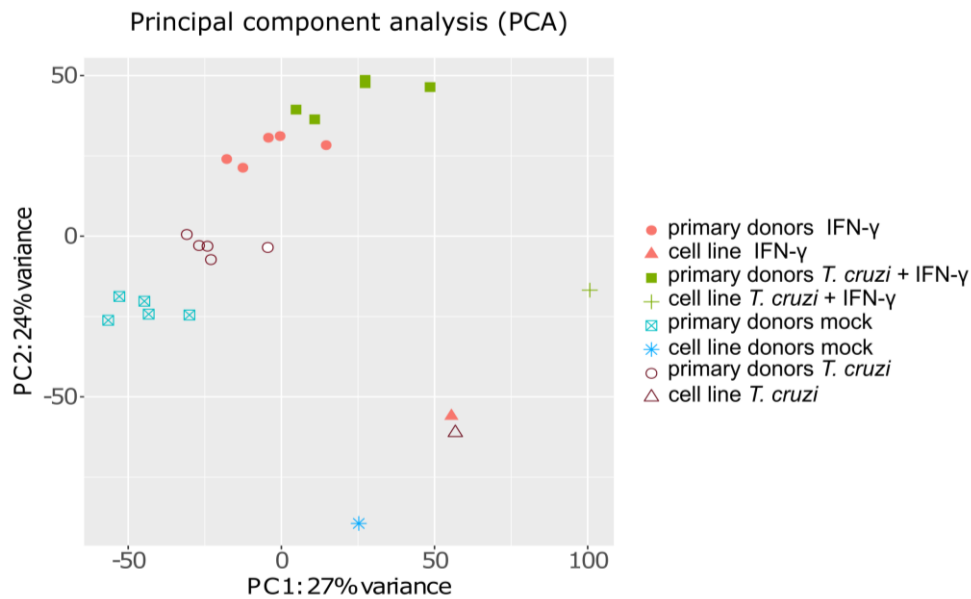


Figure 6: Principal component analysis (PCA) of the expressed genes of human primary muscle cells and the cell line LHCN-M2 after infection and/or stimulation with IFN- γ reveals comparable transcriptional changes within the treatments. Muscle cells were infected with a MOI of 5:1 and/or stimulated with 100 IU/ml IFN- γ for 48 h. RNA sequencing of five primary muscle cell donors and the cell line LHCN-M2 are depicted. In the PCA blot, mock-infected muscle cells are shown in blue, *T. cruzi*-infected muscle cells in burgundy, IFN- γ -stimulated muscle cells in bright red and *T. cruzi*-infected and IFN- γ -stimulated muscle cells in green. The PCA reduces the dimensions and clusters the samples according to their similarity.

The 2000 most highly expressed genes were used to create a heatmap to further investigate the differences and similarities between the donors and the cell line. Here, the samples were clustered according to the similarity of these 2000 genes. The primary muscle cell donors clustered in their respective treatment groups again, highlighted in black boxes (Figure 7A). The cell line clustered together independent of the treatments (grey box). A k-means diagram further characterised these highly expressed genes (Figure 7B). With this algorithm, the genes were clustered into three separate clusters, gene ontology terms (GO terms) were assigned to the genes within the clusters, the genes for each GO term were counted, and the GO terms were displayed in a table (Figure 7B). The largest cluster A (807 genes) consisted of genes essential for muscle cell function, like muscle contraction. These genes were more expressed in the primary cells than in the cell line. The second largest cluster B (703 genes) consisted of genes essential for cell proliferation. These genes were more expressed in the cell line than in the primary cells. The third cluster C (490 genes) consisted of genes essential in the defence response, the immune response and cytokine-mediated signalling pathways. For this cluster of genes, primary cells and the cell line show a similar pattern according to the respective

Results

conditions used during culture. This analysis validated that the cell line could be a suitable model for further functional assays. The cell line showed that the same genes were up-regulated in the cluster of the defence response during the infection and IFN- γ stimulation compared to the primary cells, making it a viable alternative. While differences in the proliferation capacity of the cell line were expected, the differences in muscle cell contraction did not play a role in this study.

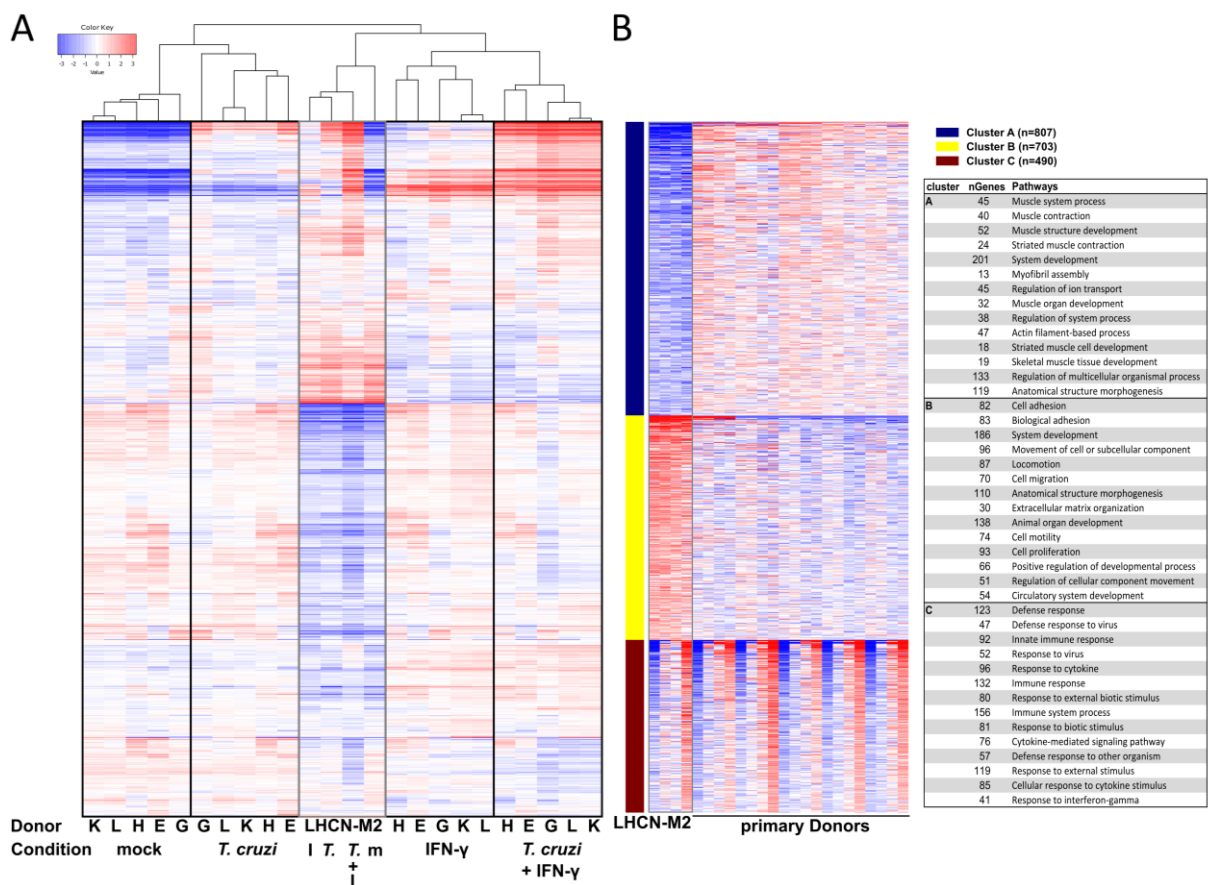


Figure 7: Heatmap and k-means diagram of 2000 highly expressed genes in human primary muscle cells and the cell line LHCN-M2 after infection (MOI 5:1) and/or stimulation with IFN- γ (100 IU/ml). A) Filtered counts of the four treatments for primary donors and the cell line were used to create a heatmap. The algorithm clustered the primary muscle cells together based on their treatments (black boxes) and the cell line, independent of its treatment (grey box). B) The k-means diagram was generated using the 2000 most differentially expressed genes. These genes were categorised into three clusters based on their GO terms (biological processes). This analysis revealed significant changes in the cell line for cluster A (muscle system process) and B (cell adhesion), but it showed a consistent response for cluster C (defence response).

For further transcriptional analysis, only the primary muscle cell donors were used. Differentially expressed genes from the treatment groups compared to mock-infected muscle

cells were calculated. The Venn diagram visualises the identical and distinct genes upregulated between different treatment groups (Figure 8). The depth of the sequencing allowed 14,983 genes to be compared between the treatments. The combination of *T. cruzi* infection and IFN- γ treatment resulted in the highest number of differentially expressed genes (1,606 genes differentially expressed, 952 distinct genes). IFN- γ treatment resulted in 817 differently expressed genes, and the majority were shared with the *T. cruzi* infection and IFN- γ treated group. However, 187 genes were distinctly expressed, indicating a potential influence of *T. cruzi* on the response of the muscle cell to IFN- γ . The *T. cruzi* infection alone led to the lowest number of differentially expressed genes (164 total). Moreover, the majority of the genes (137) were shared with the other groups.

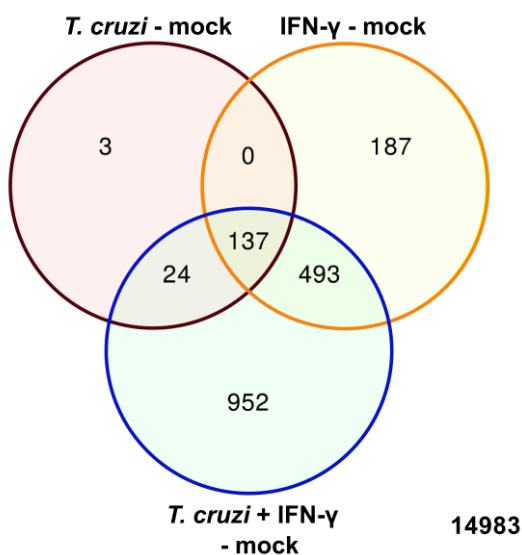


Figure 8: Venn diagram visualising the number of differentially expressed genes in primary muscle cell donors across different treatments compared to the mock control reveals the highest amount of differentially expressed genes in *T. cruzi*-infected and IFN- γ stimulated muscle cells. The results from five different donors were pooled for each condition. Genes were selected with an FDR of 0.1 and a min log fold2 change of 2. The depth of sequencing enabled the comparison of 14,983 genes.

A GO term analysis was performed to get a broad overview of the function of the differently expressed genes (Figure 9A). Moreover, the fold enrichment for each GO term and the $-\log_{10}$ (FDR) were plotted. To gain a deeper insight into the upregulated genes, a heatmap comparing the fold change of the 50 most highly expressed genes of muscle cells infected with *T. cruzi* and stimulation with IFN- γ with muscle cells only infected with *T. cruzi* or only stimulated with IFN- γ was made (Figure 9B).

For *T. cruzi* infection, many genes corresponding to GO terms for the defence response were upregulated, like the negative regulation of viral genome replication, negative regulation of viral production, defence response to other organisms and others. Examples of genes falling into this category from the Heatmap in Figure 9B are *RSAD2*, *MX1*, *OASL*, *CMPK2*, *OAS1*, *MX2*, *OAS2*, and *OAS3*, and these genes are among the top 10 differently expressed genes in all conditions, but even more highly expressed in the *T. cruzi*-infected samples. *RSAD2* can be directly induced by viruses or Type I interferons and has been shown to have antiviral properties ¹⁶⁹. Furthermore, *RSAD2* and *CMPK2* together inhibit the replication of several coronaviruses by inhibiting the RNA-dependent RNA polymerase activity ¹⁷⁰. At the same time, *MX1* and *MX2* are best known for inhibiting negative-stranded RNA viruses and are induced by interferon type I and III ¹⁷¹. *OAS1*, *OAS2* and *OAS3* are involved in the pathway of double-stranded RNA degradation and can restrict intracellular *Mycobacterium tuberculosis* replication ¹⁷². The upregulation of these genes implies that the muscle cell sensed the infection, upon which the genes were upregulated, causing a negative impact on the invading organism.

Many genes in the category of interferon-induced proteins with tetratricopeptide repeats (IFITs) were induced, like *IFIT1*, *IFIT2*, *IFI44L*, *IFIT3*, *IFITM1*, and *IFIT3*. These genes have been shown to be highly expressed during the cell-intrinsic immune response to viral infections ¹⁷³.

The second highest enriched GO term was cellular response to type I interferon, and the GO terms Type I interferon signalling pathway, response to cytokine, and cellular response to cytokine stimulus were upregulated. The majority of the genes mentioned above are described to be induced by Type I, II or III interferons. These genes are more highly expressed by *T. cruzi*-infected muscle cells than only by IFN- γ stimulated muscle cells.

For IFN- γ stimulated muscle cells, genes corresponding to the GO term cellular response to type I interferon were enriched and a defence response to viruses was initiated. Moreover, a cellular response to IFN- γ was induced. Here, the GO term showed regulation of cytokine production. The heatmap revealed that genes for immune cell-recruiting chemokines were induced, like *CXC11*, *CXCL9* and *CCL8*. Genes like *CD74* and *CTSS* were also especially induced by IFN- γ stimulation. *CD74* is the invariant γ -chain of the Human leukocyte antigen class II (HLA-II) receptor, and *CTSS* is the gene of the protein Cathepsin S, which is a lysosomal cysteine protease processing the invariant chain of the HLA-II receptor (*CD74*) and which participates

in the degradation of antigenic proteins for presentation¹⁷⁴. Additionally, for IFN- γ -stimulated muscle cells, genes that followed the GO-term regulation of the immune response were upregulated. Examples are *CD274* and *LGALS9*, which encode for the co-inhibitory receptor ligands PD-L1 and galectin-9. The infection with *T. cruzi* already induces the expression, but the expression increases upon IFN- γ stimulation.

The combination of a *T. cruzi* infection and stimulation with IFN- γ showed the same GO terms as the IFN- γ -stimulated muscle cells. Additionally, the majority of genes that were either upregulated by *T. cruzi* infection or by IFN- γ stimulation had an increased expression in muscle cells that were infected and stimulated. Interestingly, the genes *IDO1* and *IL-4I1* were induced by IFN- γ and *T. cruzi* infection as well as IFN- γ stimulation. *IDO1* and *IL-4I1* encode for the enzymes indoleamine-pyrrole 2,3-dioxygenase and L-amino acid oxidase, which are a tryptophan and an L-alanine oxidase, respectively. Both of these enzymes have been described in various cancer models and are involved in immune suppression by downregulating T cell responses⁷.

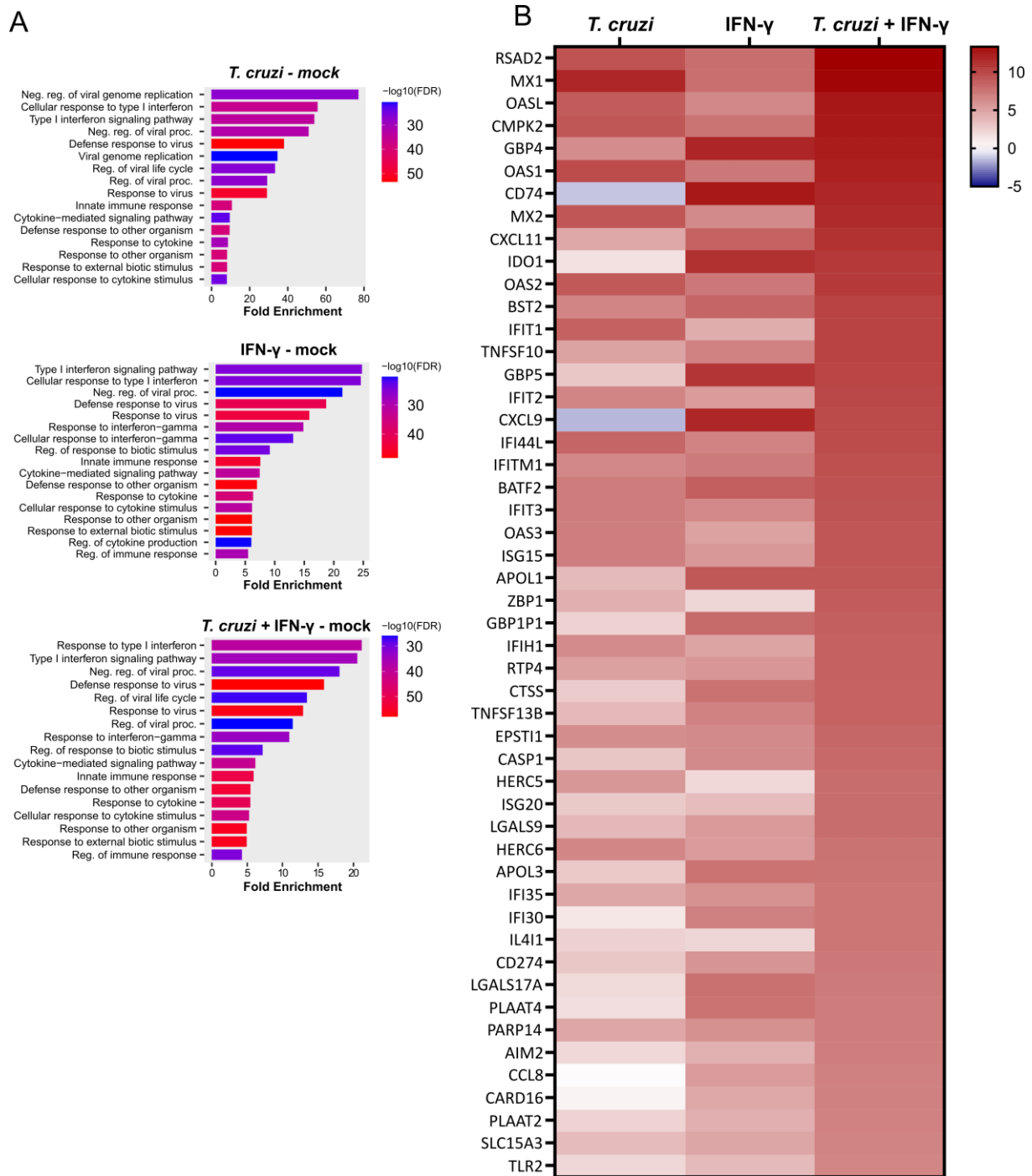


Figure 9: GO term analysis and heatmap of the 50 most highly differentially expressed genes in primary human muscle cells infected with *T. cruzi* and/or stimulated with IFN- γ , revealing upregulation of genes involved in the defence response. The results from five different donors were pooled for each condition. A) GO term enrichment for *T. cruzi* (MOI 5:1) infected and/or IFN- γ (100 IU/ml) stimulated muscle cells. The fold change and $-\log_{10}(\text{FDR})$ values are depicted for each GO term. B) Comparison of the fold change of the 50 most highly significantly differentially expressed genes in primary human muscle cells infected with *T. cruzi* and or/stimulated with IFN- γ .

In the next step, all significantly differently expressed genes (adj. p-value 0.05) of the three different treatment groups were analysed for genes involved in immune cell processes. The volcano plot depicts these genes of interest (Figure 10). Aside from the upregulation of the aforementioned genes, the analysis revealed the upregulation of CXCL10 (C-X-C motif chemokine ligand 10) and TLR3 (toll-like receptor 3) in *T. cruzi*-infected muscle cells. *APOL1*, which is described as a resistance factor for the infection with the related parasite *Trypanosoma brucei*¹⁷⁵, was also induced. Moreover, RIG-1 was upregulated, which is a helicase that can recognise single and double-stranded RNA in the cytosol¹⁷⁶.

For IFN- γ stimulation, an additional upregulation of the cytokine IL-15 and the IL-15 receptor could be seen, and the induction of the chemokine CXCL16 and CXCL8. Additionally, the co-stimulatory receptor CD40 and the TLR2 (Toll-like receptor 2) were upregulated. The transcriptional co-activator CIITA was highly upregulated by the IFN- γ stimulation. This co-activator upregulates the expression of HLA-I and HLA-II¹⁷⁷.

The infection with *T. cruzi* and stimulation with IFN- γ revealed the additional upregulation of the chemokine *CCRL2* and the upregulation of *PDCD1LG2*, which encodes for the co-inhibitory receptor ligand PD-L2 as well as the HLA-H pseudogene.

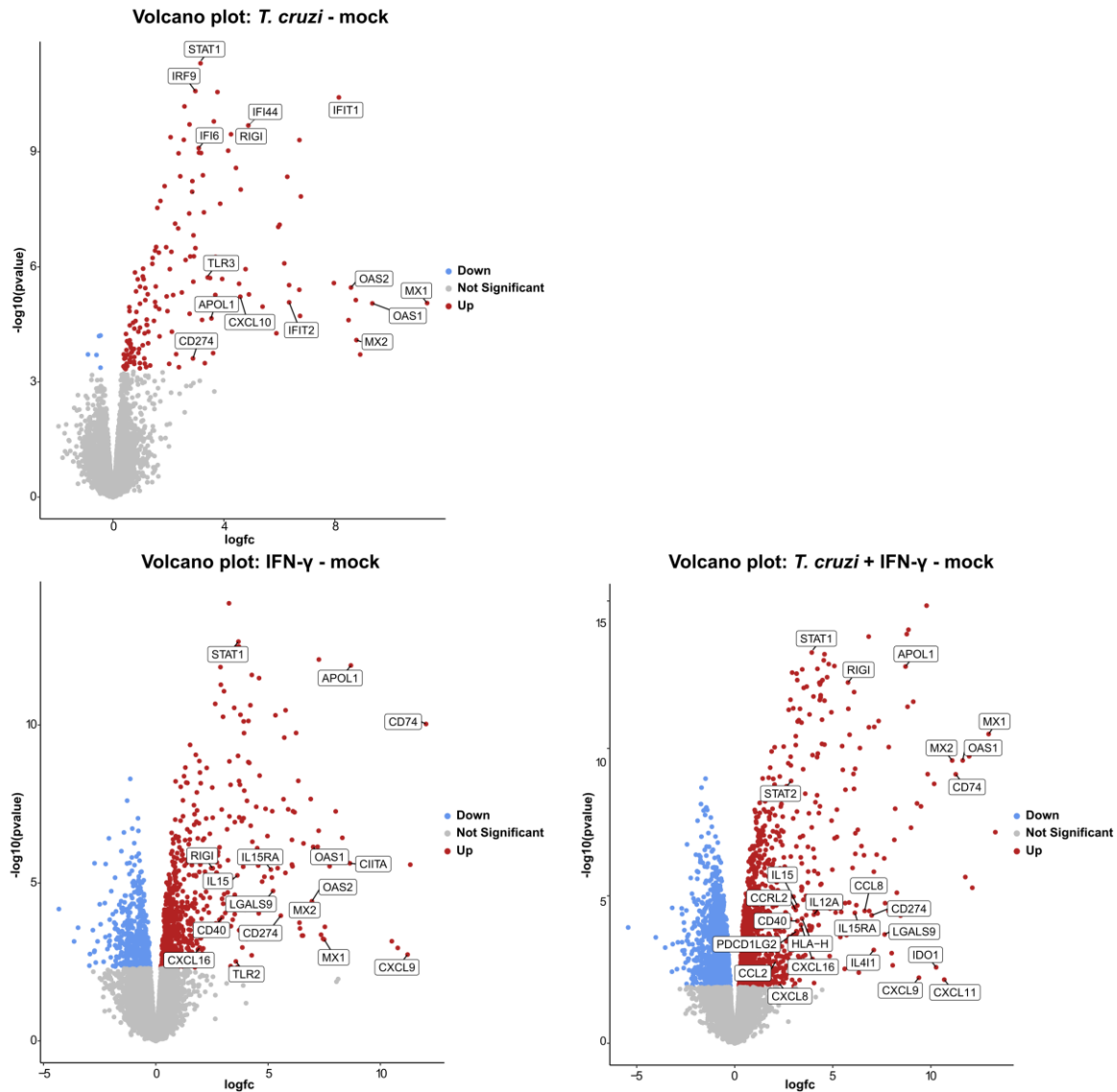


Figure 10: Volcano plot of the differentially expressed genes of the primary muscle cell donors under different conditions reveals the induction of anti-parasitic and immune-regulatory mechanisms. The results of 5 different donors were pooled for each condition. The log fold change (x-axis) is plotted against the $-\log_{10}(\text{p-value})$, and significantly differentially expressed genes are coloured in red (upregulated) and blue (downregulated). Immunologically relevant genes are labelled.

Moreover, genes potentially downregulated by a *T. cruzi* infection were investigated as these might favour the persistence of the parasite. To this end, the differentially expressed genes of IFN- γ -stimulated muscle cells in contrast to IFN- γ -stimulated and *T. cruzi*-infected muscle cells were calculated. All genes significantly upregulated by IFN- γ and showing a minimum change in expression by a log fold change of 1 upon *T. cruzi* infection were sorted. Six genes could be identified using these criteria; their log fold expression compared to the mock control is shown in a heatmap in Figure 11.

In muscle cells infected with *T. cruzi*, significant downmodulation of *TRIM17*, *PPP1R27* and *LG1* was observed. These genes are involved in autophagy, muscle membrane repair, and potential tumour suppression, respectively^{178–180}. While *CIITA* was upregulated in all samples compared to the mock control, *T. cruzi*-infected and IFN- γ -stimulated muscle cells expressed this gene in a lower magnitude than IFN- γ -stimulated muscle cells. *CIITA* is a transcriptional co-activator involved in expressing HLA-II-related genes¹⁷⁷.

MMP25 and the antisense RNA of *MMP25* were significantly down-regulated in *T. cruzi*-infected and IFN- γ -stimulated muscle cells compared to IFN- γ -stimulated muscle cells. *MMP25* is a matrix metalloprotease anchored to the cell membrane and has been associated with immune cell infiltration in cancer¹⁸¹.

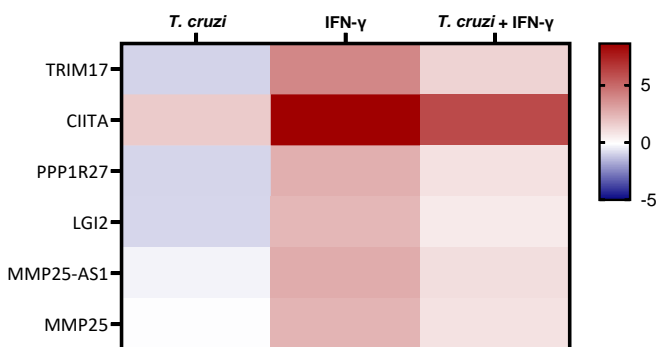


Figure 11: Heatmap of the six differentially expressed genes upregulated by IFN- γ and downregulated during *T. cruzi* infection. Muscle cell genes significantly upregulated by IFN- γ (100 U/ml) were compared to those expressed during *T. cruzi* infection and IFN- γ stimulation and sorted for genes showing a 2-fold or greater decrease.

Taken together, the results from the transcriptomic analysis show the induction of anti-parasitic mechanisms, chemokines and cytokines responsible for immune cell recruitment, antigen presentation by HLA, and immune regulatory mechanisms. These aspects will be further focused on in the following chapters. In the following chapters, only the results of primary muscle cells are shown. However, the majority of the experiments were additionally performed with the muscle cell line LHCN-M2 and showed comparable results.

4.3 Anti-parasitic mechanisms are induced in muscle cells

Transcriptomic analysis showed that the infection alone caused the induction of multiple genes involved in parasite clearance. The addition of pro-inflammatory cytokines like IFN- γ increased the expression. Therefore, determining whether the stimulation of muscle cells with pro-inflammatory cytokines resulted in a reduction of intracellular parasites is crucial. Additionally, another pro-inflammatory cytokine, TNF- α , was investigated for its effect on muscle cells, as it has previously been shown that, during a chronic *T. cruzi* infection, high amounts of TNF- α are present in the blood of mice and humans^{6,182}.

The effect of pro-inflammatory cytokines on host cell susceptibility to the parasite was investigated. To assess the impact of a pro-inflammatory environment on parasite infectivity, muscle cells were infected and treated with either IFN- γ and TNF- α alone or in combination. After 24, 48 and 72 h, the muscle cells were analysed via flow cytometry.

A significant reduction of *T. cruzi*-positive muscle cells upon stimulation with cytokines was observed (Figure 12). A trend of reduced *T. cruzi*-positive muscle cells upon stimulation with the cytokines alone was already visible after 24 hpi; however, only the IFN- γ and TNF- α -stimulated muscle cells showed a significant reduction from 18.9 % to 9 %. After 48 h, a significant reduction from 27.5 % to 20.3 % for IFN- γ stimulated muscle cells and an even higher decrease for TNF- α -stimulated muscle cells to 12.2 %, and a decrease to 11.3 % for IFN- γ and TNF- α -stimulated muscle cells was observed. A similar reduction was seen after 72 hpi. This confirms our hypothesis that a significant reduction of *T. cruzi*-positive muscle cells could be detected upon stimulation with pro-inflammatory cytokines.

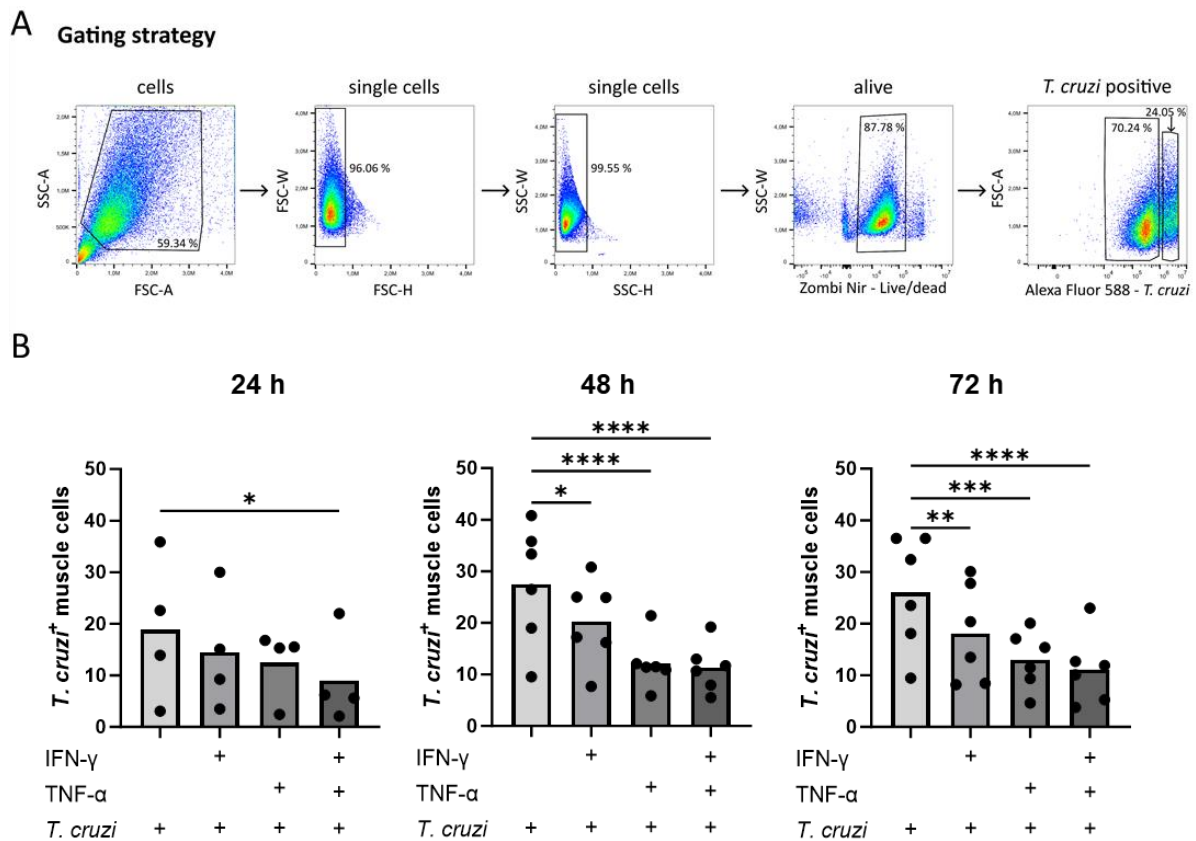


Figure 12: Percent of *T. cruzi*-positive muscle cells declines upon stimulation with pro-inflammatory cytokines after 24 h, 48 h and 72 h post-infection. Differentiated primary human muscle cells were infected and stimulated with the cytokines IFN- γ and TNF- α . After the indicated time point, cells were harvested and stained intracellularly with an antibody against *T. cruzi* and analysed by flow cytometry. A) Gating strategy for primary human muscle cells allows analysis of proteins in and on *T. cruzi*-positive and negative cells. Cells were stained intracellularly for *T. cruzi* (using a rabbit anti-*T. cruzi* serum and an AF568-conjugated anti-rabbit IgG secondary antibody) before analysis by flow cytometry. The gating strategy included excluding cell debris, setting single cell gates and viable cells, and distinguishing between *T. cruzi*-positive and negative cells. B) Graphs and statistical analysis of *T. cruzi*-positive muscle cells. Each dot represents one donor and respective means are depicted by bars. After a test for normal distribution, statistical significances were calculated by RM one-way ANOVA (normal distribution) or by Friedman test (non-normal distribution): * $p \leq 0.05$; ** $p \leq 0.01$; *** $p \leq 0.001$; **** $p \leq 0.0001$.

Immunofluorescence staining was employed to verify these results and to investigate the development of amastigotes inside the muscle cells. Images taken by the high-throughput immunofluorescence microscope Opera Phenix[®] of muscle cells pre-stimulated without cytokines or with IFN- γ and TNF- α alone or together for 16 h, at 72 hpi, are shown in Figure 13A. Muscle cells were stained with DAPI (blue) and an antibody against *T. cruzi* (red), which also faintly stained the cytoplasm red and allowed the estimation of cell dimensions. A reduction of *T. cruzi*-positive cells upon cytokine stimulation was observed. In addition, the

amount of *T. cruzi*-positive cells was reduced and the number of *T. cruzi* amastigotes per infected cell seemed to decrease, especially with a combination of IFN- γ and TNF- α (Figure 13B). Here, a statistically significant reduction of the amount of trypanosomes/nucleus was observed after 72 hpi.

This confirmed our hypothesis that the infection rate of muscle cells by *T. cruzi* is reduced after stimulation with pro-inflammatory cytokines, and the immunofluorescence staining imply that the proliferation of amastigotes might be reduced.

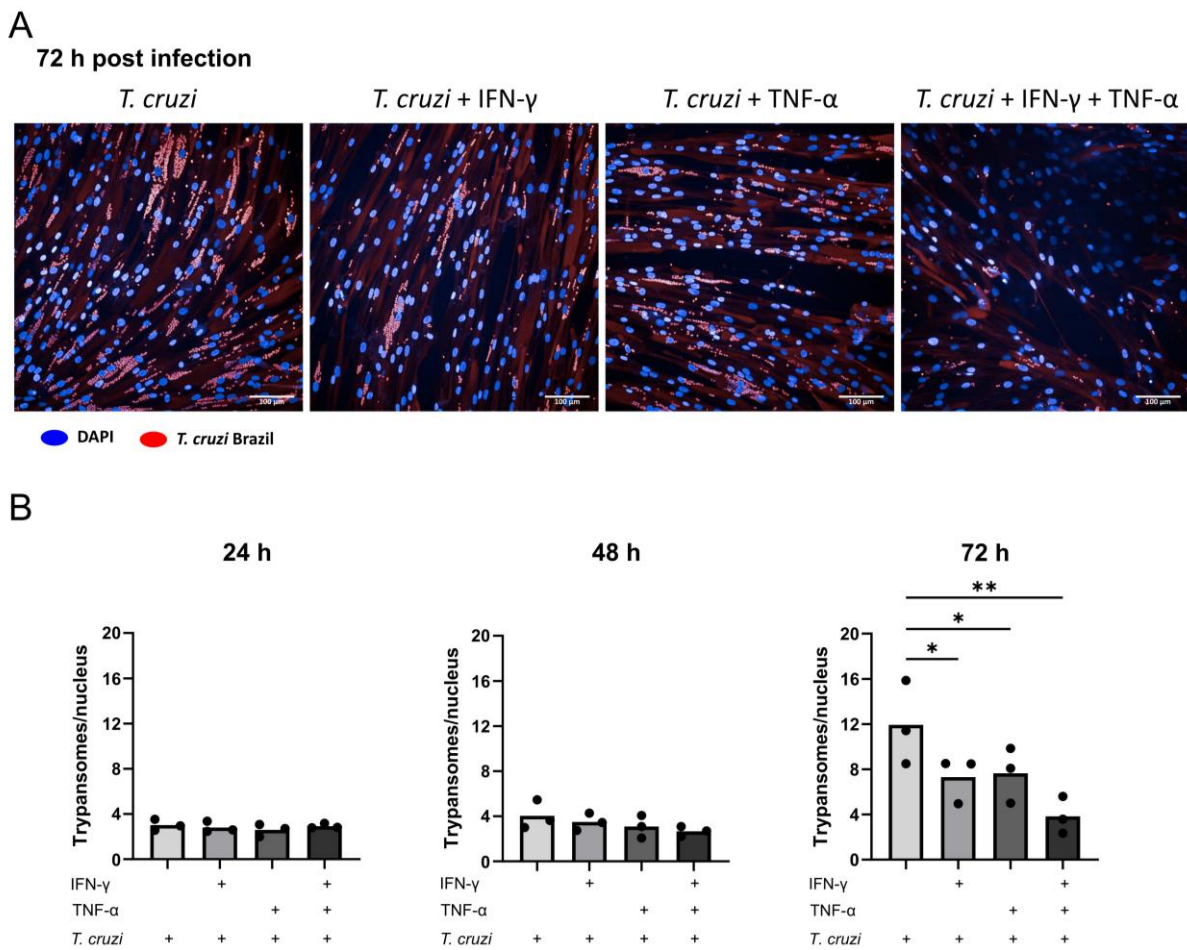


Figure 13: The amount of *T. cruzi* per muscle cell nucleus decreases after stimulation with pro-inflammatory cytokines at 72 h post infection. Differentiated primary human muscle cells were infected and stimulated with IFN- γ (100 IU/ml) and TNF- α (100 IU/ml). After the indicated time, the cells were fixed and stained intracellularly with a murine anti-*T. cruzi* serum and an AF647-conjugated anti-mouse IgG secondary antibody (red), and the nucleus was stained with DAPI (blue) and analysed using the Opera Phenix automated immunofluorescence microscope. A) Representative pictures of each treatment group from one donor. B) Graphs and statistical analysis of 3 donors. Each dot represents one donor (analysis was performed in triplicate, 15 images were taken and analysed for each well), and the respective means are represented by bars. After testing for normal distribution, statistical significance was calculated using RM one-way ANOVA (for normal distribution): * $p \leq 0.05$; ** $p \leq 0.01$.

A very conserved mechanism by which other cells such as macrophages can control the pathogens inside the cell is the induction of the induced nitrogen oxygen synthase (iNOS). iNOS has already been shown to be essential for protection in the early phase of the disease and produces reactive oxygen species¹⁸³. However, its role during the infection of skeletal muscle cells by *T. cruzi* infection has not been illuminated yet.

Therefore, whether iNOS is upregulated in muscle cells upon infection was investigated. Human primary muscle cells were infected with *T. cruzi* for 24, 48 and 72 h and stained intracellularly for *T. cruzi* and iNOS. Representative histograms of iNOS expression in *T. cruzi*-negative and positive muscle cells can be seen in Figure 14A. High amounts of iNOS are present at 24 hpi independent of an infection. However, higher amounts of iNOS are present in *T. cruzi*-positive muscle cells compared to *T. cruzi*-negative cells. Even though a trend can be observed after 24 hpi, there is only a statistically significant increase of iNOS in *T. cruzi*-positive cells compared to *T. cruzi*-negative cells after 48 hpi and 72 hpi (Figure 14B). This result confirms the elevated induction of this enzyme and implies an involvement in parasite clearance by a *T. cruzi* infection.

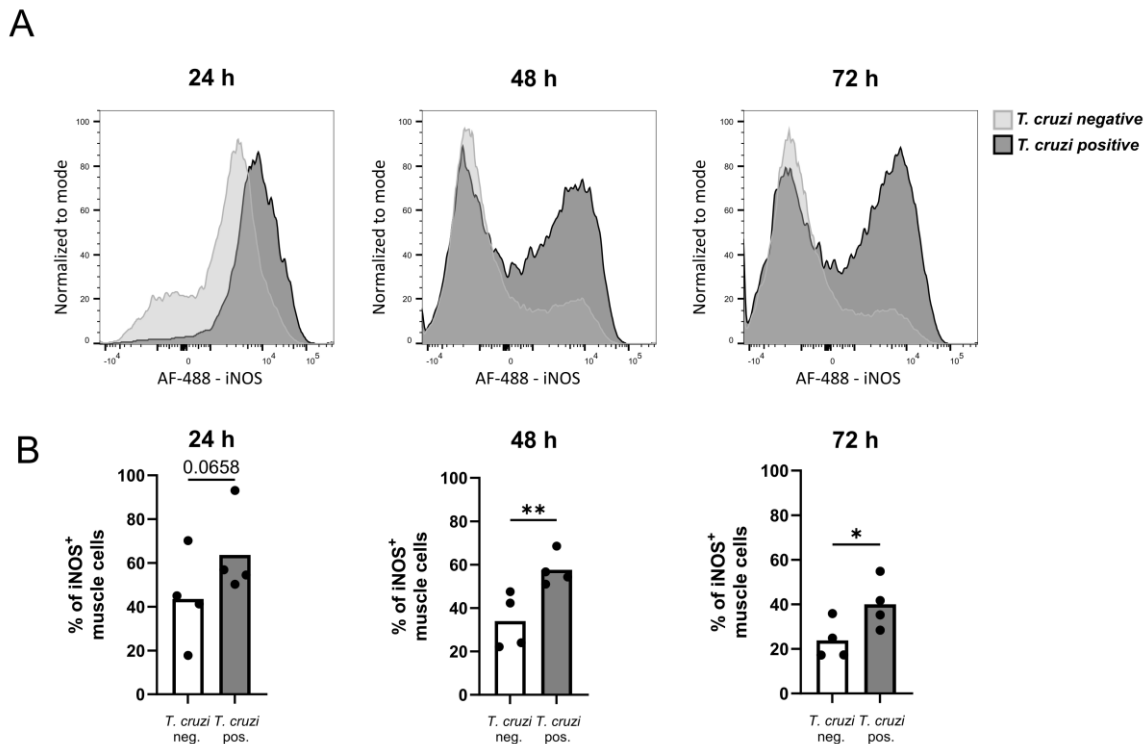


Figure 14: iNOS increases in *T. cruzi*-positive muscle cells. Differentiated primary human muscle cells were infected with *T. cruzi* (MOI 5:1) and harvested after 24, 48 and 72 hpi. Cells were stained intracellularly with an AF-488-conjugated iNOS antibody and for *T. cruzi* (using a rabbit anti-*T. cruzi* serum and an AF568-conjugated anti-rabbit IgG secondary antibody) and then analysed by flow cytometry. A) Histograms of iNOS expression in *T. cruzi*-positive and negative cells over time. B) Graphs and statistical analysis of iNOS-positive cells over time. Each point represents one donor; the respective means are shown as bars. After testing for normal distribution, statistical significance was calculated using paired t-test (for normal distribution) or Wilcoxon test (for non-normal distribution): * $p \leq 0.05$, ** $p \leq 0.01$.

To analyse the impact of iNOS on the infectivity of muscle cells by *T. cruzi*, the selective iNOS inhibitor N6-(1-iminoethyl)-L-lysine (L-Nil) was used. To this end, muscle cells were pre-incubated with L-Nil for 16 h, subsequently infected with *T. cruzi*, and analysed with the Opera Phenix® immunofluorescence microscope; representative pictures after 24, 48 and 72 hpi can be seen in Figure 15A. An increased parasitic load of the muscle cells by *T. cruzi* upon L-Nil treatment was observed. Three muscle cell donors were tested and a statistically significant increase of trypanosomes/muscle cell nucleus can be seen after 48 hpi (Figure 15B).

This confirms our hypothesis that the infectivity of muscle cells by *T. cruzi* is impaired by the expression of iNOS by the muscle cells.

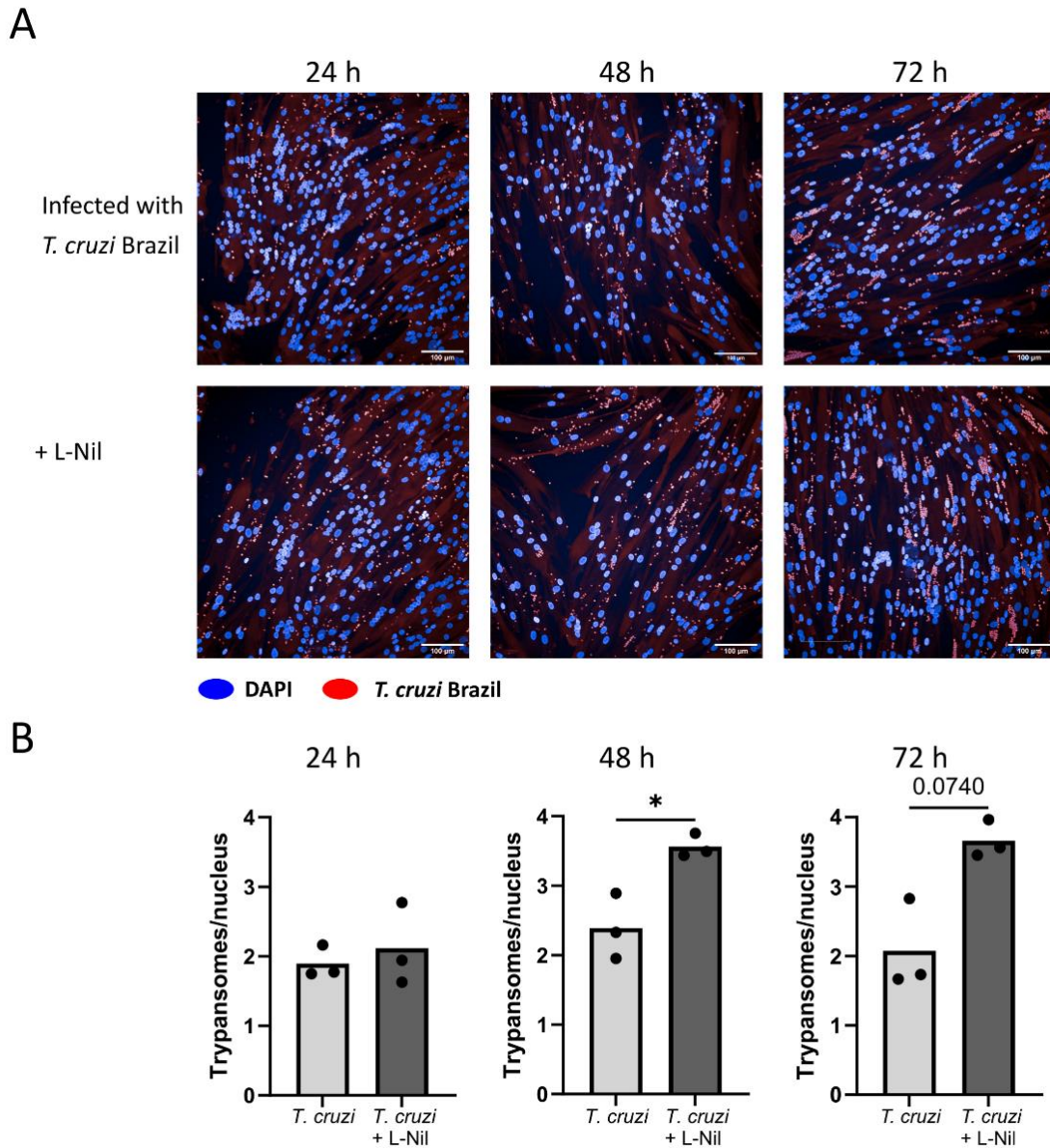


Figure 15: Inhibition of iNOS by L-Nil increases the parasitic load of *T. cruzi* in muscle cells. Differentiated primary human muscle cells were incubated with the iNOS inhibitor L-Nil for 16 h and then infected with *T. cruzi* (MOI 5:1). After the indicated time the cells were fixed and stained intracellularly with a murine anti-*T. cruzi* serum and an AF647-conjugated anti-mouse IgG secondary antibody (red), and the nucleus was stained with DAPI (blue) and analysed using Opera Phenix®. Each point represents one donor (analysis was performed in triplicate, 15 images were taken and analysed for each well), and the respective means are represented by bars. After testing for normal distribution, statistical significance was calculated using paired t-test (for normal distribution): * $p \leq 0.05$.

4.4 Cytokines responsible for immune cell recruitment are secreted by muscle cells

In the next step, whether infected muscle cells can secrete chemokines and cytokines to recruit immune cells to the site of infection was investigated. This is essential to ensure sensing of the ongoing infection inside muscle tissue by the immune system.

To this end, muscle cells were infected and/or stimulated with the cytokines IFN- γ and TNF- α and the supernatants were analysed for the chemokines and cytokines IL-6, IL15, IL8 and CCL-19 via Legendplex after 24, 48 and 72 hpi (Figure 16).

The cytokine IL-6 has been described to be secreted by muscle cells and is involved in the proliferation of CD4⁺ T cells during inflammatory conditions^{146,184}. A significant increase in the secretion of this cytokine by muscle cells 24 h after stimulation with TNF- α (mean of 4418 pg/ml) was observed and the secretion stayed consistent over time (4534 pg/ml after 48 h and 4580 pg/ml after 72 h). The combination of IFN- γ and TNF- α stimulation or an infection and TNF- α stimulation increased the secretion of this cytokine even more after 48 h, to 7439 pg/ml and 6451 pg/ml, respectively. The same was visible after 72 h. Interestingly, even though the stimulation with IFN- γ alone did not seem to have a high effect on the secretion of IL-6 after 48 h, there was a significant increase of IL-6 after IFN- γ stimulation and simultaneous *T. cruzi* infection to 3646 pg/ml.

IL-15 is a pro-inflammatory cytokine the skeletal muscle produces in response to exercise and has already been shown to be upregulated by IFN- γ and TNF- α ¹⁸⁵. This cytokine and the IL-15 receptor were significantly upregulated in the transcriptomic analysis of IFN- γ -stimulated muscle (Figure 10). It is essential for the proliferation of natural killer cells (NK-cells), a cell type which is very important in the early response against the parasite, as well as anti-apoptotic signalling to memory T cells. Here, muscle cells showed a low expression of this cytokine. Upon stimulation with IFN- γ and TNF- α , we saw a significant increase to 19 pg/ml after 48 h and to 39 pg/ml after 72h. The infection with *T. cruzi* does not seem to impact the secretion of IL-15.

IL-8 is a very important chemokine involved in the recruitment of neutrophils and mediated by the neutrophil recruitment of T cells¹⁸⁶. This chemokine was already secreted at a steady state (91 pg/ml at 24 h), and a high increase of the secretion was observed 24 h after cytokine stimulation. The secretion stayed consistently high across the analysed time points. It was not induced by an infection with *T. cruzi* but instead appeared to rely on the stimulation of the

muscle cell with TNF- α (10085 pg/ml after 24 h, 11224 pg/ml after 48 h and 8523 pg/ml after 72 h).

The cytokine CCL19 is abundantly expressed in lymph nodes and the thymus but can be expressed by other organs in smaller amounts. This chemokine can attract immune cells, like T cells, by binding to the receptor CCR7¹⁸⁷. Muscle cells secreted small amounts of this cytokine, and the secretion was significantly increased upon stimulation with IFN- γ and TNF- α (9 pg/ml after 24 h, 7 pg/ml after 48 h and 14 pg/ml after 72 h).

Taking the results together, it could be shown that muscle cells secrete the cytokines IL-6, IL-15, IL-8 and CCL19. The secretion is highly increased by the stimulation with pro-inflammatory cytokines, especially by TNF- α . This confirms the immune cell-recruiting capacity of muscle cells.

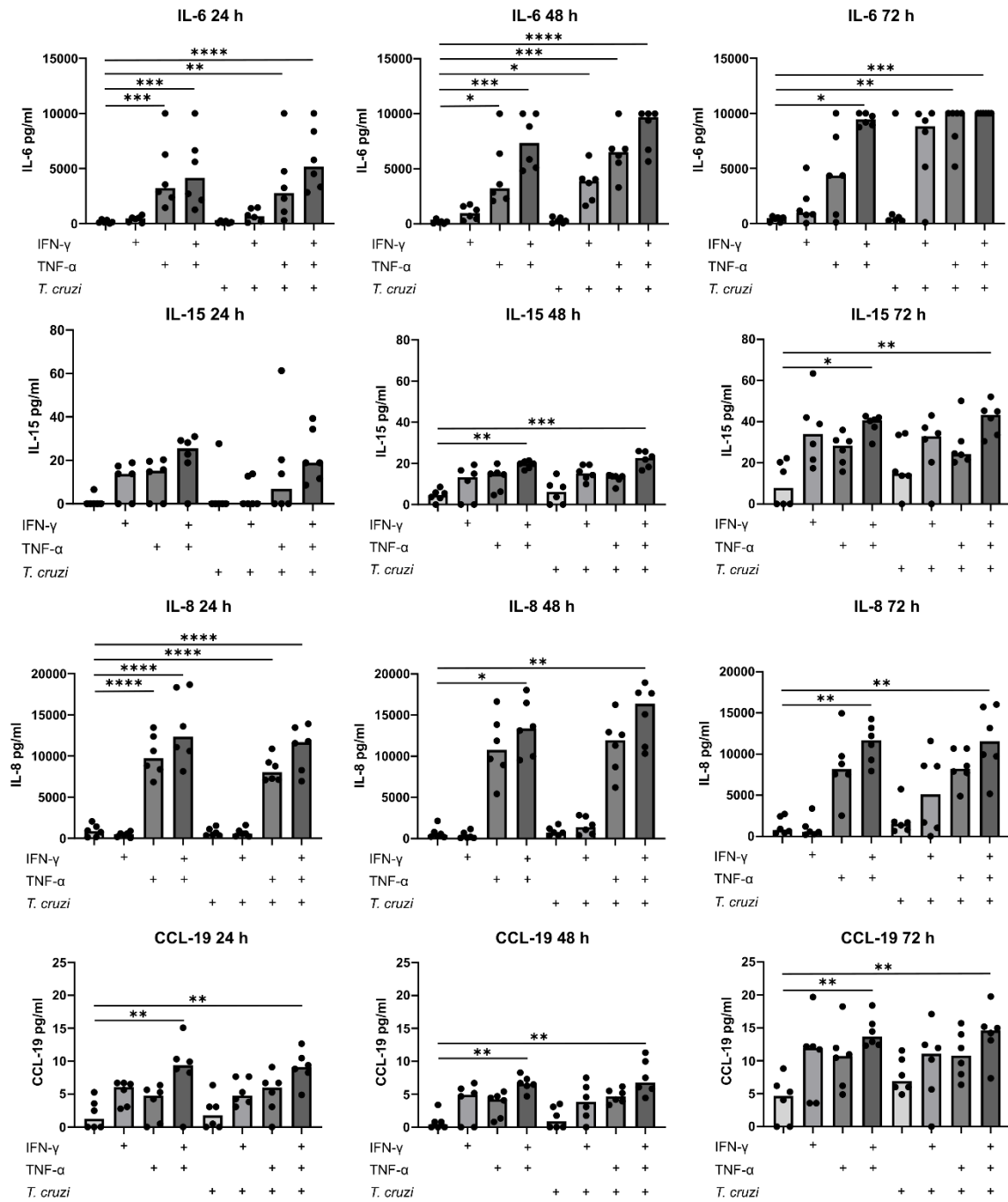


Figure 16: Immune cell-recruiting cytokines and chemokines are secreted by muscle cells infected with *T. cruzi* and/or stimulated with pro-inflammatory cytokines. The concentration of IL-6, IL-15, IL-8 and CCL-19 in the supernatant of mock, IFN- γ , TNF- α , IFN- γ and TNF- α -stimulated, *T. cruzi*-infected (MOI 5:1) and stimulated muscle cells. Supernatants were collected at the indicated time points and analysed using a customised human LEGENDplex. Non-detectable values were set to 0. Each point represents one donor and the bars represent the respective means. After testing for normal distribution, statistical significance was calculated using RM one-way ANOVA (for normal distribution) or Friedman's test (for non-normal distribution): * $p \leq 0.05$; ** $p \leq 0.01$; *** $p \leq 0.001$; **** $p \leq 0.0001$.

4.5 Muscle cells could present *T. cruzi* antigen via HLA-I and HLA-II

A crucial step for immune cells to recognise an infection is the presentation of parasite antigens on the surface of the infected cell. Therefore, all nucleated cells in the body express the human leukocyte system class I receptor (HLA-I). This receptor acts as a surveillance system and presents antigens to CD8⁺ T cells.

Muscle cells were infected and stimulated with pro-inflammatory cytokines for 24, 48 and 72 h. Infected and stimulated muscle cells were investigated for their HLA-I expression, and representative histograms of the muscle cells after the stimulation and infection can be seen in Figure 17A. Muscle cells showed a high HLA-I expression under all conditions compared to the FMO (fluorescence minus one) (dotted lines). The mean fluorescent intensity was plotted to investigate changes in expression levels of HLA-I after different treatments (Figure 17B).

An induction of HLA-I upon stimulation with pro-inflammatory cytokines was observed after 24 h (a 140-fold increase upon IFN- γ stimulation compared to mock control). Furthermore, the expression stayed elevated over the analysed time points. In contrast, infection with *T. cruzi* increased the expression of HLA-I, but only after 72 hpi (200 fold in comparison to mock control).

These results indicate that muscle cells can potentially present *T. cruzi* antigens to immune cells via HLA-I. The pro-inflammatory environment increases the number of receptors on the cell surface. As *T. cruzi* infection delayed the increase of HLA-I, this might affect the recognition of infected muscle cells.

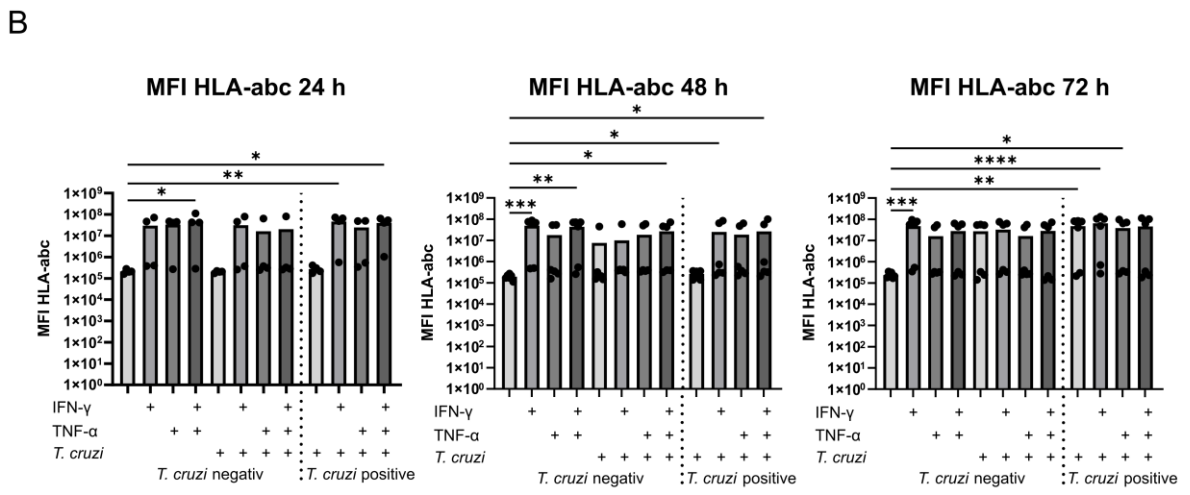
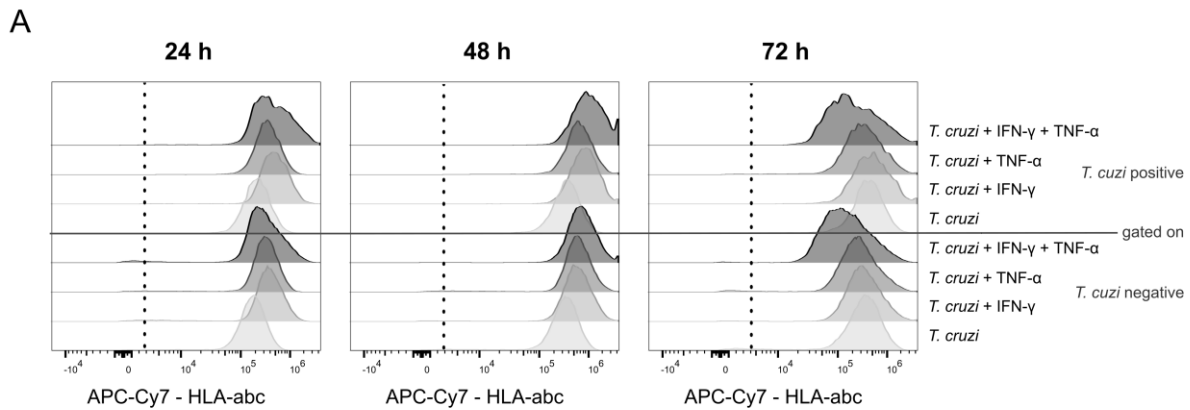


Figure 17: Human primary muscle cells express HLA-I and upregulate the receptor expression upon infection and stimulation with pro-inflammatory cytokines. Differentiated primary human muscle cells were infected with *T. cruzi* (MOI 5:1), stimulated with IFN- γ and TNF- α as indicated in the figure and harvested after 24, 48 and 72 h. Cells were surface stained with an APC-Cy7-labelled antibody against HLA-abc and intracellularly stained for *T. cruzi* as described previously and then analysed by flow cytometry. A) Histograms of HLA-abc expression in *T. cruzi*-positive and negative cells over time. B) Graphs and statistical analysis of HLA-abc-positive cells over time. Each point represents one donor; the respective means are shown as bars. After testing for normal distribution, statistical significance was calculated using RM one-way ANOVA (for normal distribution) or Friedman's test (for non-normal distribution): * $p \leq 0.05$; ** $p \leq 0.01$; *** $p \leq 0.001$; **** $p \leq 0.0001$.

Since the transcriptomic analysis revealed the up-regulation of CD74 upon IFN- γ stimulation, which is the γ -chain of the HLA-II receptor, the expression of the HLA-II receptor was investigated. This receptor is usually expressed on antigen-presenting cells and is essential for activating CD4⁺ T cells. In line with this, the transcriptomic analysis revealed an upregulation of CD40 upon IFN- γ stimulation. This co-stimulatory receptor is crucial for the activation of CD4⁺ T helper cells. The expression of both of these surface receptors was investigated on muscle cells infected and stimulated with different cytokines, as shown in Figure 18.

The expression of HLA-DR was highly increased after IFN- γ stimulation. After 48 h, a statistically significant increase from 24 % to 83 % of HLA-DR-positive muscle cells could be seen, and this expression stayed significantly high over time. However, for the IFN- γ -stimulated and infected muscle cells, an increase of the HLA-DR expression was observed early on after 24 hpi from 17 % (mock control) to 70 % of the *T. cruzi*-positive and 63 % of the *T. cruzi*-negative cells. The expression stayed high over time.

While CD40 showed a significant increase after IFN- γ and TNF- α stimulation after 24 h, an increase of CD40-positive cells from 27 % of the mock control to 62 % was observed. The expression stayed high over time. The stimulation with IFN- γ or TNF- α alone did not lead to an increase in the expression of CD40. Interestingly, CD40 was specifically increased in *T. cruzi*-infected muscle cells. Early, after 24 hpi, a statistically significant increase to 63 % of *T. cruzi*-positive muscle cells could be seen. After additional IFN- γ stimulation, an increase of CD40-positive and *T. cruzi*-positive muscle cells to 71 % was observed, with an increase to 83 % after IFN- γ and TNF- α stimulation. Similar to the HLA-DR⁺ cells, the expression level remained high over time.

These results show that muscle cells are capable of presenting *T. cruzi*-derived antigens via HLA-II and potentially give CD4⁺ T helper cells co-stimulatory signals. A pro-inflammatory environment increases the expression of the molecules HLA-DR and CD40. While IFN- γ mainly induced HLA-DR expression, CD40 was predominantly expressed on *T. cruzi*-infected muscle cells.

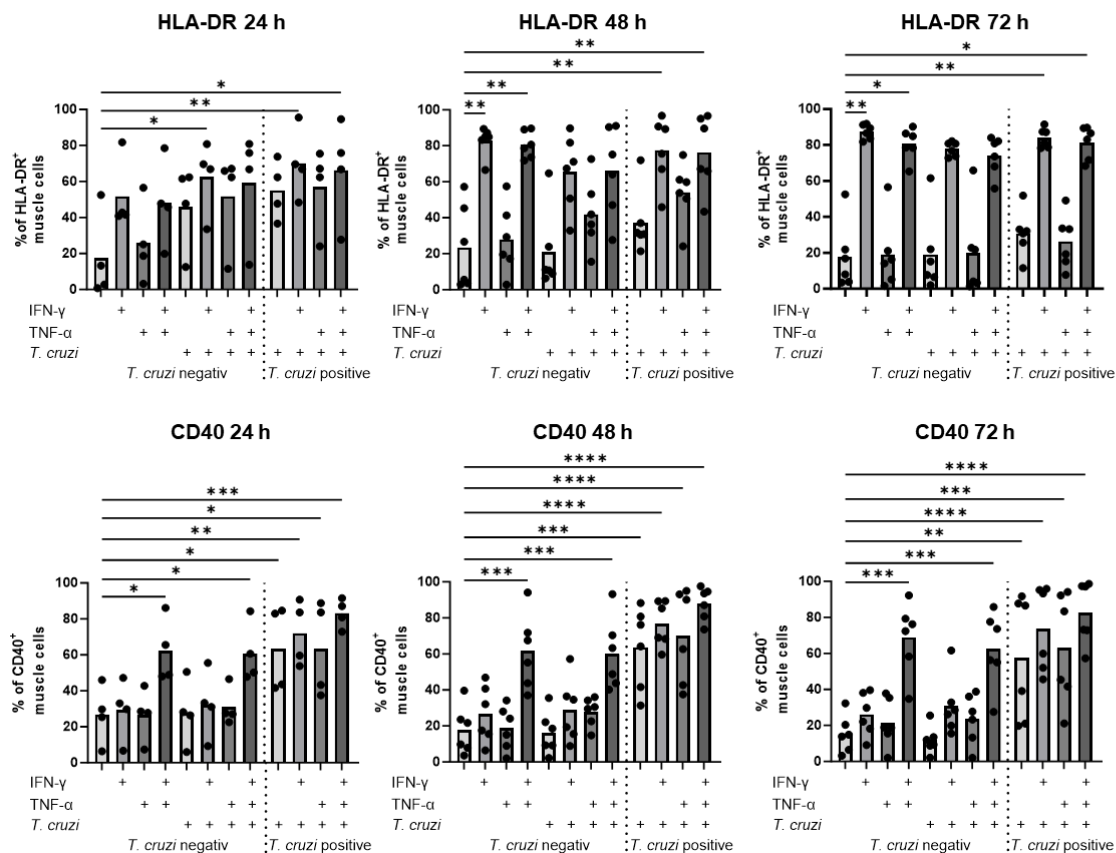


Figure 18: Human primary muscle cells express HLA-DR and CD40 and upregulate these receptors upon infection and stimulation with pro-inflammatory cytokines. Differentiated primary human muscle cells were infected with *T. cruzi* (MOI 5:1), stimulated with IFN- γ and TNF- α as indicated in the figure and harvested at 24, 48 and 72 h. Cells were surface stained with an AF-700-labelled antibody against HLA-DR and a Pacific blue-labelled antibody against CD40 and intracellularly stained for *T. cruzi* as previously described and then analysed by flow cytometry. Graphs and statistical analysis of HLA-DR and CD40-positive cells over time. Each point represents one donor; the respective means are shown as bars. After testing for normal distribution, statistical significance was calculated using RM one-way ANOVA (for normal distribution) or Friedman's test (for non-normal distribution): * $p \leq 0.05$; ** $p \leq 0.01$; *** $p \leq 0.001$; **** $p \leq 0.0001$.

After confirming that muscle cells express HLA-I and HLA-II, it was of interest to determine which antigens might be presented to immune cells by *T. cruzi*. Therefore, a transcriptomic analysis of *T. cruzi* amastigotes cultivated inside muscle cells for 48 h was conducted. The reads were mapped against the *T. cruzi* Brenner genome. The mean transcripts of the 30 most highly expressed *T. cruzi* genes are shown in Figure 19. These genes provide potential targets for immune cells to recognise intracellular amastigotes. The most highly expressed gene is enolase, followed by cyclophilin A and a pyruvate phosphate dikinase.

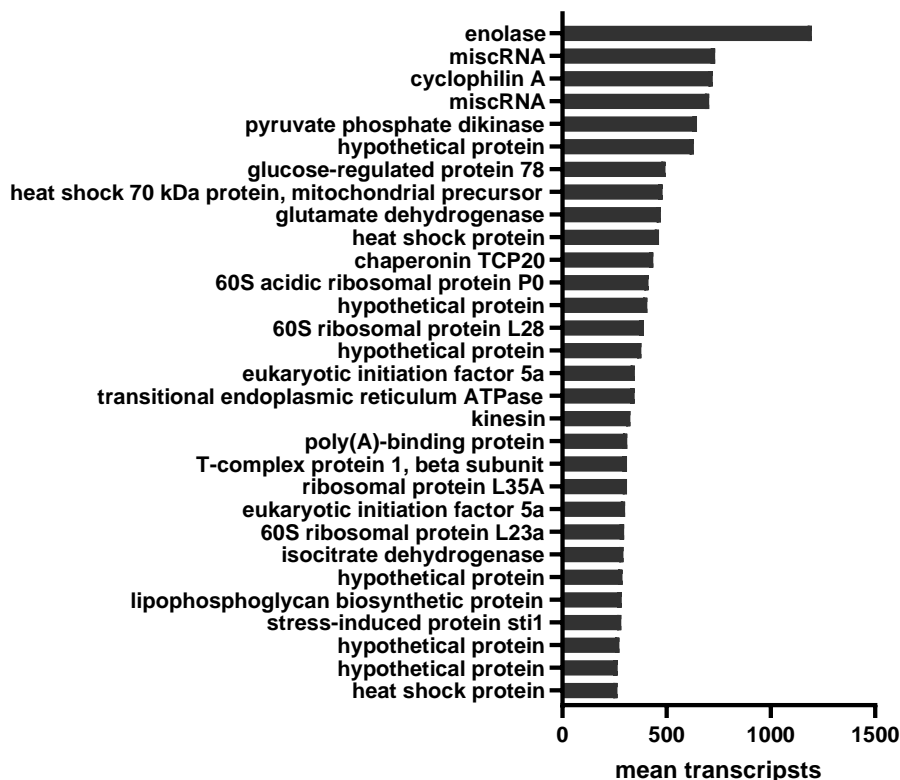


Figure 19: Highly expressed *T. cruzi* genes in muscle cells represent potential targets for HLA class I and II antigen presentation. Transcriptomic reads from *T. cruzi* Brazil amastigotes, cultivated in muscle cells for 48 h, were mapped against the genome of the *T. cruzi* Brenner strain. The figure shows the average transcripts of the 30 most highly expressed genes based on data from 5 samples.

4.6 Immunoregulatory mechanisms are induced in muscle cells

After the transcriptomic analysis revealed several genes involved in immune regulation, it was investigated whether mechanisms are induced in muscle cells which could potentially downregulate T cell activation. The transcriptomic analysis revealed the induction of the enzyme Indolamin-2,3-Dioxygenase 2 (IDO2) by IFN- γ stimulation. At the same time, IL-4I1 (Interleukin 4 Induced 1) was only induced upon IFN- γ stimulation and simultaneous infection with *T. cruzi*. IL-4I1 encodes for the enzyme L-amino acid oxidase and catalyses tryptophan. Both of these enzymes have been described to be involved in the kynurenine pathway, and the metabolites of this pathway activate the aryl hydrocarbon receptor (AHR). This transcription factor suppresses T cell proliferation and function by inducing the expression of programmed cell death protein 1 (PD1) on CD8⁺ T cells and even by inducing cell death ⁷.

To verify whether the enzyme IL-4I1 is secreted into the muscle cell supernatant and could potentially downregulate the CD8⁺ T cell response, the amount of IL-4I1 in the supernatant of

infected and IFN- γ -stimulated muscle cells was investigated over time using ELISA (Figure 20). IL-411 was only detectable in the supernatant of *T. cruzi*-infected and IFN- γ -stimulated muscle cells. After 48 h, an average of 840 pg/ml could be detected, and the amount increased to 1613 pg/ml after 72 h.

In line with the transcriptomic analysis, IL-411 was only detectable in the supernatant of *T. cruzi*-infected and IFN- γ -stimulated muscle cells, a phenomenon not observed before. This could be a new potential mechanism by which muscle cells can downregulate the T cell response during a *T. cruzi* infection.

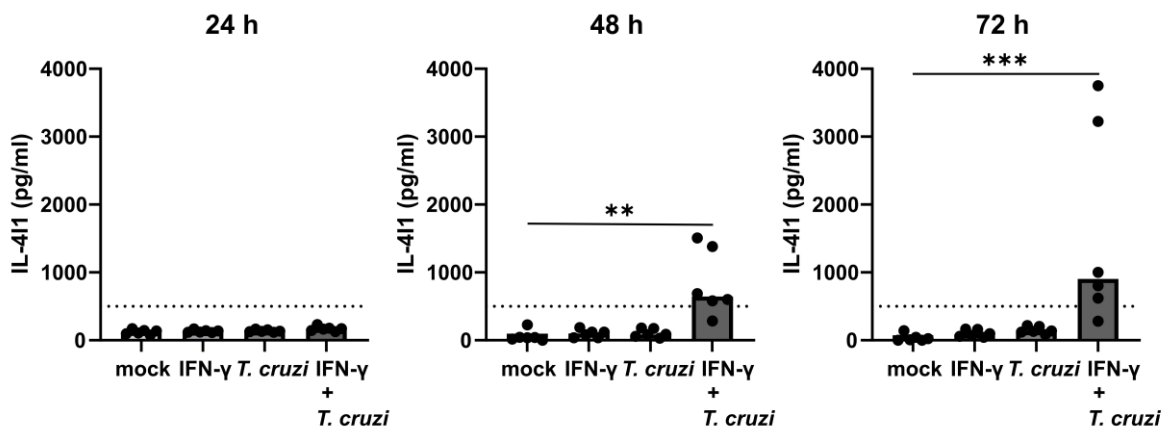


Figure 20: Muscle cells secrete IL-411 after infection with *T. cruzi* and simultaneous stimulation with IFN- γ . The supernatants of infected and stimulated muscle cells were collected at 24, 48 and 72 hpi. The concentration of IL-411 was determined in the supernatant of either mock-treated, *T. cruzi*-infected (MOI 5:1) and/or IFN- γ -stimulated primary muscle cells. The bars represent the respective mean values (n=6), and the dotted line indicates the detection limit of the ELISA. After testing for normal distribution, statistical significance was calculated using RM one-way ANOVA (for normally distributed data) or Friedman's test (for non-normally distributed data): ** p < 0.01; *** p < 0.001.

The transcriptomic analysis revealed the induction of the co-inhibitory receptor ligands PD-L1, PD-L2 and galectin-9 (Figure 10). PD-L1 and PD-L2 are the ligands of the co-inhibitory receptor PD-1. This receptor can be expressed on exhausted T cells, and the interaction with the ligands can lead to T cell anergy¹⁸⁸. In comparison, galectin-9 binds to TIM-3, a co-inhibitory receptor described to downregulate the T cell response and induce apoptosis in T cells¹⁰⁴.

Based on this, the expression of these receptors was investigated on the cell surface of the muscle cells by flow cytometry upon stimulation with IFN- γ and TNF- α (Figure 21). The analysis

revealed a significant induction of PD-L1 expression on the muscle cell surface upon stimulation with IFN- γ . The frequency of PD-L1-positive muscle cells increased compared to the mock control from 12 % to 64 % after 24 h, to 71 % after 48 and to 85 % after 72 h. A similar expression pattern could be observed in muscle cells that were additionally stimulated with TNF- α or infected with *T. cruzi*. The infection with *T. cruzi* alone did not affect PD-L1 expression.

The PD-L2 expression only showed a significant upregulation after IFN- γ and TNF- α stimulation in *T. cruzi*-positive cells after 24 h to 62 % compared to the control (25 %). After 48 hpi, a significant increase of PD-L2-positive and *T. cruzi*-positive muscle cells could be seen after stimulation with IFN- γ (to 66 %), TNF- α (to 62 %), or with both cytokines (to 68 %). The expression of PD-L2 on *T. cruzi*-positive cells stayed high at 72 hpi. After 72 h, an increase of PD-L2-positive muscle cells upon IFN- γ stimulation (47 %) was observed, although a higher amount expressing PD-L2 after IFN- γ stimulation (78 %) was detectable for *T. cruzi*-positive cells.

Low amounts of galectin-9 were expressed on the muscle cell surface. However, in *T. cruzi*-positive and IFN- γ stimulated muscle cells, a significant increase from 5 % to 20 % was observed after 24 hpi. The expression stayed stable after 48 hpi (16 %) and 72 hpi (17 %). The same effect could be detected for the additional stimulation with TNF- α .

Taking these results together, PD-L1 expression is upregulated upon IFN- γ stimulation. In contrast, PD-L2 can be upregulated by the infection and IFN- γ stimulation, but a higher frequency of *T. cruzi*⁺ muscle cells express the receptor. At the same time, galectin-9 seems to be predominantly upregulated in *T. cruzi*-positive cells.

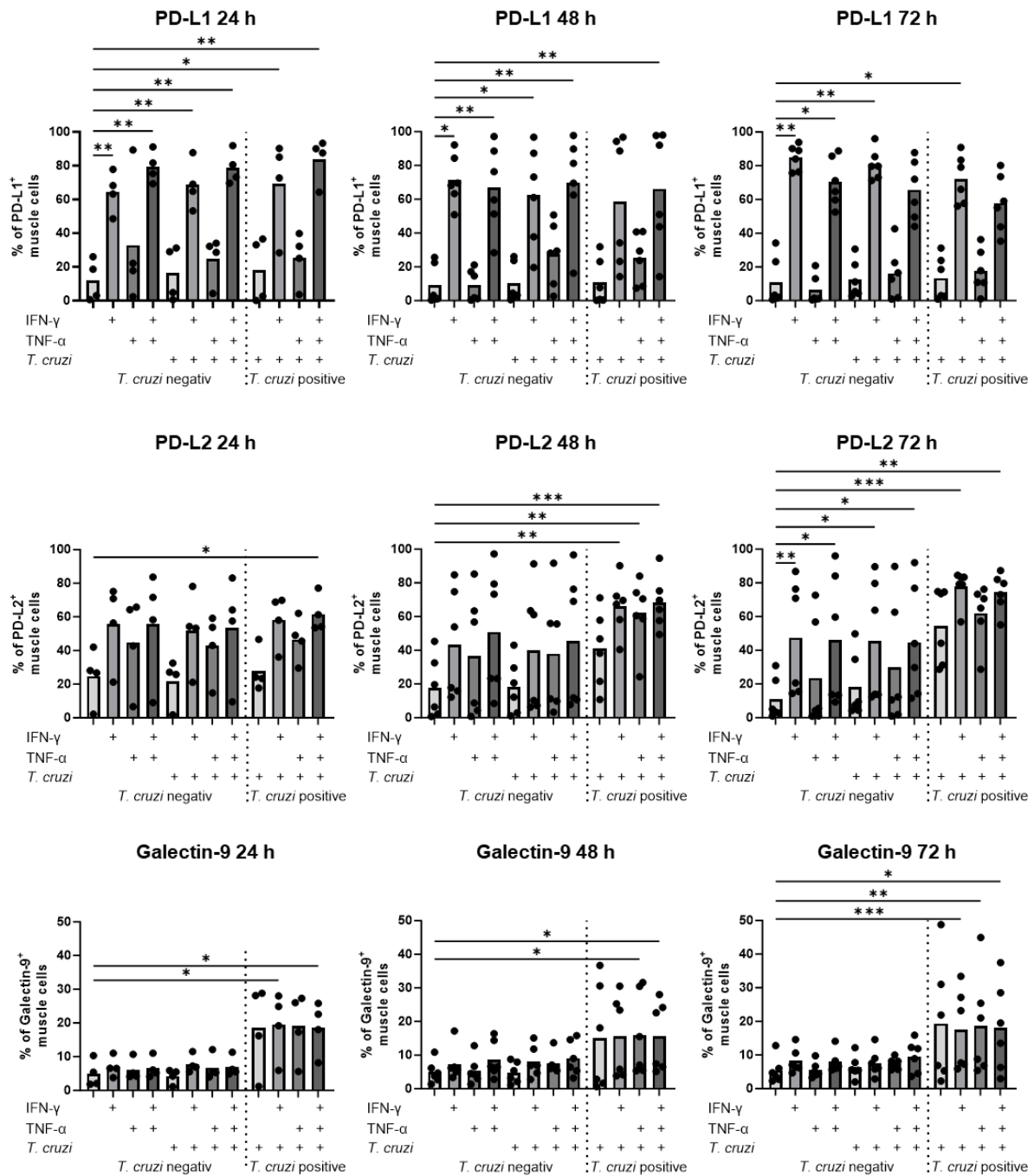


Figure 21: Human primary muscle cells express the co-inhibitory receptor ligands PD-L1, PD-L2, and galectin-9 and upregulate these receptors upon infection and stimulation with pro-inflammatory cytokines. Differentiated primary human muscle cells were infected with *T. cruzi* (MOI 5:1), stimulated with IFN- γ and TNF- α as indicated in the figure and harvested at 24, 48, and 72 hpi. Cells were surface stained with a BV421-labelled antibody against PD-L1, an AF-647-labelled antibody against PD-L2 and a PE-Cy7-labelled antibody against galectin-9. Cells were intracellularly stained for *T. cruzi* as described previously and analysed by flow cytometry. The graphs show the percentage of PD-L1, PD-L2 and galectin-9-positive cells and the statistical analysis over time. Each point represents data from one donor, with the respective mean values shown as bars. After testing for normal distribution, statistical significance was determined using RM one-way ANOVA (for normally distributed data) or Friedman's test (for non-normally distributed data): * $p \leq 0.05$; ** $p \leq 0.01$; *** $p \leq 0.001$.

Next, the supernatants of the infected and differently stimulated muscle cells were analysed for the co-inhibitory receptor ligands PD-L1, PD-L2, and galectin-9. It has previously been described that sheddases can enzymatically cut the extracellular part of these receptors off. Even though the function of these soluble forms is still being discussed, they seem to have an immune regulatory function¹⁸⁹. Moreover, it could be shown that apoptosis is induced in CD8⁺ and CD4⁺ T cells after exposure to soluble PD-L1¹⁹⁰.

Therefore, supernatants of muscle cells infected with *T. cruzi* and stimulated with IFN- γ and TNF- α were analysed for soluble forms of PD-L1, PD-L2, and galectin-9 via a bead-based immunoassay (Figure 22).

A significant increase of soluble PD-L1 could be seen in the supernatant of IFN- γ and TNF- α -stimulated muscle cells from 2 mg/ml (mock control) to 87 pg/ml after 24 h, to 66 pg/ml after 48 h, and to 230 pg/ml after 72 h. If the muscle cells were infected and stimulated with IFN- γ and TNF- α , even higher amounts of PD-L1 could be detected in the supernatant; an increase to 104 pg/ml after 24 hpi, 197 pg/ml after 48 hpi, and to 531 pg/ml after 72 hpi was visible. A statistically significant increase of PD-L1 was found in the supernatant of infected and IFN- γ -stimulated muscle cells after 48 hpi (34 pg/ml) and 72 hpi (103 pg/ml).

Significantly higher amounts of PD-L2 compared to the mock control were observed in all samples stimulated with pro-inflammatory cytokines after 48 h. For example, an increase from 33 pg/ml to 158 pg/ml after IFN- γ stimulation compared to the mock control was visible. Furthermore, the same concentration of soluble PD-L2 was present in the supernatant of *T. cruzi*-infected and stimulated muscle cells. The amount of PD-L2 increased after 72 h, for example, to 433 pg/ml in the case of IFN- γ stimulation.

For galectin-9, a significant increase of the soluble form could be observed in the supernatant of IFN- γ and TNF- α -stimulated muscle cells from 14 mg/ml (mock control) to 168 pg/ml after 24 h to 542 pg/ml after 48 h and to 1848 pg/ml after 72 h. Upon infection with *T. cruzi* and stimulation with IFN- γ and TNF- α , even higher amounts of galectin-9 were detected in the supernatant. In fact, an increase to 314 pg/ml after 24 hpi, 2288 pg/ml after 48 hpi, and to 4049 pg/ml after 72 hpi was detected. Here, a statistically significant increase of galectin-9 could be observed in the supernatant of infected and IFN- γ -stimulated muscle cells after 48 hpi (542 pg/ml) and 72 hpi (1413 pg/ml).

Results

Taken together, these results show that the co-inhibitory receptor ligands PD-L1, PD-L2, and galectin-9 can not only be expressed on the muscle cell surface but that the receptors are shed into the muscle cell supernatant, with galectin-9 being released in very high amounts.

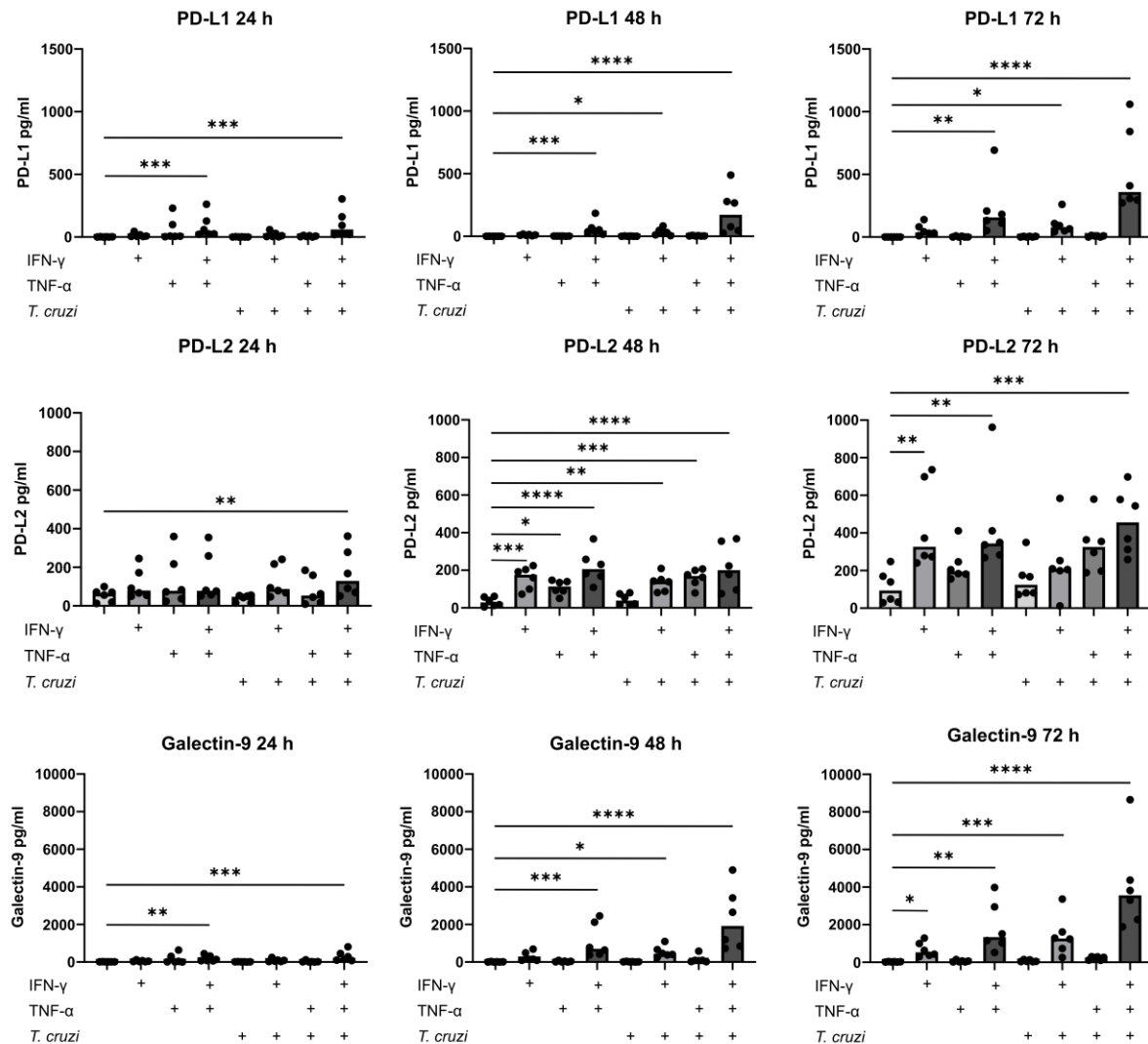


Figure 22: PD-L1, PD-L2 and galectin-9 are present in the supernatant after infection with *T. cruzi* and stimulation with IFN- γ and TNF- α . Concentration of PD-L1, PD-L2, and galectin-9 in the supernatant of mock, IFN- γ (100 IU/ml), TNF- α (100 IU/ml), IFN- γ , and TNF- α -stimulated, *T. cruzi*-infected (MOI 5:1) and stimulated muscle cells. Supernatants were collected at the indicated time points and analysed using a customised human LEGENDplex. Non-detectable values were set to 0. Each point represents one donor and the bars represent the respective means. After testing for normal distribution, statistical significance was calculated using RM one-way ANOVA (for normal distribution) or Friedman's test (for non-normal distribution): * $p \leq 0.05$; ** $p \leq 0.01$; *** $p \leq 0.001$; **** $p \leq 0.0001$.

To investigate whether galectin-9 could be found in chronic Chagas patients and could potentially play a key role in suppressing the immune response in humans, sera from Chagas

patients were analysed for galectin-9 using a bead-based immunoassay. The patients were recruited in villages in Columbia. They were screened for *T. cruzi* infection by PCR and their heart function was assessed to categorise the patients into indeterminate cases (*T. cruzi*-positive but no detectable impairment of heart function) or symptomatic cases where a cardiac dysfunction was already detectable. Patients showed very high levels of galectin-9 in their sera (Figure 23). Patients in the indeterminate phase of the disease showed a median of 18422 pg/ml galectin-9 in their serum, while patients with cardiac dysfunction showed a median of 8112 pg/ml. This difference is not statistically significant.

Considering these results, there may potentially be systemic immune suppression of Tim3⁺ T cells in Chagas patients by galectin-9.

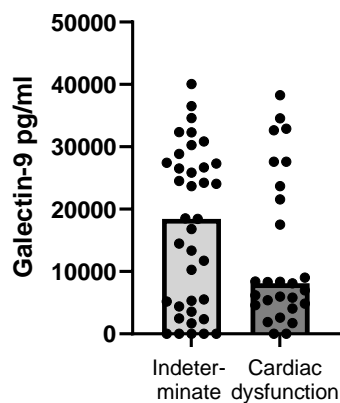


Figure 23: Patients with Chagas disease have soluble galectin-9 in their serum. Galectin-9 was analysed in the serum of patients from Columbia and analysed via LEGENDplex. Samples were divided into indeterminate cases, where *T. cruzi* was detected but there were no heart anomalies, and into patients who already showed signs of cardiac dysfunction. Non-detectable values were set to 0. Each point represents one donor, and the bars represent the respective median. After testing for normal distribution, statistical significance was calculated with a Mann-Whitney test. No statistical difference was detected.

4.7 Immunoregulatory mechanisms of the muscle cells reduce T cell proliferation *in vitro*

Lastly, whether the induction of these previously described immune regulatory mechanisms influences T cell activity was investigated. To this end, an assay was established to identify the effect of the muscle cells on T cell proliferation (Figure 24A).

Because this assay needed a high number of cells and to have a more uniform response, the human muscle cell line LHCN-M2 was used in these experiments. It could be shown in the previously described transcriptomic analysis that this cell line showed a very similar response to primary muscle cells (Figure 7). Flow cytometry analysis of different extracellular receptors was performed to compare the response to different stimuli and a comparable response was observed (data not shown).

T cells were isolated by positive selection using Iba-positive selection columns from PBMCs of healthy donors. The T cells were stained for CD4 and CD8 to determine the purity (the purity always exceeded 90 %); representative dot plots are shown in Figure 24B. The T cells were stained with the proliferation dye eFluor450 and incubated with α CD3/ α CD28-covered beads and IL-2. This led to a pre-activation of the T cells to mimic the natural activation of naïve T cells in the lymph node. After 18 h, the beads and the IL-2 were removed, and either IgG control antibodies or α -PD-1 or α -TIM-3 antibodies were added to the T cells. The antibodies used in this experiment were blocking antibodies, which inhibit the activation of the receptors they bind to by blocking the interactions with their ligands without activating them. In the meantime, differentiated muscle cells of the muscle cell line LHCN-M2 were infected with *T. cruzi* and stimulated with IFN- γ for 24 h. Afterwards, the remaining trypanosomes and the IFN- γ were washed away thoroughly, and the CD4⁺ and CD8⁺ T cells with the different antibodies were added to the muscle cells. After co-cultivation for 3 days, the T cells were removed and stained for CD4 (labelled with APC) and CD8 (labelled with AF700), and the proliferation was analysed by flow cytometry.

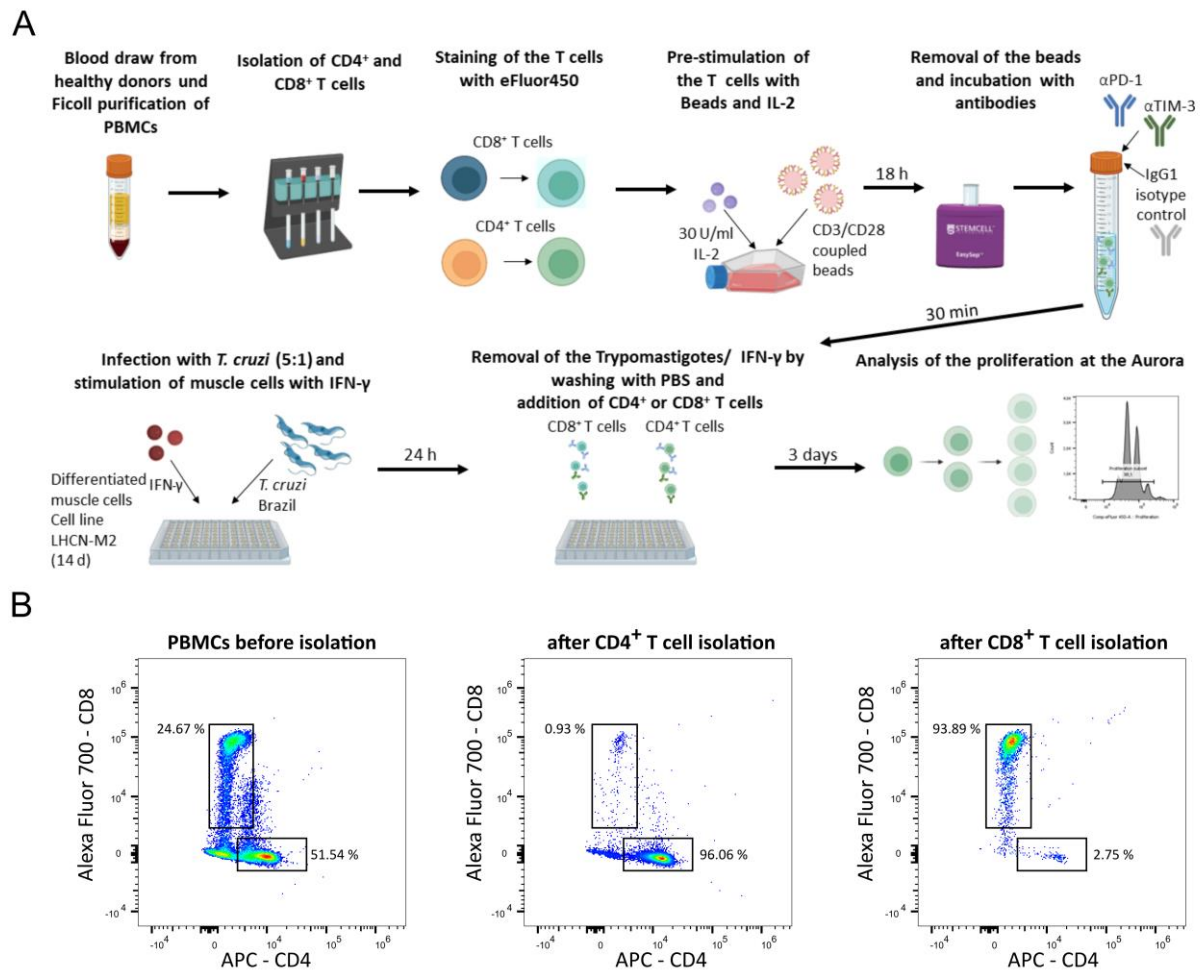


Figure 24: Co-culture of human donor CD4⁺ and CD8⁺ T cells with differently treated muscle cells.

A) T cells were purified from the blood of healthy human donors using Iba-positive selection columns, labelled with the proliferation dye eFluor450 and stimulated with α CD3/ α CD28 beads and IL-2. After 18 hours, the beads were removed using magnets and the T cells were incubated for 30 minutes with antibodies against PD-1, TIM-3, or an IgG1 isotype control. At the same time, differentiated muscle cells (cell line LHCN-M2) were infected with *T. cruzi* and stimulated with IFN- γ (100 IU/ml) for 24 hours. Any remaining trypomastigotes and IFN- γ were washed away, and the CD4⁺ and CD8⁺ T cells with the different antibodies were added. Proliferation was analysed on the Aurora flow cytometer using the decrease in intensity of the proliferation dye eFluor450 as an indicator of proliferation. B) Successful isolation and purity of CD4⁺ and CD8⁺ T cells were confirmed by staining with AF-700-labelled antibodies against CD8 and APC-labelled antibodies against CD4. Representative staining of PBMCs before and after CD4 and CD8 T cell isolation are shown.

The co-culture revealed that CD4⁺ and CD8⁺ T cells incubated with unstimulated muscle cells showed a significantly reduced proliferation compared to T cells incubated with α CD3/ α CD28 beads (Figure 25 A). Reduced proliferation from 90 % to 58 % could be observed for CD8⁺ T cells, with a reduction from 96 % to 61 % for CD4⁺ T cells. The co-cultivation with *T. cruzi*-infected muscle cells significantly reduced proliferation to 51 % and 58 % for CD8⁺ and CD4⁺ T

cells, respectively. This shows that the muscle cells already have a T cell suppressing phenotype at steady state conditions, and a *T. cruzi* infection only induces a slightly higher suppressive state in muscle cells.

Upon stimulation with IFN- γ , muscle cells could suppress T cell proliferation even more, with the percentage of proliferated T cells dropping to 26 % and 13 % for CD8⁺ and CD4⁺ T cells, respectively. For *T. cruzi*-infected and IFN- γ -stimulated muscle cells, a reduction in proliferation to 30 % and 13 % for CD8⁺ and CD4⁺ T cells, respectively, could be detected.

The next step was to investigate whether the co-inhibitory receptor ligands PD-L1 and PD-L2, which bind to PD-1 on the T cell side, and galectin-9, which binds to TIM-3, are responsible for the suppression. Representative histograms of the proliferation of CD8⁺ and CD4⁺ T cells after the co-culture and inhibition of the co-inhibitory receptors PD-1 and TIM-3 are shown in Figure 25B and D. The proliferation of the T cells increased after the incubation with blocking antibodies against PD-1 and TIM-3. Additionally, the effect of these two antibodies was similar, but the combination of both antibodies did not have a synergistic effect. Moreover, it is possible to see, that the amount of T cells that proliferated and the amount of proliferation steps compared to the mock control were lower for the co-culture with IFN- γ stimulated muscle cells.

The percentage of proliferated CD8⁺ T cells was calculated and is shown in Figure 25C. To account for inter-experimental diversity, the amount of proliferated T cells was normalised to the control, which was only stimulated with α CD3/ α CD28 beads. For mock-infected muscle cells, there was an apparent increase in the proliferation rate of CD8⁺ T cells from 66 % to 88 % after incubation with an α PD-1 antibody compared to an IgG isotype control. The same applies for *T. cruzi*-infected muscle cells (increase from 58 % to 85 %). While IFN- γ stimulation of muscle cells reduced the proliferation to 30 % for the IgG Isotype control, incubation with an α PD-1 antibody increased the proliferation to 54 %. Again, comparable results were observed after the co-culture with infected and IFN- γ -stimulated muscle cells, from 35 % after adding an IgG antibody to 63 % after adding α PD-1.

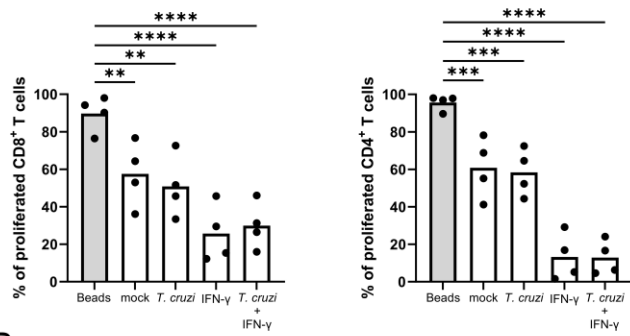
The results for CD4⁺ T cells show the same trend upon co-cultivation with muscle cells and the addition of α PD-1 and α TIM-3 antibodies (Figure 25E). However, IFN- γ stimulated muscle cells could reduce the proliferation of CD4⁺ T cells even more than the proliferation of CD8⁺ T cells,

with a decrease to 14 % after the addition of an IgG antibody, and the addition of an α PD-1 antibody increasing the proliferation to 45 %.

Combining these results, muscle cells already exhibit a suppressive phenotype for T cells in steady-state conditions. This phenotype is primarily caused by the expression of ligands of the co-inhibitory receptors PD-1 and TIM-3, as blocking these receptors can significantly improve T cell proliferation to nearly 90 %. While IFN- γ stimulation increases their suppressive capacity, this effect is only partially dependent on T cell suppression by PD-1 and TIM-3; adding these antibodies can only increase the proliferation to about 50 % of the control.

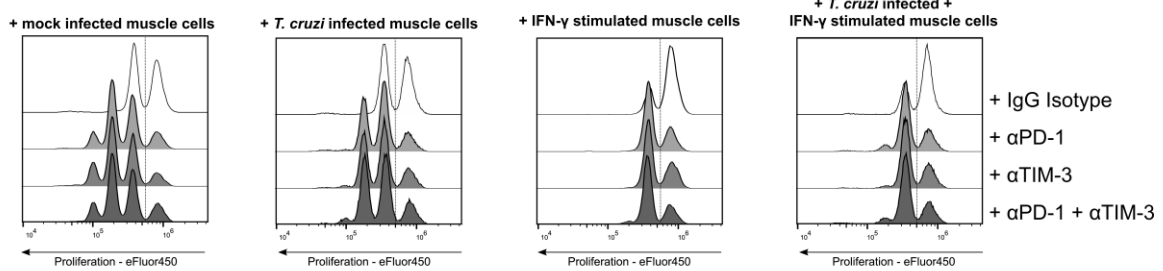
Co culture of CD8⁺ and CD4⁺ T cells with muscle cells

A



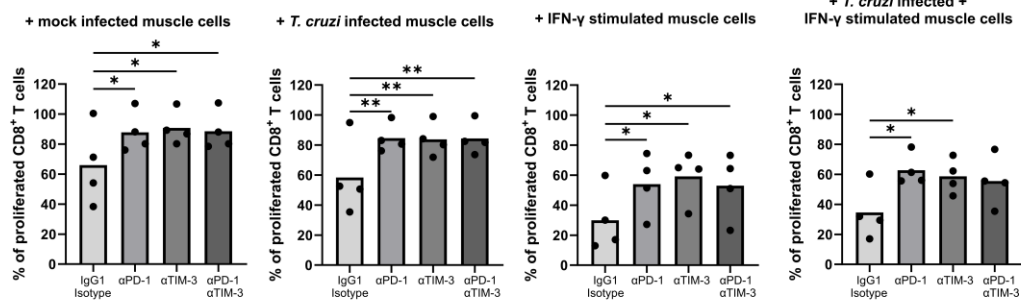
B

CD8⁺ T Zellen



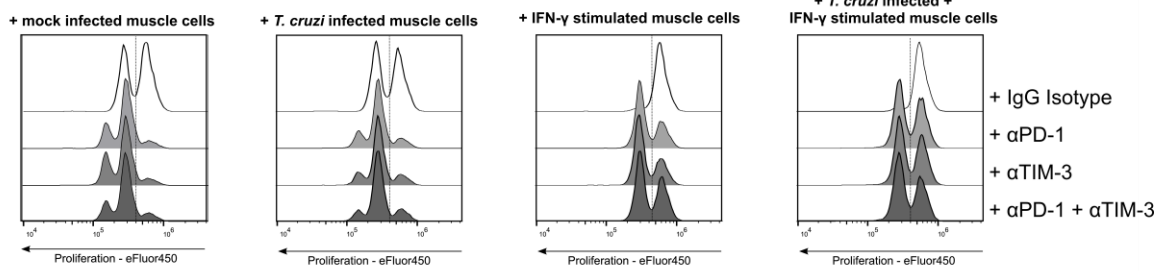
C

CD8⁺ T Zellen



D

CD4⁺ T Zellen



E

CD4⁺ T Zellen

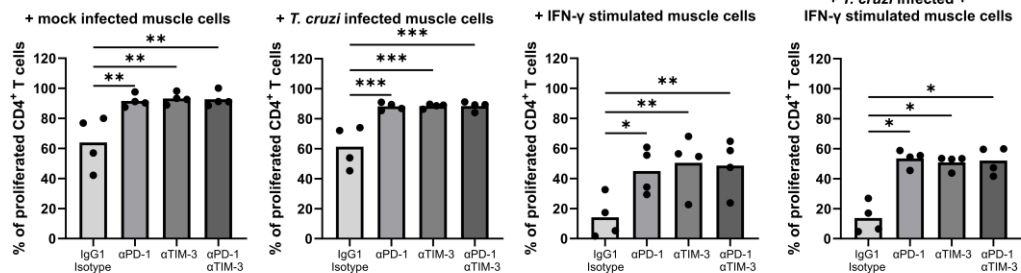


Figure 25: Proliferation of CD8⁺ and CD4⁺ T cells from human donors is reduced after co-incubation with differently treated muscle cells. A) Proliferation of CD8⁺ and CD4⁺ T cells is reduced after co-incubation with mock-infected, *T. cruzi*-infected, IFN- γ (100 IU/ml) stimulated, and *T. cruzi*-infected and IFN- γ -stimulated muscle cells compared to T cells stimulated with α CD3/ α CD28 beads alone. B) and D) Representative histograms of CD8⁺ and CD4⁺ T cells incubated with α PD-1 and α TIM-3 antibodies after co-incubation with differently treated muscle cells. C) and E) Graphs and statistical analyses of CD8⁺ and CD4⁺ T cells incubated with α PD-1 and α TIM-3 antibodies after co-incubation with variously treated muscle cells, normalised to control cells stimulated with α CD3/ α CD28 beads only. Each point represents data from one donor (each condition was performed in duplicates or triplicates; n=4), and the bars represent the respective means. After testing for normal distribution, statistical significance was calculated using RM one-way ANOVA (for normally distributed data) or Friedman's test (for non-normally distributed data): * p \leq 0.05; ** p \leq 0.01; *** p \leq 0.001; **** p \leq 0.0001.

Interestingly, it could be shown in the co-culture that muscle cells stimulated with IFN- γ use other suppressive mechanisms besides the expression of the co-inhibitory receptor ligands PD-L1, PD-L2, and galectin-9. As could be observed in the co-culture, the addition of α -TIM-3 and α -PD-1 antibodies could only increase the proliferation to about 50 % of the bead control, and the antibodies were not able to increase the proliferation of T cells in the same manner, as observed for unstimulated or *T. cruzi*-infected muscle cells. Therefore, other co-inhibitory receptors were investigated for their expression on muscle cells to potentially explain the higher suppressive capacity. A deeper transcriptomic analysis revealed an induction of *NECTIN2*, the gene for the co-inhibitory receptor ligand CD122 in IFN- γ -stimulated and infected muscle cells, with a log-fold change of 1. CD122 can bind to the co-inhibitory receptor TIGIT¹⁹¹. The other receptor that can bind to TIGIT is the receptor CD155, which is mainly known as an extracellular receptor involved in forming junctions with neighbouring cells. Another well-described co-inhibitory receptor ligand is Herpes Virus Entry Mediator (HVEM). This ligand can bind to the co-inhibitory receptor B and T-lymphocyte attenuator (BTLA) and CD160¹⁹².

Therefore, CD122, CD155, and HVEM were analysed for their expression on the muscle cell surface after infection and stimulation with IFN- γ and TNF- α . The results of the flow cytometry analysis can be seen in Figure 26.

The expression of CD122 seems to be highly dependent on the muscle cell donor, with some donors showing a low baseline expression and some having a higher expression without any addition of the stimulus. However, a significant increase of the expression could be detected overall 48 h after the stimulation with IFN- γ and TNF- α , from 35 % of CD122-positive muscle

cells to 64 %. More *T. cruzi*-positive muscle cells stimulated with IFN- γ showed expression of CD122 (69 %).

CD155 was constitutively expressed by muscle cells, and the amount of CD155-positive cells did not change significantly after infection with *T. cruzi* or stimulation with IFN- γ or TNF- α .

HVEM expression was significantly increased in muscle cells after the stimulation with IFN- γ after 24 h (from 9 % HVEM-positive muscle cells of the control to 39 %). Moreover, the number of HVEM-positive cells increased even further to 46 % after 48 h and to 62 % after 72 h. However, no statistically significant increase of the HVEM expression was visible in *T. cruzi*-positive muscle cells, even after an additional IFN- γ stimulation. Therefore, the expression of HVEM might be responsible for the higher suppressive capacity of IFN- γ stimulated muscle cells besides the expression of PD-L1, PD-L2 and galectin-9.

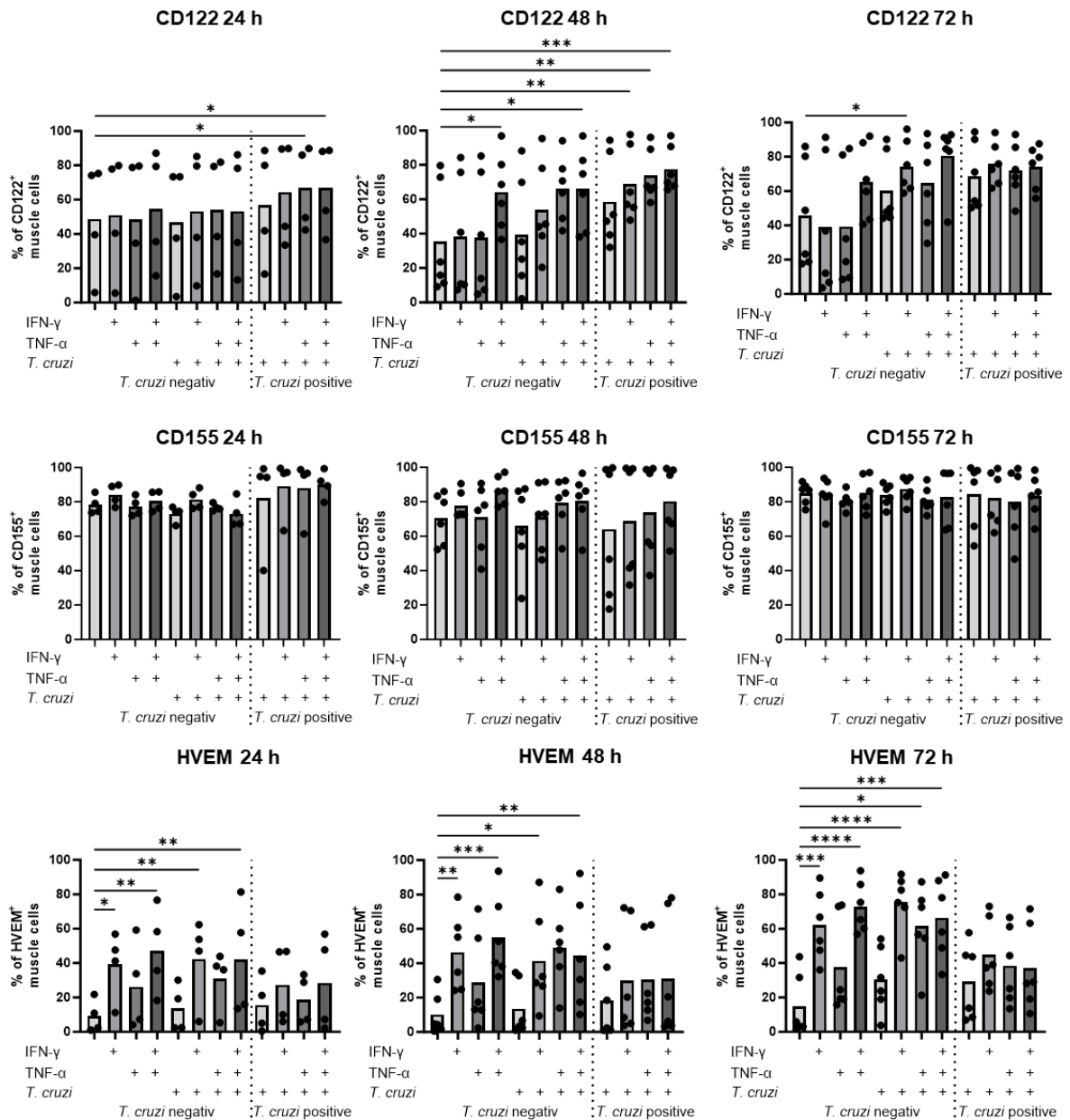


Figure 26: Human primary muscle cells express the co-inhibitory receptor ligands CD155, CD122, and HVEM and upregulate these receptors upon infection and infection and stimulation with pro-inflammatory cytokines. Differentiated primary human muscle cells were infected with *T. cruzi* (MOI 5:1), stimulated with IFN- γ (100 IU/ml) and TNF- α (100 IU/ml) as indicated in the figure and harvested at 24, 48, and 72 hpi. Cells were surface stained with an APC-labelled antibody against CD155, a PerCP-Cy5.5-labelled antibody against CD122 and a PE-labelled antibody against HVEM. Cells were intracellularly stained for *T. cruzi* as described previously and analysed by flow cytometry. The graphs show the percentage of CD155, CD122, and HVEM-positive cells and the statistical analysis over time. Each point represents data from one donor, with the respective mean values shown as bars. After testing for normal distribution, statistical significance was determined using RM one-way ANOVA (for normally distributed data) or Friedman's test (for non-normally distributed data): * $p \leq 0.05$; ** $p \leq 0.01$; *** $p \leq 0.001$; **** $p \leq 0.0001$.

5. Discussion

The present study aimed to elucidate the pathways activated in muscle cells following *T. cruzi* infection and their subsequent immunomodulatory capabilities. Furthermore, the effects of a pro-inflammatory environment present during a *T. cruzi* infection on immunomodulatory mechanisms were investigated. To this end, primary human myoblasts were differentiated *in vitro* to explore their responses. Altogether, the results confirmed that muscle cells detect *T. cruzi* infection and activate anti-parasitic mechanisms, notably iNOS induction, reducing the parasite burden. Transcriptomic profiling revealed additional intracellular pathways that might inhibit parasite replication. A pro-inflammatory environment amplified the anti-parasitic response, limiting both the number of infected muscle cells and intracellular parasite development. In addition, a phenotypical analysis of muscle cells was performed, highlighting the relevance of co-inhibitory receptor ligand expression. The expression of these ligands resulted in a suppression of T cells by muscle cells via PD-1 and TIM-3 receptor interactions. Moreover, we found that infected muscle cells secrete IL-4I1, which might be a potential factor in T cell suppression during *T. cruzi* infection. These findings reveal that muscle cells play multifaceted immunoregulatory roles, suggesting that singular pathway inhibition might not sufficiently augment T cell activity.

5.1 Sensing of *T. cruzi* infection and induction of an anti-parasitic response in muscle cells

In line with studies of *T. cruzi* infection in fibroblasts, the present transcriptional analysis demonstrated the upregulation of anti-parasitic or anti-viral proteins in skeletal muscle cells (Figure 9)^{193,194}. In primary fibroblasts and primary skeletal muscle cells, MX1 (interferon-induced GTP-binding protein MX1) was the highest differently expressed gene upon *T. cruzi* infection¹⁹⁴. MX1 has been described as a resistance factor against viral infections by interacting with the ribonucleoprotein complex during influenza infections¹⁹⁵. The upregulation in both cell types might reveal an essential role during the *T. cruzi* infection. However, further investigation of how this protein can impact *T. cruzi* replication is needed. Moreover, the infection induced genes such as RSAD2, OASL, CMPK2, OAS1, MX2, OAS2, and OAS, which are known to inhibit the transcription and translation of viruses and bacteria^{169,171,172}. These genes belong to the interferon-regulated gene family (ISG), and their

expression is triggered by interferons.¹⁹⁶ Indeed, in skeletal muscle cells, IFN- γ stimulation increased the expression of these genes (Figure 9).

Interferons are evolutionally conserved signalling proteins used by cells to communicate with nearby cells to heighten their anti-viral defences⁴⁷. They can bind to the interferon- α and - β receptors, activate the JAK-STAT signalling pathway and induce gene transcription. STAT1 was significantly up-regulated in muscle cells both during a *T. cruzi* infection and by IFN- γ stimulation (Figure 10). Depending on the receptor and signalling cascade involved in its activation, STAT1 binds to adaptor proteins and induces transcriptional changes. Upon stimulation with type I interferon, this transcription factor can form a heterotrimeric transcription factor complex with STAT2 and IFN regulatory factor 9 (IRF9), which were also upregulated in muscle cells in *T. cruzi* infection and IFN- γ stimulation¹⁹⁷. STAT1 is an essential transcription factor involved in controlling the parasite during the infection with *T. cruzi*¹⁹⁸. The absence of STAT-1 resulted in a more robust infection, with increased numbers of parasites in the blood and tissues and significantly decreased survival rates. Moreover, IFN- γ -dependent activation of STAT1 reduced the susceptibility of human cells to infection with *T. cruzi*¹⁹⁹. Additionally, IFN- γ -induced activation of STAT1 upregulated iNOS transcription in macrophages²⁰⁰. *T. cruzi* is highly susceptible to iNOS-dependent killing, as the parasite lacks two crucial reductase systems to neutralise reactive oxygen species²⁰¹. Furthermore, pathogenic *T. cruzi* strains can reduce iNOS production in macrophages to evade this intracellular defence mechanism²⁰².

Therefore, it can be assumed that a defence response is induced via IFN- γ and STAT1-dependent induction of anti-viral genes in IFN- γ -stimulated muscle cells. However, for *T. cruzi*-infected skeletal muscle cells, the GO-term enrichment analysis revealed cellular response to type I interferons as the second highest enriched GO-term (Figure 9). Moreover, skeletal muscle cells were shown to upregulate ISG-related proteins upon stimulation with IFN- β ²⁰³. This indicates that a type 1 interferon response takes place upon *T. cruzi* infection in skeletal muscle cells and leads to autocrine and paracrine stimulation.

Nevertheless, the question remains how infected muscle cells sense the presence of intracellular amastigotes. It has been described that cells can sense parasites through pattern recognition receptors, which are present inside the cytosol or in other cellular compartments like the endosome²⁰⁴. For macrophages, it has been shown that TLR-9 can sense double-

stranded DNA from *T. cruzi* and, in conjunction with TLR-2, increase cytokine production in a MyD88-dependent manner^{51,205}. Moreover, previous studies have shown that TLR2 and TLR-4 can sense the trypomastigote's cell surface lipids, the glycosylphosphatidylinositol anchor and glycoinositolphospholipids, respectively^{50,206}. However, in this study, there was no induction of the expression of these three receptors in the transcriptomic analysis. Nevertheless, the transcriptomic analysis revealed increased expression of the pattern recognition receptor Toll-like receptor 3 (TLR3) and RNA helicase retinoic acid-inducible gene I (RIG-1) (Figure 10). These receptors sense double-stranded RNA (dsRNA) in the endosome (TLR3) or the cytosol (RIG-1)^{176,207}. Although RIG-1 has not been described to be involved in *T. cruzi* sensing so far, it has been discussed that RIG-1 can sense double-stranded DNA (ds-DNA) by converting ds-DNA to ds-RNA through RNA Polymerase III²⁰⁸. Although TLR3 and RIG-1 have mainly been described to sense viral double-stranded RNA, it could be hypothesised that these pattern recognition receptors can also sense the ds-RNA of *T. cruzi*. However, a study by Chessler et al. in fibroblasts and macrophages investigated the *T. cruzi*-dependent release of IFN- β and showed that the release was independent of Toll-like receptor signalling and RIG-1²⁰⁹. The authors hypothesised that a pathway of *T. cruzi* sensing involving TBK-binding kinase one and IFN regulatory factor 3 exists, but this has not yet been described in further detail²⁰⁹. Therefore, it will be necessary to further investigate how exactly skeletal muscle cells sense *T. cruzi*, especially considering that, in contrast to viruses, *T. cruzi* parasite replication is not performed in the cytosol, the parasites are surrounded by a plasma membrane. Therefore, the RNA and DNA of the parasite would not be accessible to receptors in the cytosol.

Taken together, the induction of TLR3, RIG-I, STAT1, STAT2 and IRF9 and of genes that are part of the ISG was shown. This may indicate direct sensing of the pathogen inside the muscle cells, a subsequent production and release of type I interferons and activation of non-infected muscle cells and STAT1-dependent gene transcription of anti-viral proteins. These proteins could inhibit pathogen proliferation by blocking RNA synthesis or degrading ds-RNA, thereby limiting parasite distribution. Thus, it would be interesting to investigate the supernatant of infected muscle cells for type I interferons released by the skeletal muscle cells, particularly because for fibroblasts and macrophages, an induction of IFN- β could already be shown upon *T. cruzi* infection¹⁹⁴.

The transcriptomic analysis alone cannot decipher the complex signalling cascade elicited in muscle cells after a *T. cruzi* infection. Hence, a deeper analysis of the protein expression, phosphorylation status and the secretion of type I interferons would be necessary to determine how an infection with *T. cruzi* is sensed, which signalling pathways are activated and which cytokines are released.

5.2 Reduced parasite replication in muscle cells by pro-inflammatory cytokines is due to the induction of anti-parasitic mechanisms

Primary human skeletal muscle cells showed fewer infected cells and fewer parasites inside the cells upon stimulation with the pro-inflammatory cytokines IFN- γ and TNF- α using flow cytometry analysis and immunofluorescence (Figures 12 and 13). Moreover, combining IFN- γ and TNF- α strengthened the cells' defence against *T. cruzi*, indicating these proteins might limit the parasite's growth. IFN- γ was described as one of the most essential iNOS-activating factors, and it directly induced the expression of iNOS²¹⁰. In line with this, a high proportion of muscle cells produced iNOS (Figure 14) and the inhibition of iNOS by the selective iNOS inhibitor L-Nil could improve parasite growth inside the muscle cell (Figure 15). Furthermore, electrophoretic mobility shift assay analysis in macrophages revealed that STAT1 is essential for IFN- γ -inducible iNOS expression²¹¹, suggesting that the observed upregulation of STAT1 expression in infected muscle cells could lead to the induction of iNOS.

This enzyme catalyses the formation of nitrogen oxide (NO) from L-arginine. NO can either directly kill parasites or limit the parasite's growth²¹². Muscle cells express neuronal NOS (nNOS) and endothelial NOS (eNOS) constitutively and can express iNOS upon inflammation²¹³. For *Toxoplasma gondii* infection, induction of iNOS in skeletal muscle cells and reduced parasite growth upon IFN- γ stimulation has previously been reported²¹⁴. Moreover, the mechanism of iNOS-dependent killing of *T. cruzi* parasites has been demonstrated in macrophages²¹⁵. However, this is the first description of skeletal muscle cells producing higher amounts of iNOS upon *T. cruzi* infection and the inhibition of *T. cruzi* development inside the muscle cell through the expression of this enzyme.

For macrophages, IFN- γ is described to induce iNOS, while TNF- α was also essential for parasite clearance²¹⁰. Furthermore, in skeletal muscle cells, IFN- γ significantly inhibited the

growth of the parasite *Toxoplasma gondii* via iNOS production ²¹⁴. Here, an increased expression of iNOS in skeletal muscle cells was also observed upon stimulation with the pro-inflammatory cytokines (supplement Figure 27). This data suggests that skeletal muscle cells stimulated with pro-inflammatory cytokines might be able to reduce the parasite burden even more.

The immunofluorescence images showed that there was a reduction not only in the number of infected cells, but also the numbers of parasites visible in skeletal muscle cells infected and stimulated with pro-inflammatory cytokines, primarily upon stimulation with both IFN- γ and TNF- α (Figure 13). In mouse studies, *T. cruzi* parasites displayed reduced proliferation rates in the chronic phase of the disease in smooth muscle cells of the gastrointestinal tract ²¹⁶. Here, a DNA-incorporating dye was used to provide 'snapshots' of the parasite replication status. Amastigotes in the chronic stage of the disease were three times less likely to be in the S-phase of the cell cycles than in the acute stage of the infection. For the related protozoan parasite *Leishmania major*, it could be shown that iNOS inhibited the metabolic activity of intracellular parasites without necessarily killing them ²¹⁷. Consistently, in preliminary experiments of the present study, it could be demonstrated that not only does the amount of *T. cruzi*-positive cells decrease over time, but the release of trypomastigotes into the media also decreases upon stimulation with pro-inflammatory cytokines. The combination of IFN- γ and TNF- α significantly reduced the release of trypomastigotes after 96 hpi for one donor (Supplement Figure 28).

5.3 *T. cruzi* infection leads to downregulation of genes in skeletal muscle cells

To identify genes essential for the persistence of *T. cruzi* in muscle cells and potential targets to inhibit *T. cruzi* development, the transcriptome of infected and IFN- γ -stimulated muscle cells was compared. Six genes showed a significant downregulation upon infection with *T. cruzi* (Figure 11). The highest downregulated transcript was *TRIM-17* (tripartite motif family-17), which encodes a ubiquitin ligase involved in multiple processes, including apoptosis, autophagy and cell division and has been described to be upregulated by cellular stress ¹⁷⁸. It can only be speculated how TRIM-17 is involved in the cellular process during a *T. cruzi* infection. However, it has been described to have a pro-apoptotic function by leading to the degradation of the anti-apoptotic protein induced myeloid leukemia cell differentiation

protein (MCL1)²¹⁸. Therefore, downregulation by TRIM-17 might inhibit premature apoptosis of the muscle cells before the amastigotes have developed into infectious trypomastigotes. Moreover, TRIM-17 was revealed to have a complex role in the induction of autophagy, recruiting autophagic factors in a localised and limited area of the cell but also inducing degradation of some targets, such as p62, IFT20, TRIM-5 α or TRIM-22²¹⁹. In line with this, it has been reported that autophagy plays a protective role during *T. cruzi* infection²²⁰. Selective autophagy has been described to promote the elimination of *T. cruzi* amastigotes from macrophages and cardiac cells²²¹. Therefore, TRIM-17 might be essential for muscle cells' autophagic degradation of *T. cruzi*.

While the transcriptional co-activator *CIITA* was upregulated in *T. cruzi*-infected muscle cells, its expression was significantly lower in *T. cruzi*-infected and IFN- γ -stimulated muscle cells compared to IFN- γ -stimulated muscle cells. The expression of *CIITA* induces HLA-II expression upon IFN- γ stimulation in a STAT1-dependent manner²²². An immune evasion mechanism by *T. cruzi* infection is to downregulate the MHC-II molecules on antigen-presenting cells, thereby limiting the T cell stimulatory activity of dendritic cells²²³. Consequently, the downregulation of antigen-presenting receptors on muscle cells might also have an immune regulatory effect. However, no downregulation of the protein HLA-DR could be seen in FACS staining of *T. cruzi*-infected and IFN- γ -stimulated muscle cells (Figure 18). Further studies inhibiting *CIITA* potentially by silencing RNA (siRNA) have to be performed to determine the influence on the expression of different HLA class II molecules, like HLA-DR, on muscle cells.

Additionally, the infection led to a significant downregulation of the matrix metalloprotease MMP25 gene and its antisense RNA. The expression of this matrix-metalloprotease could be found in cancer and has been associated with T cell, neutrophil and monocyte infiltration¹⁸¹. It could also be demonstrated that MMP25 expression increased neutrophil infiltration, generated pro-phagocytic signals upon vimentin cleavage and increased phagocytic removal of neutrophils to resolve inflammation²²⁴. IFN- γ can induce MMP25 expression, and the overexpression of the antisense RNA of MMP25, MMP25-AS1, significantly reduces MMP25 mRNA and protein expression in primary human colonic epithelial and human small intestinal epithelial cells *in vitro*²²⁵. Therefore, by downregulating MMP-25, *T. cruzi* might inhibit immune cell recruitment.

5.4 Immune cell recruitment and modulation by secretion of chemokines and cytokines

Muscle cells can secrete different immune-recruiting chemokines and cytokines after stimulation with pro-inflammatory cytokines. The secretion of IL-6, IL-8, IL-15 and CCL19 was observed, and it was evident that TNF- α significantly enhanced the secretion (Figure 16). In contrast, anti-inflammatory cytokines such as IL-10 and TGF- β could not be detected in the supernatant (data not shown).

IL-6 production has been described as a response to infections and tissue injuries and contributes to host defence against pathogens^{226,227}. A *T. cruzi* infection triggers the production of IL-6 during the acute phase of the disease and plays a crucial role in limiting parasitaemia^{228,229}. IL-6 is involved in various immune processes stretching from neutrophil infiltration at the site of infection to the shaping of the T cell response²³⁰. Furthermore, it has been shown to induce the differentiation of CD8⁺ T cells into cytotoxic T cells, which are essential in killing infected muscle cells²³¹.

IL-15 is expressed in the skeletal muscle and could be shown to be upregulated by IFN- γ and TNF- α ¹⁸⁵. IL-15 stimulation is involved in the maturation process of NK cells²³². NK cells are essential during the early immune response against *T. cruzi* because they can kill *T. cruzi*-infected cells and could even be shown to kill free trypomastigotes directly^{58,194}. IL-15 is closely related to IL-2 and is a critical cytokine involved in T cell proliferation, function and survival²³³. It has been shown to provide a survival signal to effector CD8⁺ T cells during the responses to *Listeria* infection²³⁴. Additionally, IL-15 can be trans-presented with the IL-15 receptor, stimulating memory CD8⁺ T cells²³⁵.

IL-8 is a chemoattractant of neutrophils²³⁶. Indeed, during the acute phase of a *T. cruzi* infection, neutrophils were recruited to the skeletal muscle in mice (data not shown). Neutrophils are involved in parasite clearance by phagocytosis and secretion of extracellular traps but can also induce tissue damage²³⁷. Moreover, IL-8 could promote the bacterial killing of neutrophils in the lung²³⁸. Additionally, it could be shown to be involved in the recruitment of T cells by chemokines released by the neutrophils¹⁸⁶. Consequently, increased IL-8 might enhance neutrophil and T cell numbers and consequently reduce parasite burden.

CCL19 is described to be abundantly expressed by endothelial cells in the lymph nodes and the thymus and is involved in the recruitment of T cells to these organs through the chemokine receptor CCR7¹⁸⁷. Here, naive T cells and a subset of memory T cells survey these secondary

lymphoid tissues for antigens⁴⁷. However, it can be expressed by other cell types in smaller amounts, like bone marrow stromal cells, and stimulation with IFN- γ and TNF- α increased the transcription of this chemokine²³⁹. Nevertheless, there have been no descriptions of this cytokine in the skeletal muscle. *In vitro* experiments showed that CCL19 enhanced the frequencies of antigen-responsive IFN- γ ⁺ CD8⁺ T cells from hepatitis B virus patients²⁴⁰. This function could imply that increased CCL19 from muscle cells might help to induce antigen-specific CD8⁺ T cells during infection.

Therefore, skeletal muscle cells can actively shape the immune response by recruiting different immune cell types such as neutrophils and T cells and by promoting T cell and NK cell effector function, cell types that play a crucial role in the defence against *T. cruzi* infections.

5.5 Presentation of *T. cruzi* antigens by HLA-I and HLA-II

Under steady-state conditions, an anti-inflammatory, regenerative environment is present in the muscle tissue¹⁶⁸. This is necessary to improve tissue repair by muscle stem cells during injuries²⁴¹. Therefore, many anti-inflammatory cells are present at steady-state, such as regulatory T cells and anti-inflammatory tissue regenerative macrophages¹³³. Moreover, the skeletal muscle cells express HLA-I in low amounts, while HLA-II is absent²⁴². In contrast, upregulation of HLA-I and HLA-II in infected cells and upon stimulation with pro-inflammatory cytokines was observed in the present study (Figures 17 and 18). These findings align with the literature reporting the upregulation of antigen-presenting molecules after injury and IFN- γ stimulation²⁴³. However, while IFN- γ stimulation induced the upregulation of these receptors early on, infected cells only upregulated these receptors after 72 hpi. This suggests a different mechanism is involved in the upregulation of these receptors in case of a *T. cruzi* infection.

HLA-I and HLA-II can present antigens to CD8⁺ and CD4⁺ T cells, respectively⁴⁷. While HLA-I is expressed by all nucleated cells and presents peptides from the cell cytoplasm, HLA-II is primarily found on professional antigen-presenting cells and presents exogenous antigens⁴⁷. Using the C2C12 myoblast cell line, myoblasts have been demonstrated to present antigens to T cells via HLA-I and HLA-II, and the presentation elicited the secretion of IL-2 by T cell hybridoma cells²⁴⁴. Therefore, it was concluded that muscles can activate or inhibit T cells by providing co-stimulatory or co-inhibitory signals¹⁶⁸.

Moreover, muscle cells can express the co-stimulatory molecule of CD4⁺ T cells, CD40, upon IFN- γ stimulation in a dose-dependent manner ²⁴⁵. Similarly, in the present work, it could be shown that muscle cells express the co-stimulatory molecule CD40 upon stimulation with the pro-inflammatory cytokines IFN- γ and TNF- α (Figure 18). In addition, a significantly higher amount of muscle cells infected with *T. cruzi* expressed CD40. Furthermore, it has been shown that myoblasts can present endogenous antigens and elicit the release of IFN- γ by CD4⁺ T cells in an HLA-II-dependent manner ²⁴⁶. Moreover, IFN- γ stimulated muscle cells can activate autologous CD4⁺ T cells ²⁴³. Conversely, upon stimulation with pro-inflammatory cytokines, muscle cells do not express the co-stimulatory receptors CD80 and CD86, which are necessary for CD8⁺ T cells. Nevertheless, it could be shown *in vitro* that these receptors are only upregulated upon stimulation with IL-4 ²⁴⁷. It can be hypothesised that muscle cells act as non-professional antigen-presenting cells and activate previously primed CD4⁺ and CD8⁺ T cells with peptides from *T. cruzi*.

Additionally, the interaction of CD40 with its ligand CD40L elicits a response in the muscle cells as, *in vitro*, it has been shown that the interaction of soluble CD40L with CD40 on the muscle cells leads to the induction of different cytokines such as IL-6, IL-8, IL-15 and monocyte chemoattractant protein-1 ²⁴⁵. These findings align with the previously described results, showing the secretion of IL-6, IL-8 and IL-15 in the supernatant of muscle cells stimulated with pro-inflammatory cytokines (Figure 16).

It was investigated which RNA transcripts of *T. cruzi* are highly expressed in muscle cells to elucidate which peptides of *T. cruzi* might be presented to T cells by the muscle cell via HLA-I and HLA-II. For the infection of human fibroblasts, it could be demonstrated that *T. cruzi* significantly changes their expression profile upon transitioning from the trypomastigote to the amastigote stage ¹⁹³. Therefore, the highly expressed transcripts of intracellular amastigotes in skeletal muscle cells were investigated to find possible targets to be used for a vaccination approach.

The most highly expressed RNA transcript of *T. cruzi* in muscle cells at 48 hpi is the enzyme enolase (Figure 19). This enzyme is part of the glycolytic pathway and is highly expressed in the parasite in the trypomastigote and the amastigote stage ²⁴⁸. This enzyme has recently been identified as an ideal target for a vaccine against *T. cruzi* ²⁴⁹. Using an enolase consensus sequence, the authors showed that the protein has a high immunogenic potential, with six

epitopes for HLA-I and seven epitopes for HLA-II. If a vaccine is developed against the enolase, there is a high chance that T cells induced by the vaccine could also detect *T. cruzi* parasites in the muscle. Moreover, it could be shown that two peptides of the HSP70 protein were recognised in CD8⁺ T cells of Chagas disease patients²⁵⁰. Concordantly, the RNA of this protein was also highly expressed in *T. cruzi* amastigotes in muscle cells.

5.6 Muscle cells downregulate the immune response by providing co-inhibitory signals to T cells via PD-L1 and PD-L2

Modulation of the activation of T cells by muscle cells is of high interest since T cells are essential to fight *T. cruzi* parasites during the disease²⁵¹. While muscle tissue has been shown to be a niche of persistence for *T. cruzi* Brazil in mice, CD8⁺ T cells can kill intracellular parasites and have been shown to be crucial for controlling parasite burden during chronic infection^{6,68}. Furthermore, induction of a T_H1 T cell response is essential to protect from lethal *T. cruzi* infection in mice²⁵². The present study demonstrated that muscle cells can express co-inhibitory ligands to downregulate an immune response. It was evident that IFN- γ induced the expression of the co-inhibitory ligands PD-L1 and PD-L2 on muscle cells (Figure 21).

While PD-L1 has been shown to be induced by IFN- γ via the JAK2/STAT1 signalling pathway, PD-L2 can be induced by IFN- γ and IFN- β ⁹⁵. This further supports the hypothesis that type I interferons may be involved during *T. cruzi* infection. However, while it has been reported that skeletal muscle cells can express the ligand PD-L1 during muscle myopathies¹⁵⁰, the present study describes the expression of PD-L2 expression on skeletal muscle cells for the first time. Moreover, a higher proportion of *T. cruzi*-infected muscle cells expressed PD-L2, indicating a *T. cruzi*-specific induction of this ligand (Figure 21). Both of these ligands bind to the co-inhibitory receptor PD-1, and T cells expressing PD-1 could be found in the heart in a mouse model of Chagas disease²⁵³. The same study reported that inhibition of the interaction of PD-1 and PD-L1 increased the amount of infiltrating T cells but also increased immune pathology²⁵³. Additionally, exhausted PD-1⁺ T cells could be found in the chronic phase of the disease⁶. In humans with Chagas disease, higher proportions of CD8⁺ T cells expressed PD-1 during the chronic phase²⁵⁴. T cells progressively showed reduced cytokine production, advanced differentiation and increased inhibitory receptor expression.

The presented results support the hypothesis that muscle cells downregulate T cell proliferation via the interaction of PD-L1 and PD-L2 with PD-1 (Figure 25). Blockage of this interaction resulted in elevated proliferation of CD4⁺ and CD8⁺ T cells. This suppression of T cell function by muscle cells was demonstrated without stimulation and during *T. cruzi* infection, but elevated during IFN- γ stimulation. Thus, muscle cells might inhibit T cell function during a *T. cruzi* infection via the expression of PD-L1 and PD-L2. Nevertheless, mouse studies using a PD-L1 antibody could not find a significant improvement in parasite clearance ¹²². However, the binding of PD-L2 could compensate for the loss of the binding of PD-L1. Additionally, it has been shown that PD-L2 cannot only bind to PD-1 on CD8⁺ T cells but also to repulsive guidance molecule b (RGMb)²⁵⁵. In a tumour setting, it could be shown that targeting the PD-L2 and RGMb interaction can overcome resistance to PD-1 pathway inhibitors ²⁵⁶. Therefore, it would be interesting to investigate whether T cells express RGMb during a *T. cruzi* infection and whether this interaction might also downregulate the immune response independently of PD-1.

Moreover, this study reveals for the first time the expression of galectin-9, HVEM, CD122 and CD155 on muscle cells (Figures 21 and 26). These molecules are the ligands of the co-inhibitory receptors TIM-3, CD160, BTLA and TIGIT ^{257,258}. Furthermore, the co-inhibitory receptor LAG-3 can bind to HLA-II ²⁵⁹; this receptor's expression has been shown and discussed before. Thus, it is possible that inhibiting a single immunoregulatory pathway is insufficient to augment T cell function during a *T. cruzi* infection to improve parasite clearance in the muscle.

5.7 Involvement of soluble co-inhibitory ligands

Besides membrane-bound PD-L1 and PD-L2, soluble PD-L1 (sPD-L1) and sPD-L2 were detected in the supernatant of infected and IFN- γ and TNF- α -stimulated muscle (Figure 22). Even though their function has not been studied in detail, it has been observed in multiple cancers and described to be involved in immune regulation ²⁶⁰. Different mechanisms of producing the soluble form of PD-L1 have been described. Cleavage of cell surface PD-L1 by a disintegrin and metalloproteinase-10 (ADAM10) and ADAM17 resulted in an active sPD-L1 and induced apoptosis of CD8⁺ T cells, thereby attenuating the killing of tumour cells ²⁶¹. At the same time, multiple splicing variants of PD-L1 and PD-L2 which do not contain the transmembrane part of the molecule have been described ²⁶². Moreover, it could be shown that mature dendritic

cells produce and release sPD-L1, and that the exposure of CD4⁺ and CD8⁺ T cells to sPD-L1 induces apoptosis¹⁹⁰. Soluble PD-L1 can be found in human sera, and the concentration increases with age²⁶³. Additionally, elevated levels of sPD-L1 could be found in patients with cystic echinococcosis, which was shown to have an immune suppressive effect²⁶⁴. This suggests that muscle cells' release of soluble co-inhibitory receptor ligands during the *T. cruzi* infection might contribute to immune suppression in the muscle and systemic downregulation of immune cell function by induction of apoptosis in T cells.

Nevertheless, matrix metalloproteases 13 and 9 (MMP-9) have been shown to cleave the extracellular part of PD-L1 and PD-L2 expressed by fibroblasts²⁶⁵. This cleavage resulted in the lack of a PD-1 binding domain and was postulated as a mechanism for reducing the immunosuppressive capacity. It could be shown that macrophages in the heart of chronically *T. cruzi*-infected mice exhibited a significant increase in the expression, activity and release of MMP-9²⁶⁶. Therefore, more studies on the functionality of this secreted PD-L1 and PD-L2 are needed to identify their immune regulatory capacity during a *T. cruzi* infection.

5.8 Role of galectin-9 in immune suppression during *T. cruzi* infection

Galectin-9 is the ligand of TIM-3, a co-inhibitory receptor that is highly expressed on CD8⁺ T cells in mice throughout the infection with *T. cruzi* Brazil and has also been found to be expressed on muscle-infiltrating CD8⁺ T cells during the acute stage of the infection⁶. Furthermore, a higher frequency of TIM-3⁺ CD8⁺ T cells could be found in Chagas patients compared to healthy donors²⁵⁴, and exposure of PBMCs of Chagas patients to parasite antigens increased the expression of TIM-3 on CD4⁺ T cells, especially in those with cardiac symptoms²⁶⁷. It could be demonstrated that the binding of galectin-9 to TIM-3 induced apoptosis of CD8⁺ T cells and T_H1 cells and induced regulatory T cells^{103,268–270}. Besides the effect on T cells, galectin-9 drives monocyte differentiation towards an anti-inflammatory phenotype²⁷¹. For macrophages, it could be shown that an anti-inflammatory phenotype and the expression of Arginase 1 is beneficial for parasite survival and proliferation inside the macrophages but also limit tissue damage²⁷².

In this study, it was observed that muscle cells infected with *T. cruzi* and additionally stimulated with pro-inflammatory cytokines expressed galectin-9 on the surface (Figure 21).

Additionally, high amounts of soluble galectin-9 were found in the supernatant of muscle cells stimulated with IFN- γ , and the amount increased upon infection with *T. cruzi* (Figure 22). Co-culture experiments of muscle cells with human T cells revealed improved T cell proliferation upon blocking of TIM-3 with a blocking α TIM-3 antibody (Figure 25). This data indicates that muscle cells can influence T cell proliferation via the co-inhibitory receptor TIM-3, potentially via the expression of the before-shown ligand galectin-9.

Even though galectin-9 is expressed in the skeletal muscle tissue in mice ²⁶⁹, this is the first description of primary human skeletal muscle cells producing galectin-9. The expression of galectin-9 depends on IFN- α and - β , once more indicating the potential involvement of type I interferons during the infection with *T. cruzi* ²⁷³.

Taking these described functions together, it could be speculated that galectin-9 expression by muscle cells upon *T. cruzi* infection in a pro-inflammatory environment downregulates the T cell response in the muscle. Moreover, cell death could be induced in TIM-3⁺ T_H1 cells through exposure to galectin-9, and CD4⁺ T cells upregulated TIM-3 upon exposure to *T. cruzi* antigens^{267,268}. Therefore, galectin-9 may deplete or suppress *T. cruzi*-specific TIM-3⁺ T_H1 cells, thereby contributing to the many immune evasion mechanisms described for *T. cruzi* ²⁷⁴. To test this hypothesis, TIM3⁺ T cells from Chagas patients could be sorted and incubated with the supernatant of infected and IFN- γ -stimulated muscle cells and analysed for the induction of apoptosis. Incubation of monocytes with the supernatant of infected and IFN- γ -stimulated muscle cells and analysis of anti-inflammatory markers, such as Arginase 1, and the growth of parasites would reveal the influence on other immune cells.

Moreover, and described for the first time, this thesis found high levels of galectin-9 in the serum of individuals from Columbia chronically infected with *T. cruzi* (Figure 23). Galectin-9 can be produced by muscle cells, potentially released into the bloodstream and be systemically distributed. However, other sources of galectin-9, such as the endometrial epithelium in human females, have also previously been described ²⁷⁵. Indeed, a negative correlation between galectin-9 in the plasma and age could be found in the samples from female donors (Supplement Figure 29). However, high amounts of galectin-9 could also be found in males; no correlation with age was visible here. Unfortunately, the levels of galectin-9 could not be compared with individuals from the same area without a *T. cruzi* infection. However, in a study of COVID patients, similar levels of galectin-9 could be found ²⁷⁶. In this

study, healthy individuals had a range of 0 to 2,042 pg/ml, while the galectin-9 levels were substantially greater in those with severe disease (median around 13,000 pg/ml) compared to those with mild/moderate disease (median around 28,000 pg/ml). Indetermined, asymptomatic Chagas cases showed a comparable level of galectin-9 in the sera, a median expression of around 18,000 pg/ml. In contrast, in symptomatic Chagas cases, galectin-9 concentration decreased to 8,000 pg/ml, but this decrease was not statistically significant. However, different ages have to be considered, as there is a significant difference in age between the groups, with a median of 26.5 years for asymptomatic cases and a median of 50 years in the group with cardiac dysfunction.

Combining all these results, it could be hypothesised that TIM-3⁺ T cells are systemically suppressed and depleted in humans during chronic *T. cruzi* infection, as could be shown for viral infections. It has previously been demonstrated that for chronic Hepatitis B Infection, galectin-9 is significantly upregulated in the serum of chronic Hepatitis B-related liver inflammation²⁷⁷. Furthermore, the authors could show that TIM-3⁺ CD8⁺ T cells were induced, which were susceptible to galectin-9-triggered cell death²⁷⁷. Moreover, another study investigated the effect of systemic inhibition of TIM-3 using a TIM-3 blocking antibody could show a trend towards a reduced parasite burden in the muscle⁶. However, as previously hypothesised, inhibition of a single immunoregulatory pathway may not be sufficient to lead to the clearance of a *T. cruzi* infection.

5.9 Potential new immune regulatory pathway in *T. cruzi*-infected muscle cells

T cells co-cultured with infected and IFN- γ -stimulated muscle cells significantly downregulated T cell proliferation (Figure 25). While the addition of α PD-1 and α TIM-3 antibodies could improve T cell proliferation, T cells exhibited only half of the proliferation capacity of control T cells stimulated only with beads. These findings suggest the existence of additional immunoregulatory mechanisms in the muscle cell. Besides the aforementioned expression of other co-inhibitory receptor ligands, the transcriptomic analysis revealed the induction of another potential immune regulatory mechanism. It could be shown that *IDO* (Indoleamine 2, 3-dioxygenase 1) and *IL-41* were significantly induced in infected and IFN- γ -stimulated muscle cells (Figure 10). Moreover, IL-411 was released into the supernatant of infected and IFN- γ -

stimulated muscle cells (Figure 20). Both enzymes are involved in the kynurenine pathway and have been described as immune suppressive in cancer ⁷.

While *IDO* is constitutively expressed in some cell types, such as type I conventional dendritic cells, it has been shown that gene transcription can be induced by IFN- γ ^{278,279}. The enzyme *IDO* metabolises the essential amino acid tryptophan ²⁸⁰. In contrast, *IL-4I1* is an L-amino acid oxidase and catalyses L-phenylalanine ²⁸¹. T cells have high metabolic requirements upon activation²⁸². Therefore, both of these enzymes can modify the T cell response by limiting the nutrient availability by catabolising essential amino acids ²⁸³.

Additionally, immune suppression of T cell apoptosis facilitated by *IDO* has been demonstrated for dendritic cells and CD8⁺ T_{regs} ^{284,285}. It has been shown that the produced metabolites of tryptophan by *IDO*, such as 3-hydroxy anthranilic and quinolinic acids, induced the selective apoptosis of murine thymocytes and of T_{H1} but not T_{H2} cells as well as B-cells and NK cells *in vitro* ^{285,286}. Similar to the function of *IDO*, immune suppression of T cells by *IL-4I1* has been reported ²⁸¹. In the study, the authors could demonstrate the secretion of *IL-4I1* by dendritic cells and an inhibition of T cell proliferation after CD3 stimulation *in vitro*. The metabolites of the kynurenine pathway produced by *IDO* and *IL-4I1* bind and activate the aryl hydrocarbon receptor (AHR) ^{287,288}. The AHR translocates into the nucleus, where it induces transcription of different genes involved in immune modulation ²⁸⁹. It could be shown that kynurenine binds to the AHR in T cells, leading to AHR-dependent T_{reg} cell differentiation ²⁹⁰. Additionally, it has been demonstrated for CD8⁺ T cells that the expression of the co-inhibitory receptor PD-1 was upregulated, and even cell death could be induced upon activation of the AHR ^{291,292}.

In contrast, it was also hypothesised that *IDO* can inhibit *T. cruzi* proliferation by depletion of the essential amino acid tryptophan ²⁹³. *T. cruzi* is auxotrophic for aromatic amino acids, meaning the parasite depends on its host cell to provide these amino acids ²⁹⁴. This hypothesis would be supported by the finding that *IDO* is expressed in IFN- γ stimulated muscle cells and the reduction in parasite load upon stimulation with pro-inflammatory cytokines. *IL-4I1* might suppress *T. cruzi* proliferation by depleting L-phenylalanine.

Moreover, skeletal muscle stem cells could be shown to express *IL-4I1* after stimulation with IFN- γ and TNF- α and were found to inhibit the infiltration of neutrophils into sites of inflammation ²⁹⁵. Taking together the described functions of these enzymes and the results of

this study, it can be hypothesised that *T. cruzi*-infected muscle cells inhibit T cell function through the expression of these enzymes. Therefore, the kynurenine pathway, specifically IDO and IL-4I1, are promising targets to improve the immune response against *T. cruzi*, particularly T cells in the skeletal muscle. Nevertheless, further experiments are needed to verify the potential downregulation of the T cell response by IL-4I1.

6. Future Perspectives

This study could shed light upon the induction of an anti-parasitic response and the immune-modulating capacities of skeletal muscle cells during a *T. cruzi* infection. Nevertheless, some questions regarding the induction of an anti-parasitic response and the modulation of the T cell response by skeletal muscle cells remain and need to be addressed in further experiments.

Induction of anti-parasitic response in skeletal muscle cells

In this study, it could be shown that skeletal muscle cells induce iNOS upon infection, which reduces the parasitic load. However, the transcriptomic analysis revealed the induction of additional proteins involved in viral replication, such as MX1, MX2 and RSAD. Consequently, knockouts of these proteins using a CRISPR/Cas9 system or silencing via siRNAs could be used to dissect their influence on the parasite development inside the skeletal muscle cells.

Furthermore, it could be shown that many genes described to be induced by type I interferons were expressed by skeletal muscle cells following a *T. cruzi* infection. It would be necessary to analyse the supernatant of infected muscle cells regarding the expression of type I interferons such as interferon- α and - β .

Moreover, it should be investigated whether the parasites are cleared from the skeletal muscle cells or whether the amastigote parasites reduce their proliferative rate. A DNA-incorporating dye in addition to fluorescence images at different time points could be used to determine the proliferation status of *T. cruzi* under pro-inflammatory conditions.

Modulation of the T cell response by skeletal muscle cells

Here, the inhibition of T cell proliferation via PD-L1, PD-L2 and galectin-9 by skeletal muscle cells could be demonstrated. However, other co-inhibitory receptor ligands, such as HVEM, CD155 and CD122, were also expressed on skeletal muscle cells. To further investigate the involvement of these ligands, co-culture assays blocking the interaction with the receptors on the T cell side, i.e., TIGIT, CD160 and BTLA, should be performed. In addition, the presence of soluble PD-L1, PD-L2 and galectin 9 could be shown in the supernatant of infected and stimulated muscle cells. Therefore, to dissect the involvement of these soluble forms, the supernatant of the muscle cells should be co-incubated with T cells to investigate their influence on T cell proliferation. Comparable to the performed experiments, blocking

antibodies against the corresponding receptors or the ligands themselves could be used to analyse the influence of the difference in receptor and ligand interactions.

While co-inhibitory receptor ligands were shown to have an effect on the proliferation capacity of T cells, their impact on the cytotoxicity of CD8⁺ T cells should also be investigated. A FATAL assay (fluorometric assessment of T lymphocyte antigen-specific lysis) could be performed as previously described²⁹⁶. In brief, muscle cells would be stained with two dyes, one present in the cytoplasm and one incorporated into the plasma membrane. Autologous CD8⁺ T cells would be activated *in vitro* and co-incubated with the muscle cells. Upon muscle cell lysis by the CD8⁺ T cell, the fluorescent dye would leak from the cytosol. Subsequently, the muscle cells would be analysed for the expression of the two fluorescent dyes and a ratio would be calculated. If reduced cytotoxicity of CD8⁺ T cells could be described, it would be interesting to see the influence of the blockage of the different co-inhibitory receptor and ligand interactions, as seen here for their proliferation capacity.

In addition, it would be interesting to investigate the effect of IL-4I1 and IDO. The supernatant of infected and IFN- γ stimulated muscle cells should be investigated for the presence of kynurenine derivatives, which IDO and IL-4I1 can produce. To this end, the supernatant could be used to identify the effect of these enzymes on T cell function, such as proliferation and cytotoxicity, and whether cell death can be induced, as shown in other studies²⁹⁷. To directly prove that IL-4I1 causes a negative effect on the T cell response, phenylalanine derivatives such as Cp2-SO4 could be used to rescue the T cell response. Cp2-SO4 has recently been described as a potent inhibitor of the activity of IL-4I1²⁹⁸.

Zhu et al. demonstrated that galectin-9 can induce cell death in CD4⁺ T cells²⁶⁸. Thus, it could be investigated whether the infected and IFN- γ -stimulated muscle cells' supernatant can induce apoptosis in the T cells of Chagas patients. This would be of high relevance, as it has been shown that CD4⁺ T cells express TIM-3 upon stimulation with *T. cruzi* antigens, which could be a mechanism by which antigen-specific CD4⁺ T cells are depleted during *T. cruzi* infection. Additionally, it could be explored whether galectin-9 is also expressed in the muscle during the *T. cruzi* infection *in vivo*. For this purpose, histological cuts of the skeletal muscle tissues of humans or mice could be stained for galectin-9.

Literature

1. Tarleton, R. L., Sun, J., Zhang, L. & Postan, M. Depletion of T-cell subpopulations results in exacerbation of myocarditis and parasitism in experimental Chagas' disease. *Infect Immun* **62**, 1820–1829 (1994).
2. Lasso, P. *et al.* Inhibitory Receptor Expression on CD8+ T Cells Is Linked to Functional Responses against *Trypanosoma cruzi* Antigens in Chronic Chagasic Patients . *The Journal of Immunology* **195**, 3748–3758 (2015).
3. Cardillo, F., Voltarelli, J. C., Reed, S. G. & Silva, J. S. Regulation of *Trypanosoma cruzi* infection in mice by gamma interferon and interleukin 10: role of NK cells. *Infect Immun* **64**, 128–134 (1996).
4. Dotiwala, F. *et al.* Killer lymphocytes use granzysin, perforin and granzymes to kill intracellular parasites. *Nat Med* **22**, 210–216 (2016).
5. Martin, D. & Tarleton, R. Generation, specificity, and function of CD8+ T cells in *Trypanosoma cruzi* infection. *Immunol Rev* **201**, 304–317 (2004).
6. Gálvez, R. I. & Jacobs, T. Exhausted PD-1+ TOX+ CD8+ T Cells Arise Only in Long-Term Experimental *Trypanosoma cruzi* Infection. *Front Immunol* **13**, (2022).
7. Sadik, A. *et al.* IL4I1 Is a Metabolic Immune Checkpoint that Activates the AHR and Promotes Tumor Progression. *Cell* **182**, 1252–1270 (2020).
8. World Health Organization. *Integrating neglected tropical diseases into global health and development: fourth WHO report on neglected tropical diseases*. World Health Organization (2017).
9. Guhl, F. & Ramírez, J. D. Poverty, Migration, and Chagas Disease. *Curr Trop Med Rep* **8**, 52–58 (2021).
10. Wirth, M. *et al.* Knowledge, attitudes, behaviors, and serological status related to Chagas disease among Latin American migrants in Germany: A cross-sectional study in six German cities. *Front Cell Infect Microbiol* **12**, (2023).

11. Monroy, C. *et al.* Comparison of indoor searches with whole house demolition collections of the vectors of Chagas disease and their indoor distribution. *Medical Entomology and Zoology* **49**, 195–200 (1998).
12. Beatty, N. L. & Klotz, S. A. Perspective Piece Autochthonous Chagas Disease in the United States: How Are People Getting Infected? *American Journal of Tropical Medicine and Hygiene* **103**, 967–969 (2020).
13. Harris, N. *et al.* Autochthonous Chagas disease in the southern United States: A case report of suspected residential and military exposures. *Zoonoses Public Health* **64**, 491–493 (2017).
14. Chagas, C. Nova tripanozomíase humana: estudos sobre a morfologia e o ciclo evolutivo do *Schizotrypanum cruzi* n. gen., n. sp., agente etiológico de nova entidade morbida do homem. *Memórias do Instituto Oswaldo Cruz* **1**, 159–218 (1909).
15. Pan American Health Organization. *Guidelines for the diagnosis and treatment of Chagas disease*. *Pan American Health Organization* **6**, (2019).
16. Hughes, A. L. & Piontkivska, H. Phylogeny of Trypanosomatidae and Bodonidae (Kinetoplastida) Based on 18S rRNA: Evidence for Paraphyly of Trypanosoma and Six Other Genera. *Mol Biol Evol* **20**, 644–652 (2003).
17. Kelly, F. D., Sanchez, M. A. & Landfear, S. M. Touching the Surface: Diverse Roles for the Flagellar Membrane in Kinetoplastid Parasites. *Microbiology and Molecular Biology Reviews* **84**, (2020).
18. Noireau, F., Diosque, P. & Jansen, A. M. Trypanosoma cruzi: adaptation to its vectors and its hosts. *Vet Res* **40**, (2009).
19. Bern, C., Kjos, S., Yabsley, M. J. & Montgomery, S. P. Trypanosoma cruzi and Chagas' Disease in the United States. *Clin Microbiol Rev* **24**, 655–681 (2011).
20. Andrade, L. O. *et al.* Differential tissue tropism of Trypanosoma cruzi strains: An in vitro study. *Mem Inst Oswaldo Cruz* **105**, 834–837 (2010).
21. Melo, R. C. & Brener, Z. Tissue Tropism of Different Trypanosoma cruzi Strains. *J Parasitol* **64**, 475–482 (1978).

22. Pech-Canul, Á. de la C., Monteón, V. & Solís-Oviedo, R.-L. A Brief View of the Surface Membrane Proteins from *Trypanosoma cruzi*. *J Parasitol Res* **2017**, (2017).
23. Tyler, K. M. & Engman, D. M. The life cycle of *Trypanosoma cruzi* revisited. *Int J Parasitol* **31**, 472–481 (2001).
24. Milder, R. & Kloetzel, J. The development of *Trypanosoma cruzi* in macrophages in vitro. Interaction with lysosomes and host cell fate. *Parasitology* **80**, 139–145 (1980).
25. Tardieux, I. *et al.* Lysosome recruitment and fusion are early events required for trypanosome invasion of mammalian cells. *Cell* **71**, 1117–1130 (1992).
26. Lidani, K. C. F. *et al.* Chagas Disease: From Discovery to a Worldwide Health Problem. *Frontiers in Public Health* **7**, (2019).
27. Prata A. Clinical and epidemiological aspects of chagas disease. *Lancet infection disease* **1**, 92–100 (2001).
28. Suárez, C., Nolder, D., García-Mingo, A., Moore, D. A. J. & Chiodini, P. L. Diagnosis and Clinical Management of Chagas Disease: An Increasing Challenge in Non-Endemic Areas. *Res Rep Trop Med* **13**, 25–40 (2022).
29. Tarleton, R. L. Parasite persistence in the aetiology of Chagas disease. *Int J Parasitol* **31**, 550–554 (2001).
30. Ward, A. I., Olmo, F., Atherton, R. L., Taylor, M. C. & Kelly, J. M. *Trypanosoma cruzi* amastigotes that persist in the colon during chronic stage murine infections have a reduced replication rate: *Trypanosoma cruzi* proliferation. *Open Biol* **10**, (2020).
31. Ferreira, A. V. M. *et al.* Evidence for *Trypanosoma cruzi* in adipose tissue in human chronic Chagas disease. *Microbes Infect* **13**, 1002–1005 (2011).
32. García Sánchez, L. T. *et al.* Disagreement between PCR and serological diagnosis of *Trypanosoma cruzi* infection in blood donors from a Colombian endemic region. *Biomedica* **41**, 47–59 (2021).
33. Bocchi, E. A., Bestetti, R. B., Scanavacca, M. I., Cunha Neto, E. & Issa, V. S. Chronic Chagas Heart Disease Management: From Etiology to Cardiomyopathy Treatment. *J Am Coll Cardiol* **70**, 1510–1524 (2017).

34. Matsuda, N. M., Miller, S. M. & Evora, P. R. B. The chronic gastrointestinal manifestations of Chagas disease. *Clinics (Sao Paulo)* **64**, 1219–1224 (2009).
35. Morrot, A., Villar, S. R., González, F. B. & Pérez, A. R. Evasion and Immuno-Endocrine Regulation in Parasite Infection: Two Sides of the Same Coin in Chagas Disease? *Frontiers in Microbiology* **7**, (2016).
36. Medei, E. H., Nascimento, J. H. M., Pedrosa, R. C. & Carvalho, A. C. C. de. Role of autoantibodies in the physiopathology of Chagas' disease. *Arq Bras Cardiol* **91**, 257–286 (2008).
37. Bivona, A. E., Alberti, A. S., Cerny, N., Trinitario, S. N. & Malchiodi, E. L. Chagas disease vaccine design: the search for an efficient *Trypanosoma cruzi* immune-mediated control. *Biochim Biophys Acta Mol Basis Dis.* **1866**, (2020).
38. Filardi, L. S. & Brener, Z. Susceptibility and natural resistance of *Trypanosoma cruzi* strains to drugs used clinically in Chagas disease. *Trans R Soc Trop Med Hyg* **81**, 755–759 (1987).
39. Rajão, M. A. *et al.* Unveiling benznidazole's mechanism of action through overexpression of DNA repair proteins in *Trypanosoma cruzi*. *Environ Mol Mutagen* **55**, 309–321 (2014).
40. Bern, C. *et al.* Evaluation and Treatment of Chagas Disease in the United States. *J Am Med Assoc* **298**, 2171–2181 (2007).
41. Castro, J. A. & Diaz de Toranzo, E. G. Toxic effects of nifurtimox and benznidazole, two drugs used against American trypanosomiasis (Chagas' disease). *Biomedical and environmental sciences* **1**, 19–33 (1988).
42. Morillo, C. A. *et al.* Randomized trial of benznidazole for chronic Chagas' cardiomyopathy. *N Engl J Med* **373**, 1295–1306 (2015).
43. Han, C. Y., Issa, H., Rychtář, J., Taylor, D. & Umana, N. A voluntary use of insecticide treated nets can stop the vector transmission of Chagas disease. *PLoS Negl Trop Dis* **14**, (2020).
44. WHO. Chagas disease (American trypanosomiasis). https://www.who.int/health-topics/chagas-disease#tab=tab_1 (2021).
45. Espinoza-Gómez, F., Maldonado-Rodríguez, A., Coll-Cárdenas, R., Hernández-Suárez, C. M. & Fernández-Salas, I. Presence of triatominae (Hemiptera, Reduviidae) and risk of transmission of Chagas disease in Colima, México. *Mem Inst Oswaldo Cruz* **97**, 25–30 (2002).

46. Rao, S. P. S. *et al.* Cyanotriazoles are selective topoisomerase II poisons that rapidly cure trypanosome infections. *Science* **380**, 1349–1356 (2023).
47. Murphy, K. M., Travers, P. & Walport, M. *Janeway Immunologie*. 7th ed. (2009).
48. Acevedo, G. R., Girard, M. C. & Gómez, K. A. The Unsolved Jigsaw Puzzle of the Immune Response in Chagas Disease. *Front Immunol* **9**, (2018).
49. Oliveira, A. *et al.* Expression of Functional TLR4 Confers Proinflammatory Responsiveness to *Trypanosoma cruzi* Glycoinositolphospholipids and Higher Resistance to Infection with *T. cruzi*. *The Journal of Immunology* **173**, 5688–5696 (2004).
50. Campos, M. A. S. *et al.* Activation of Toll-Like Receptor-2 by Glycosylphosphatidylinositol Anchors from a Protozoan Parasite. *The Journal of Immunology* **167**, 416–423 (2001).
51. Bafica, A. *et al.* Cutting Edge: TLR9 and TLR2 Signaling Together Account for MyD88-Dependent Control of Parasitemia in *Trypanosoma cruzi* Infection. *The Journal of Immunology* **6**, 3515-3519 (2006).
52. Roffê, E. *et al.* IL-10 Limits Parasite Burden and Protects against Fatal Myocarditis in a Mouse Model of *Trypanosoma cruzi* Infection. *The Journal of Immunology* **188**, 649–660 (2012).
53. Rezende-Oliveira, K., Sarmiento, R. R. & Junior, V. R. Production of cytokine and chemokines by human mononuclear cells and whole blood cells after infection with *Trypanosoma cruzi*. *Rev Soc Bras Med Trop* **45**, 45–50 (2012).
54. Scharon-Kersten, T., Afonso, L. C., Wyszocka, M., Trinchieri, G. & Scott, P. IL-12 is required for natural killer cell activation and subsequent T helper 1 cell development in experimental leishmaniasis. *The Journal of Immunology* **154**, 5320–5330 (1995).
55. Silva, J. S., Machado, F. S. & Martins, G. A. The role of nitric oxide in the pathogenesis of Chagas disease. *Front Biosci* **8**, 314-25 (2003).
56. Alvarez, M. N., Peluffo, G., Piacenza, L. & Radi, R. Intraphagosomal Peroxynitrite as a Macrophage-derived Cytotoxin against Internalized *Trypanosoma cruzi*. *J Biol Chem* **286**, 6627–6640 (2011).

57. Muñoz-Fernández, M. A., Fernández, M. A. & Fresno, M. Activation of human macrophages for the killing of intracellular *Trypanosoma cruzi* by TNF- α and IFN- γ through a nitric oxide-dependent mechanism. *Immunol Lett* **33**, 35–40 (1992).
58. Lieke, T., Graefe, S. E. B., Klauenberg, U., Fleischer, B. & Jacobs, T. NK cells contribute to the control of *Trypanosoma cruzi* infection by killing free parasites by perforin-independent mechanisms. *Infect Immun* **72**, 6817–6825 (2004).
59. Christoffersson, G. & Phillipson, M. The neutrophil: one cell on many missions or many cells with different agendas? *Cell Tissue Res* **371**, 415–423 (2018).
60. de Andrade, M. F. *et al.* Involvement of neutrophils in Chagas disease pathology. *Parasite Immunol* **40**, (2018).
61. Sousa-Rocha, D. *et al.* *Trypanosoma cruzi* and its soluble antigens induce NET release by stimulating toll-like receptors. *PLoS One* **10**, (2015).
62. Lidani, K. C. F., Bavia, L., Ambrosio, A. R. & de Messias-Reason, I. J. The complement system: A prey of *Trypanosoma cruzi*. *Front Microbiol* **8**, (2017).
63. Cardillo, F. *et al.* B cells modulate T cells so as to favour T helper type 1 and CD8 + T-cell responses in the acute phase of *Trypanosoma cruzi* infection. *Immunology* **122**, 584–595 (2007).
64. Kumar, S. & Tarleton, R. L. The relative contribution of antibody production and CD8+ T cell function to immune control of *Trypanosoma cruzi*. *Parasite Immunol* **20**, 207–216 (1998).
65. Padilla, A. M., Simpson, L. J. & Tarleton, R. L. Insufficient TLR activation contributes to the slow development of CD8+ T cell responses in *Trypanosoma cruzi* infection. *The Journal of Immunology* **183**, 1245–1252 (2009).
66. Low, H. P., Santos, M. A., Wizel, B. & Tarleton, R. L. Amastigote surface proteins of *Trypanosoma cruzi* are targets for CD8+ CTL. *The Journal of Immunology* **160**, 1817–1823 (1998).
67. Wizel, B., Nunes, M. & Tarleton, R. L. Identification of *Trypanosoma cruzi* trans-sialidase family members as targets of protective CD8+ TC1 responses. *The Journal of Immunology* **159**, 6120–6130 (1997).

68. Pack, A. D., Collins, M. H., Rosenberg, C. S. & Tarleton, R. L. Highly competent, non-exhausted CD8+ T cells continue to tightly control pathogen load throughout chronic *Trypanosoma cruzi* infection. *PLoS Pathog* **14**, (2018).
69. Martin, D. & Tarleton, R. Generation, specificity, and function of CD8+ T cells in *Trypanosoma cruzi* infection. *Immunol Rev* **201**, 304–317 (2004).
70. Laucella, S. A., Rottenberg, M. E. & de Titto, E. H. Role of cytokines in resistance and pathology in *Trypanosoma cruzi* infection. *Rev Argent Microbiol* **28**, 99–109 (1996).
71. Barbosa, C.-H. D. *et al.* Cytotoxic CD4+ T cells driven by T-cell intrinsic IL-18R/MyD88 signaling predominantly infiltrate *Trypanosoma cruzi*-infected hearts. *Elife* **11**, (2022).
72. Tarleton, R. L. Parasite persistence in the aetiology of Chagas disease. *Int J Parasitol* **31**, 550–554 (2001).
73. Salvador, F. *et al.* Immunosuppression and Chagas disease; experience from a non-endemic country. *Clinical Microbiology and Infection* **21**, 854–860 (2015).
74. Andrews, N. W. From lysosomes into the cytosol: the intracellular pathway of *Trypanosoma cruzi*. *Braz J Med Biol Res* **27**, 471–475 (1994).
75. Silva, J. S. *et al.* The role of IL-12 in experimental *Trypanosoma cruzi* infection. *Braz J Med Biol Res* **31**, 111–115 (1998).
76. de Diego, J., Punzón, C., Duarte, M. & Fresno, M. Alteration of macrophage function by a *Trypanosoma cruzi* membrane mucin. *The Journal of Immunology* **159**, 4983–4989 (1997).
77. Freire-de-Lima, C. G. *et al.* Proapoptotic activity of a *Trypanosoma cruzi* ceramide-containing glycolipid turned on in host macrophages by IFN-gamma. *The Journal of Immunology* **161**, 4909–4916 (1998).
78. Pereira-Chioccola, V. L. *et al.* Mucin-like molecules form a negatively charged coat that protects *Trypanosoma cruzi* trypomastigotes from killing by human anti- α -galactosyl antibodies. *J Cell Sci* **113**, 1299–1307 (2000).
79. Joiner, K., Sher, A., Gaither, T. & Hammer, C. Evasion of alternative complement pathway by *Trypanosoma cruzi* results from inefficient binding of factor B. *Proc Natl Acad Sci U S A* **83**, 6593–6597 (1986).

80. Bermejo, D. A. *et al.* Trypanosoma cruzi infection induces a massive extrafollicular and follicular splenic B-cell response which is a high source of non-parasite-specific antibodies. *Immunology* **132**, 123–133 (2011).
81. Gao, W., Wortis, H. H. & Pereira, M. A. The Trypanosoma cruzi trans-sialidase is a T cell-independent B cell mitogen and an inducer of non-specific Ig secretion. *Int Immunol* **14**, 299–308 (2002).
82. Somoza, M. *et al.* Trypanosoma cruzi Induces B Cells That Regulate the CD4(+) T Cell Response. *Front Cell Infect Microbiol* **11**, (2021).
83. Nunes, M. P. *et al.* Inhibitory effects of Trypanosoma cruzi sialoglycoproteins on CD4+ T cells are associated with increased susceptibility to infection. *PLoS One* **8**, (2013).
84. Erdmann, H., Steeg, C., Koch-Nolte, F., Fleischer, B. & Jacobs, T. Sialylated ligands on pathogenic Trypanosoma cruzi interact with Siglec-E (sialic acid-binding Ig-like lectin-E). *Cell Microbiol* **11**, 1600–1611 (2009).
85. Chen, L. & Flies, D. B. Molecular mechanisms of T cell co-stimulation and co-inhibition. *Nat Rev Immunol* **13**, 227–242 (2013).
86. Linsley, P. S. *et al.* Human B7-1 (CD80) and B7-2 (CD86) bind with similar avidities but distinct kinetics to CD28 and CTLA-4 receptors. *Immunity* **1**, 793–801 (1994).
87. Walunas, T. L. *et al.* CTLA-4 can function as a negative regulator of T cell activation. *Immunity* **1**, 405–413 (1994).
88. Baumeister, S. H., Freeman, G. J., Dranoff, G. & Sharpe, A. H. Coinhibitory Pathways in Immunotherapy for Cancer. *Annu Rev Immunol* **34**, 539–573 (2016).
89. Okazaki, T., Chikuma, S., Iwai, Y., Fagarasan, S. & Honjo, T. A rheostat for immune responses: the unique properties of PD-1 and their advantages for clinical application. *Nat Immunol* **14**, 1212–1218 (2013).
90. Ahn, E. *et al.* Role of PD-1 during effector CD8 T cell differentiation. *Proc Natl Acad Sci U S A* **115**, 4749–4754 (2018).
91. Latchman, Y. *et al.* PD-L2 is a second ligand for PD-1 and inhibits T cell activation. *Nat Immunol* **2**, 261–268 (2001).

92. Keir, M. E. *et al.* Tissue expression of PD-L1 mediates peripheral T cell tolerance. *Journal of Experimental Medicine* **203**, 883–895 (2006).
93. Saunders, P. A., Hendrycks, V. R., Lidinsky, W. A. & Woods, M. L. PD-L2:PD-1 involvement in T cell proliferation, cytokine production, and integrin-mediated adhesion. *Eur J Immunol* **35**, 3561–3569 (2005).
94. Hui, E. *et al.* T cell costimulatory receptor CD28 is a primary target for PD-1-mediated inhibition. *Science* **355**, 1428–1433 (2017).
95. Wurdeman, S. R. *et al.* Interferon Receptor Signaling Pathways Regulating PD-L1 and PD-L2 Expression. *Physiol Behav* **6**, 1189–1201 (2017).
96. Chen, R. Y. *et al.* The role of PD-1 signaling in health and immune-related diseases. *Front Immunol* **14**, (2023).
97. Tang, Q. *et al.* The role of PD-1/PD-L1 and application of immune-checkpoint inhibitors in human cancers. *Front Immunol* **13**, (2022).
98. Monney, L. *et al.* Th1-specific cell surface protein Tim-3 regulates macrophage activation and severity of an autoimmune disease. *Nature* **415**, 536–541 (2002).
99. Joller, N. & Kuchroo, V. K. Tim-3, Lag-3, and TIGIT. *Curr Top Microbiol Immunol.* **410**, 127–156 (2017).
100. Sánchez-Fueyo, A. *et al.* Tim-3 inhibits T helper type 1-mediated auto- and alloimmune responses and promotes immunological tolerance. *Nat Immunol* **4**, 1093–1101 (2003).
101. Kuespert, K., Pils, S. & Hauck, C. R. CEACAMs: their role in physiology and pathophysiology. *Curr Opin Cell Biol* **18**, 565–571 (2006).
102. Zhu, C. *et al.* The Tim-3 ligand galectin-9 negatively regulates T helper type 1 immunity. *Nat Immunol* **6**, 1245–1252 (2005).
103. Yang, S. *et al.* Elevated Galectin-9 Suppresses Th1 Effector Function and Induces Apoptosis of Activated CD4+ T Cells in Osteoarthritis. *Inflammation* **40**, 1062–1071 (2017).
104. Kang, C. W. *et al.* Apoptosis of tumor infiltrating effector TIM-3+CD8+ T cells in colon cancer. *Sci Rep* **5**, (2015).

105. Nakayama, M. *et al.* Tim-3 mediates phagocytosis of apoptotic cells and cross-presentation. *Blood* **113**, 3821–3830 (2009).
106. Yu, X. *et al.* The surface protein TIGIT suppresses T cell activation by promoting the generation of mature immunoregulatory dendritic cells. *Nat Immunol* **10**, 48–57 (2009).
107. Joller, N. *et al.* Cutting Edge: TIGIT Has T Cell-Intrinsic Inhibitory Functions. *Journal of immunology* **186**:, 1338–1342 (2011).
108. Murphy, K. M., Nelson, C. A. & Sedý, J. R. Balancing co-stimulation and inhibition with BTLA and HVEM. *Nat Rev Immunol* **6**, 671–681 (2006).
109. del Rio, M. L., Lucas, C. L., Buhler, L., Rayat, G. & Rodriguez-Barbosa, J. I. HVEM/LIGHT/BTLA/CD160 cosignaling pathways as targets for immune regulation. *J Leukoc Biol* **87**, 223–235 (2009).
110. Cai, G. & Freeman, G. J. The CD160, BTLA, LIGHT/HVEM pathway: a bidirectional switch regulating T-cell activation. *Immunol Rev* **229**, 244–258 (2009).
111. Šedý, J. R. *et al.* CD160 activation by herpesvirus entry mediator augments inflammatory cytokine production and cytolytic function by NK cells. *The Journal of Immunology* **191**, 828–836 (2013).
112. McKinney, E. F., Lee, J. C., Jayne, D. R. W., Lyons, P. A. & Smith, K. G. C. T-cell exhaustion, co-stimulation and clinical outcome in autoimmunity and infection. *Nature* **523**, 612–616 (2015).
113. Baitsch, L. *et al.* Exhaustion of tumor-specific CD8⁺ T cells in metastases from melanoma patients. *J Clin Invest* **121**, 2350–2360 (2011).
114. Quigley, M. *et al.* Transcriptional analysis of HIV-specific CD8⁺ T cells shows that PD-1 inhibits T cell function by upregulating BATF. *Nat Med* **16**, 1147–1151 (2010).
115. Collier, J. L., Weiss, S. A., Pauken, K. E., Sen, D. R. & Sharpe, A. H. Not-so-opposite ends of the spectrum: CD8⁺ T cell dysfunction across chronic infection, cancer and autoimmunity. *Nat Immunol* **22**, 809–819 (2021).
116. Lasso, P. *et al.* Inhibitory Receptor Expression on CD8⁺ T Cells Is Linked to Functional Responses against *Trypanosoma cruzi* Antigens in Chronic Chagasic Patients. *The Journal of Immunology* **195**, 3748–3758 (2015).

117. Mateus, J. *et al.* An animal model of acute and chronic chagas disease with the reticulotropic Y strain of *Trypanosoma cruzi* that depicts the multifunctionality and dysfunctionality of T cells. *Front Immunol* **10**, (2019).
118. Ribas, A. & Wolchok, J. D. Cancer immunotherapy using checkpoint blockade. *Science* **359**, 1350–1355 (2018).
119. Silverio, J. C. *et al.* CD8+ T-cells expressing interferon gamma or perforin play antagonistic roles in heart injury in experimental *Trypanosoma cruzi*-elicited cardiomyopathy. *PLoS Pathog* **8**, (2012).
120. Rodrigues, V. *et al.* Impairment of T Cell Function in Parasitic Infections. *PLoS Negl Trop Dis* **8**, (2014).
121. Laugier, L. *et al.* Whole-Genome Cardiac DNA Methylation Fingerprint and Gene Expression Analysis Provide New Insights in the Pathogenesis of Chronic Chagas Disease Cardiomyopathy. *Clin Infect Dis* **65**, 1103–1111 (2017).
122. Arana, Y., Gálvez, R. I. & Th. Role of the PD-1/PD-L1 Pathway in Experimental *Trypanosoma cruzi* Infection and Potential Therapeutic Options. *Front Immunol* **13**, (2022).
123. Gálvez, R. I. & Jacobs, T. Exhausted PD-1+ TOX+ CD8+ T Cells Arise Only in Long-Term Experimental *Trypanosoma cruzi* Infection. *Front Immunol* **13**, (2022).
124. Pack, A. D. & Tarleton, R. L. Cutting Edge: Augmenting Muscle MHC Expression Enhances Systemic Pathogen Control at the Expense of T Cell Exhaustion. *The Journal of Immunology* **205**, 573–578 (2020).
125. Marcon, G. E. B. *et al.* *Trypanosoma cruzi*: Parasite persistence in tissues in chronic chagasic Brazilian patients. *Mem Inst Oswaldo Cruz* **106**, 85–91 (2011).
126. Sciorati, C., Rigamonti, E., Manfredi, A. A. & Rovere-Querini, P. Cell death, clearance and immunity in the skeletal muscle. *Cell Death Differ* **23**, 927–937 (2016).
127. Benhar, I., London, A. & Schwartz, M. The privileged immunity of immune privileged organs: The case of the eye. *Front Immunol* **3**, (2012).
128. Boegel, S. *et al.* HLA and proteasome expression body map. *BMC Med Genomics* **11**, (2018).

129. Gama, J. F. G. *et al.* Role of Regulatory T Cells in Skeletal Muscle Regeneration: A Systematic Review. *Biomolecules* **12**, (2022).
130. Villalta, S. A. *et al.* Regulatory T cells suppress muscle inflammation and injury in muscular dystrophy. *Sci Transl Med* **6**, (2014).
131. Sousa-Victor, P., García-Prat, L. & Muñoz-Cánoves, P. Control of satellite cell function in muscle regeneration and its disruption in ageing. *Nat Rev Mol Cell Biol* **23**, 204–226 (2022).
132. Brigitte, M. *et al.* Muscle resident macrophages control the immune cell reaction in a mouse model of notexin-induced myoinjury. *Arthritis Rheum* **62**, 268–279 (2010).
133. Tidball, J. G. Regulation of muscle growth and regeneration by the immune system. *Nat Rev Immunol* **17**, 165–178 (2017).
134. Peake, J. M., Neubauer, O., Gatta, P. A. D. & Nosaka, K. Muscle damage and inflammation during recovery from exercise. *J Appl Physiol* **122**, 559–570 (2017).
135. Cheng, M., Nguyen, M.-H., Fantuzzi, G. & Koh, T. J. Endogenous interferon-gamma is required for efficient skeletal muscle regeneration. *Am J Physiol Cell Physiol* **294**, (2008).
136. Dort, J., Fabre, P., Molina, T. & Dumont, N. A. Macrophages Are Key Regulators of Stem Cells during Skeletal Muscle Regeneration and Diseases. *Stem Cells Int* **2019**, (2019).
137. Sciorati, C., Rigamonti, E., Manfredi, A. A. & Rovere-Querini, P. Cell death, clearance and immunity in the skeletal muscle. *Cell Death Differ* **23**, 927–937 (2016).
138. Butterfield, T. a, Best, T. M. & Merrick, M. a. The Dual Roles of Neutrophils and. *J Athl Train* **41**, 457–465 (2006).
139. Deng, B., Wehling-Henricks, M., Villalta, S. A., Wang, Y. & Tidball, J. G. IL-10 triggers changes in macrophage phenotype that promote muscle growth and regeneration. *The Journal of Immunology* **189**, 3669–3680 (2012).
140. Lu, H. *et al.* Macrophages recruited via CCR2 produce insulin-like growth factor-1 to repair acute skeletal muscle injury. *The FASEB Journal* **25**, 358–369 (2011).
141. Wang, X., Zhao, W., Ransohoff, R. M. & Zhou, L. Identification and Function of Fibrocytes in Skeletal Muscle Injury Repair and Muscular Dystrophy. *The Journal of Immunology* **197**, 4750–4761 (2016).

142. Lee, H.-O. *et al.* FAP-overexpressing fibroblasts produce an extracellular matrix that enhances invasive velocity and directionality of pancreatic cancer cells. *BMC Cancer* **11**, (2011).
143. Joe, A. W. B. *et al.* Muscle injury activates resident fibro/adipogenic progenitors that facilitate myogenesis. *Nat Cell Biol* **12**, 153–163 (2010).
144. Goebels, N., Michaelis, D., Wekerle, H. & Hohlfeld, R. Human myoblasts as antigen-presenting cells. *The Journal of Immunology* **149**, 661–667 (1992).
145. Afzali, A. M., Müntefering, T., Wiendl, H., Meuth, S. G. & Ruck, T. Skeletal muscle cells actively shape (auto)immune responses. *Autoimmun Rev* **17**, 518–529 (2018).
146. Muñoz-Cánoves, P., Scheele, C., Pedersen, B. K. & Serrano, A. L. Interleukin-6 myokine signaling in skeletal muscle: A double-edged sword? *FEBS Journal* **280**, 4131–4148 (2013).
147. Sugiura, T. *et al.* Increased CD40 Expression on Muscle Cells of Polymyositis and Dermatomyositis: Role of CD40-CD40 Ligand Interaction in IL-6, IL-8, IL-15, and Monocyte Chemoattractant Protein-1 Production. *The Journal of Immunology* **164**, 6593–6600 (2000).
148. Schmidt, J., Rakocevic, G., Raju, R. & Dalakas, M. C. Upregulated inducible co-stimulator (ICOS) and ICOS-ligand in inclusion body myositis muscle: significance for CD8+ T cell cytotoxicity. *Brain* **127**, 1182–1190 (2004).
149. Wiendl, H. *et al.* Muscle fibers in inflammatory myopathies and cultured myoblasts express the nonclassical major histocompatibility antigen HLA-G. *Ann Neurol* **48**, 679–684 (2000).
150. Wiendl, H. *et al.* Human muscle cells express a B7-related molecule, B7-H1, with strong negative immune regulatory potential: a novel mechanism of counterbalancing the immune attack in idiopathic inflammatory myopathies. *The FASEB Journal* **17**, (2003).
151. Adams, E. M., Kirkley, J., Eidelman, G., Dohlman, J. & Plotz, P. H. The predominance of beta (CC) chemokine transcripts in idiopathic inflammatory muscle diseases. *Proc Assoc Am Physicians* **109**, 275–285 (1997).
152. Leavey, J. K. & Tarleton, R. L. Cutting Edge: Dysfunctional CD8 + T Cells Reside in Nonlymphoid Tissues During Chronic *Trypanosoma cruzi* Infection . *The Journal of Immunology* **170**, 2264–2268 (2003).

153. Wiendl, H. *et al.* Human muscle cells express a B7-related molecule, B7-H1, with strong negative immune regulatory potential: a novel mechanism of counterbalancing the immune attack in idiopathic inflammatory myopathies. *The FASEB Journal* **17**, (2003).
154. Andrews, S. FastQC A Quality Control tool for High Throughput Sequence Data.
155. Bolger, A. M., Lohse, M. & Usadel, B. Trimmomatic: A flexible trimmer for Illumina sequence data. *Bioinformatics* **30**, 2114–2120 (2014).
156. Kim, D., Langmead, B. & Salzberg, S. L. HISAT: a fast spliced aligner with low memory requirements. *Nat Methods* **12**, 357–360 (2015).
157. El-Sayed, N. M. *et al.* The Genome Sequence of *Trypanosoma cruzi*, Etiologic Agent of Chagas Disease. *Science* **309**, 409–415 (2005).
158. Liao, Y., Smyth, G. K. & Shi, W. featureCounts: an efficient general purpose program for assigning sequence reads to genomic features. *Bioinformatics* **30**, 923–930 (2014).
159. Smyth, G. K., Michaud, J. & Scott, H. S. Use of within-array replicate spots for assessing differential expression in microarray experiments. *Bioinformatics* **21**, 2067–2075 (2005).
160. Phipson, B., Lee, S., Majewski, I. J., Alexander, W. S. & Smyth, G. K. Robust hyperparameter estimation protects against hypervariable genes and improves power to detect differential expression. *Ann Appl Stat* **10**, 946–963 (2016).
161. Ritchie, M. E. *et al.* Limma powers differential expression analyses for RNA-sequencing and microarray studies. *Nucleic Acids Res* **43**, (2015).
162. Liu, R. *et al.* Why weight? Modelling sample and observational level variability improves power in RNA-seq analyses. *Nucleic Acids Res* **43**, (2015).
163. Benjamini, Y. & Hochberg, Y. Controlling the False Discovery Rate: A Practical and Powerful Approach to Multiple Testing. *Journal of the Royal Statistical Society: Series B (Methodological)* **57**, 289–300 (1995).
164. Ge, S. X., Son, E. W. & Yao, R. iDEP: An integrated web application for differential expression and pathway analysis of RNA-Seq data. *BMC Bioinformatics* **19**, (2018).
165. Marg, A. *et al.* Human satellite cells have regenerative capacity and are genetically manipulable. *Journal of Clinical Investigation* **124**, 4257–4265 (2014).

166. Puerta, C. J., Cuellar, A., Lasso, P., Mateus, J. & Gonzalez, J. M. Trypanosoma cruzi-specific CD8+ T cells and other immunological hallmarks in chronic Chagas cardiomyopathy: Two decades of research. *Front Cell Infect Microbiol* **12**, (2023).
167. D'Ávila, D. A. *et al.* Immunological imbalance between IFN- γ and IL-10 levels in the sera of patients with the cardiac form of Chagas disease. *Mem Inst Oswaldo Cruz* **104**, 100–105 (2009).
168. Wiendl, H., Hohlfeld, R. & Kieseier, B. C. Immunobiology of muscle: Advances in understanding an immunological microenvironment. *Trends Immunol* **26**, 373–380 (2005).
169. Mattijssen, S. & Pruijn, G. J. M. Viperin, a key player in the antiviral response. *Microbes Infect* **14**, 419–426 (2012).
170. Zhu, M. *et al.* CMPK2 is a host restriction factor that inhibits infection of multiple coronaviruses in a cell-intrinsic manner. *PLoS Biol* **21**, (2023).
171. Verhelst, J., Hulpiau, P. & Saelens, X. Mx Proteins: Antiviral Gatekeepers That Restrain the Uninvited. *Microbiology and Molecular Biology Reviews* **77**, 551–566 (2013).
172. Leisching, G., Cole, V., Ali, A. T. & Baker, B. OAS1, OAS2 and OAS3 restrict intracellular M. tb replication and enhance cytokine secretion. *International Journal of Infectious Diseases* **80**, 77–84 (2019).
173. Vladimer, G. I., Gónna, M. W. & Superti-Furga, G. IFITs: Emerging roles as key anti-viral proteins. *Front Immunol* **5**, (2014).
174. Smyth, P., Sasiwachirangkul, J., Williams, R. & Scott, C. J. Cathepsin S (CTSS) activity in health and disease - A treasure trove of untapped clinical potential. *Mol Aspects Med* **88**, (2022).
175. Vanhollebeke, B. & Pays, E. The trypanolytic factor of human serum: Many ways to enter the parasite, a single way to kill: MicroReview. *Mol Microbiol* **76**, 806–814 (2010).
176. Ablasser, A. *et al.* RIG-I-dependent sensing of poly(dA:dT) through the induction of an RNA polymerase III-transcribed RNA intermediate. *Nat Immunol* **10**, 1065–1072 (2009).
177. Masternak, K. *et al.* CIITA is a transcriptional coactivator that is recruited to MHC class II promoters by multiple synergistic interactions with an enhanceosome complex. *Genes Dev* **14**, 1156–1166 (2000).

178. Basu-Shrivastava, M., Kozoriz, A., Desagher, S. & Lassot, I. To ubiquitinate or not to ubiquitinate: Trim17 in cell life and death. *Cells* **10**, (2021).
179. de Morrée, A. *et al.* Proteomic analysis of the dysferlin protein complex unveils its importance for sarcolemmal maintenance and integrity. *PLoS One* **5**, (2010).
180. Xie, Y. J. *et al.* Leucine-Rich Glioma Inactivated 1 Promotes Oligodendrocyte Differentiation and Myelination via TSC-mTOR Signaling. *Front Mol Neurosci* **11**, (2018).
181. Liang, Y. *et al.* MMP25 Regulates Immune Infiltration Level and Survival Outcome in Head and Neck Cancer Patients. *Front Oncol* **10**, (2020).
182. Talvani, A. *et al.* Elevated concentrations of CCL2 and tumor necrosis factor- α in chagasic cardiomyopathy. *Clinical Infectious Diseases* **38**, 943–950 (2004).
183. Saeftel, M., Fleischer, B. & Hoerauf, A. Stage-dependent role of nitric oxide in control of *Trypanosoma cruzi* infection. *Infect Immun* **69**, 2252–2259 (2001).
184. Li, B., Jones, L. L. & Geiger, T. L. IL-6 Promotes T Cell Proliferation and Expansion under Inflammatory Conditions in Association with Low-Level ROR γ t Expression. *The Journal of Immunology* **201**, 2934–2946 (2018).
185. Huang, P. L. *et al.* Skeletal muscle interleukin 15 promotes CD8⁺ T-cell function and autoimmune myositis. *Skelet Muscle* **5**, (2015).
186. Taub, D. D., Anver, M., Oppenheim, J. J., Longo, D. L. & Murphy, W. J. T lymphocyte recruitment by interleukin-8 (IL-8): IL-8-induced degranulation of neutrophils releases potent chemoattractants for human T lymphocytes both in vitro and in vivo. *Journal of Clinical Investigation* **97**, 1931–1941 (1996).
187. Bromley, S. K., Thomas, S. Y. & Luster, A. D. Chemokine receptor CCR7 guides T cell exit from peripheral tissues and entry into afferent lymphatics. *Nat Immunol* **6**, 895–901 (2005).
188. Klenerman, P. & Hill, A. T cells and viral persistence: Lessons from diverse infections. *Nat Immunol* **6**, 873–879 (2005).
189. Oh, S. Y. *et al.* Soluble PD-L1 is a predictive and prognostic biomarker in advanced cancer patients who receive immune checkpoint blockade treatment. *Sci Rep* **11**, (2021).

190. Frigola, X. *et al.* Soluble B7-H1: Differences in production between dendritic cells and T cells. *Immunol Letters* **142**, 78–82 (2012).
191. Harjunpää, H. & Guillerey, C. TIGIT as an emerging immune checkpoint. *Clin Exp Immunol* **200**, 108–119 (2020).
192. Cai, G. & Freeman, G. J. The CD160, BTLA, LIGHT/HVEM pathway: A bidirectional switch regulating T-cell activation. *Immunol Rev* **229**, 244–258 (2009).
193. Li, Y. *et al.* Transcriptome Remodeling in *Trypanosoma cruzi* and Human Cells during Intracellular Infection. *PLoS Pathog* **12**, (2016).
194. Barton, J. M. Deciphering mechanisms shaping Natural Killer cell responses to *Trypanosoma cruzi* -infected dermal fibroblasts. (2022).
195. Verhelst, J., Parthoens, E., Schepens, B., Fiers, W. & Saelens, X. Interferon-Inducible Protein Mx1 Inhibits Influenza Virus by Interfering with Functional Viral Ribonucleoprotein Complex Assembly. *J Virol* **86**, 13445–13455 (2012).
196. Malterer, M. B., Glass, S. J. & Newman, J. P. Interferon-stimulated genes: A complex web of host defenses. *Annu Rev Immunol* **44**, 735–745 (2014).
197. Au-Yeung, N., Mandhana, R. & Horvath, C. M. Transcriptional regulation by STAT1 and STAT2 in the interferon JAK-STAT pathway. *JAKSTAT* **2**, (2013).
198. Kulkarni, M. M. *et al.* Signal transducer and activator of transcription 1 (STAT-1) plays a critical role in control of *Trypanosoma cruzi* infection. *Immunology* **145**, 225–231 (2015).
199. Stahl, P., Ruppert, V., Schwarz, R. T. & Meyer, T. *Trypanosoma cruzi* evades the protective role of interferon-gamma-signaling in parasite-infected cells. *PLoS One* **9**, (2014).
200. Bergeron, M. & Olivier, M. *Trypanosoma cruzi* -Mediated IFN- γ -Inducible Nitric Oxide Output in Macrophages Is Regulated by iNOS mRNA Stability . *The Journal of Immunology* **177**, 6271–6280 (2006).
201. Paes, M. C., Cosentino-Gomes, D., Souza, C. F. De, Nogueira, N. P. D. A. & Meyer-Fernandes, J. R. The role of heme and reactive oxygen species in proliferation and survival of *Trypanosoma cruzi*. *J Parasitol Res* **2011**, (2011).

202. Koo, S., Chowdhury, I. H., Szczesny, B., Wan, X. & Garg, N. J. Generation in Response to *Trypanosoma cruzi*. *Infect Immun* **84**, 3527–3541 (2016).
203. Greenberg, S. A. Type 1 interferons and myositis. *Arthritis Res Ther* **12**, (2010).
204. Cerbán, F. M. *et al.* Signaling pathways that regulate *Trypanosoma cruzi* infection and immune response. *Biochim Biophys Acta Mol Basis Dis* **1866**, (2020).
205. Wagner, H. The immunobiology of the TLR9 subfamily. *Trends Immunol* **25**, 381–386 (2004).
206. Oliveira, A. *et al.* Expression of Functional TLR4 Confers Proinflammatory Responsiveness to. *The Journal of Immunology* **173**, 5688–5696 (2004).
207. McNab, F., Mayer-Barber, K., Sher, A., Wack, A. & O’Garra, A. Type I interferons in infectious disease. *Nat Rev Immunol* **15**, 87–103 (2015).
208. Goubau, D., Deddouche, S. & Reis e Sousa, C. Cytosolic Sensing of Viruses. *Immunity* **38**, 855–869 (2013).
209. Chessler, A.-D. C., Ferreira, L. R. P., Chang, T.-H., Fitzgerald, K. A. & Burleigh, B. A. A novel IFN regulatory factor 3-dependent pathway activated by trypanosomes triggers IFN-beta in macrophages and fibroblasts. *The Journal of Immunology* **181**, 7917–7924 (2008).
210. Silva, J. S., Vespa, G. N. R., Cardoso, M. A. G., Aliberti, J. C. S. & Cunha, F. Q. Tumor necrosis factor alpha mediates resistance to *Trypanosoma cruzi* infection in mice by inducing nitric oxide production in infected gamma interferon-activated macrophages. *Infect Immun* **63**, 4862–4867 (1995).
211. Blanchette, J., Jaramillo, M. & Olivier, M. Signalling events involved in interferon- γ -inducible macrophage nitric oxide generation. *Immunology* **108**, 513–522 (2003).
212. Vespa, G. N. R., Cunha, F. Q. & Silva, J. S. Nitric oxide is involved in control of *Trypanosoma cruzi*-induced parasitemia and directly kills the parasite in vitro. *Infect Immun* **62**, 5177–5182 (1994).
213. Stamler, J. S. & Meissner, G. Physiology of nitric oxide in skeletal muscle. *Physiol Rev* **81**, 209–237 (2001).

214. Takács, A. C., Swierzy, I. J. & Lüder, C. G. K. Interferon- γ Restricts *Toxoplasma gondii* Development in Murine Skeletal Muscle Cells via Nitric Oxide Production and Immunity-Related GTPases. *PLoS One* **7**, (2012).
215. Denicola, A., Rubbo, H., Rodriguez, D. & Radi, R. Peroxynitrite-Mediated Cytotoxicity to *Trypanosoma cruzi*. *Archives of Biochemistry and Biophysics* **304** 279–286 (1993).
216. Ward, A. I. *et al.* *Trypanosoma cruzi* amastigotes that persist in the colon during chronic stage murine infections have a reduced replication rate. *Open Biol* **10**, (2020).
217. Müller, A. J. *et al.* Photoconvertible pathogen labeling reveals nitric oxide control of leishmania major infection in vivo via dampening of parasite metabolism. *Cell Host Microbe* **14**, 460–467 (2013).
218. Magiera, M. M. *et al.* Trim17-mediated ubiquitination and degradation of Mcl-1 initiate apoptosis in neurons. *Cell Death Differ* **20**, 281–292 (2013).
219. Mandell, M. A. *et al.* Correction: TRIM17 contributes to autophagy of midbodies while actively sparing other targets from degradation. *J Cell Sci* **130**, (2017).
220. Casassa, A. F., Vanrell, M. C., Colombo, M. I., Gottlieb, R. A. & Romano, P. S. Autophagy plays a protective role against *Trypanosoma cruzi* infection in mice. *Virulence* **10**, 151–165 (2019).
221. Vanrell, M. C. *et al.* Induction of Autophagy by Ursolic Acid Promotes the Elimination of *Trypanosoma cruzi* Amastigotes From Macrophages and Cardiac Cells. *Front Cell Infect Microbiol* **12**, (2022).
222. Lee, Y. J. & Benveniste, E. N. Stat1 alpha expression is involved in IFN-gamma induction of the class II transactivator and class II MHC genes. *The Journal of Immunology* **157**, 1559–1568 (1996).
223. Soto, C. D. A., Mirkin, G. A., Solana, M. E. & González Cappa, S. M. *Trypanosoma cruzi* infection modulates in vivo expression of major histocompatibility complex class II molecules on antigen-presenting cells and T-cell stimulatory activity of dendritic cells in a strain-dependent manner. *Infect Immun* **71**, 1194–1199 (2003).
224. Starr, A. E., Bellac, C. L., Dufour, A., Goebeler, V. & Overall, C. M. Biochemical characterization and N-terminomics analysis of leukolysin, the membrane-type 6 matrix metalloprotease

- (MMP25): Chemokine and vimentin cleavages enhance cell migration and macrophage phagocytic activities. *Journal of Biological Chemistry* **287**, 13382–13395 (2012).
225. Premadasa, L. S. *et al.* Cannabinoid enhancement of lncRNA MMP25-AS1/MMP25 interaction reduces neutrophil infiltration and intestinal epithelial injury in HIV/SIV infection. *JCI Insight* **8**, (2023).
226. Tanaka, T., Narazaki, M. & Kishimoto, T. IL-6 in Inflammation, Immunity, and Disease. *Cold Spring Harb Perspect Biol.* **6**, (2014).
227. Pedersen, B. K., Steensberg, A. & Schjerling, P. Muscle-derived interleukin-6: Possible biological effects. *Journal of Physiology* **536**, 329–337 (2001).
228. Gao, W. & Pereira, M. A. Interleukin-6 is required for parasite specific response and host resistance to Trypanosomacruzi. *Int J Parasitol* **32**, 167–170 (2002).
229. Truysens, C. *et al.* Interleukin-6 (IL-6) production in mice infected with Trypanosoma cruzi: Effect of its paradoxical increase by anti-IL-6 monoclonal antibody treatment on infection and acute-phase and humoral immune responses. *Infect Immun* **62**, 692–696 (1994).
230. Rose-John, S., Winthrop, K. & Calabrese, L. The role of IL-6 in host defence against infections: Immunobiology and clinical implications. *Nat Rev Rheumatol* **13**, 399–409 (2017).
231. Okada, M. *et al.* IL-6/BSF-2 functions as a killer helper factor in the in vitro induction of cytotoxic T cells. *The Journal of Immunology* **141**, 1543–1549 (1988).
232. Wang, X. & Zhao, X. Y. Transcription Factors Associated With IL-15 Cytokine Signaling During NK Cell Development. *Front Immunol* **12**, (2021).
233. Brincks, E. L. & Woodland, D. L. Novel roles for IL-15 in T cell survival. *Biol Rep* **2**, 8–10 (2010).
234. Sanjabi, S., Mosaheb, M. M. & Flavell, R. A. Opposing effects of TGF-beta and IL-15 cytokines control the number of short-lived effector CD8+ T cells. *Immunity* **31**, 131–144 (2009).
235. Kokaji, A. I., Hockley, D. L. & Kane, K. P. IL-15 Transpresentation Augments CD8 η T Cell Activation and Is Required for Optimal Recall Responses by Central Memory CD8 η T Cells. *The Journal of Immunology* **132**, (2008).
236. Martin, T. A. Interleukin-8 and Angiogenesis BT - Growth Factors and their Receptors in Cancer Metastasis. *Cancer Metastasis - Biology and Treatment* **2**, 51–65 (2001).

237. Díaz-Godínez, C. & Carrero, J. C. The state of art of neutrophil extracellular traps in protozoan and helminthic infections. *Biosci Rep* **39**, (2019).
238. Hartl, D. *et al.* Cleavage of CXCR1 on neutrophils disables bacterial killing in cystic fibrosis lung disease. *Nat Med* **13**, 1423–1430 (2007).
239. Jin, P. *et al.* Interferon- γ and Tumor Necrosis Factor- α Polarize Bone Marrow Stromal Cells Uniformly to a Th1 Phenotype. *Sci Rep* **6**, (2016).
240. Yan, Y. *et al.* CCL19 enhances CD8+ T-cell responses and accelerates HBV clearance. *J Gastroenterol* **56**, 769–785 (2021).
241. Wang, X. & Zhou, L. The Many Roles of Macrophages in Skeletal Muscle Injury and Repair. *Front Cell Dev Biol* **10**, (2022).
242. Boegel, S. *et al.* HLA and proteasome expression body map. *BMC Med Genomics* **11**, (2018).
243. Goebels, N., Michaelis, D., Wekerle, H. & Hohlfield, R. Human myoblasts as antigen-presenting cells. *The Journal of Immunology* **149**, 661–667 (1992).
244. Garlepp, M. J. *et al.* Antigen processing and presentation by a murine myoblast cell line. *Clin Exp Immunol* **102**, 614–619 (1995).
245. Sugiura, T. *et al.* Increased CD40 Expression on Muscle Cells of Polymyositis and Dermatomyositis: Role of CD40-CD40 Ligand Interaction in IL-6, IL-8, IL-15, and Monocyte Chemoattractant Protein-1 Production. *The Journal of Immunology* **164**, 6593–6600 (2000).
246. Curnow, J., Corlett, L., Willcox, N. & Vincent, A. Presentation by myoblasts of an epitope from endogenous acetylcholine receptor indicates a potential role in the spreading of the immune response. *J Neuroimmunol* **115**, 127–134 (2001).
247. Behrens, L. *et al.* Human muscle cells express a functional costimulatory molecule distinct from B7.1 (CD80) and B7.2 (CD86) in vitro and in inflammatory lesions. *The Journal of Immunology* **161**, 5943–5951 (1998).
248. Paba, J. *et al.* Proteomic analysis of the human pathogen *Trypanosoma cruzi*. *Proteomics* **4**, 1052–1059 (2004).
249. Diaz-Hernandez, A. *et al.* Consensus Enolase of *Trypanosoma cruzi*: Evaluation of Their Immunogenic Properties Using a Bioinformatics Approach. *Life* **12**, (2022).

250. Ferragut, F., Acevedo, G. R. & Gómez, K. A. T Cell Specificity: A Great Challenge in Chagas Disease. *Front Immunol* **12**, (2021).
251. Tarleton, R. L. CD8+ T Cells in Trypanosoma cruzi Infection. *Semin Immunopathol* **37**, 233–238 (2015).
252. Kumar, S. & Tarleton, R. L. Antigen-Specific Th1 But Not Th2 Cells Provide Protection from Lethal Trypanosoma cruzi Infection in Mice. *The Journal of Immunology* **166**, 4596–4603 (2001).
253. Fonseca, R. *et al.* Programmed cell death protein 1-PDL1 interaction prevents heart damage in chronic Trypanosoma cruzi infection. *Front Immunol* **9**, (2018).
254. Lasso, P. *et al.* Inhibitory Receptor Expression on CD8+ T Cells Is Linked to Functional Responses against Trypanosoma cruzi Antigens in Chronic Chagasic Patients. *The Journal of Immunology* **195**, 3748–3758 (2015).
255. Xiao, Y. *et al.* RGMb is a novel binding partner for PD-L2 and its engagement with PD-L2 promotes respiratory tolerance. *Journal of Experimental Medicine* **211**, 943–959 (2014).
256. Park, J. S. *et al.* Targeting PD-L2–RGMb overcomes microbiome-related immunotherapy resistance. *Nature* **617**, 377–385 (2023).
257. Rodriguez-Barbosa, J. I. *et al.* HVEM, a cosignaling molecular switch, and its interactions with BTLA, CD160 and LIGHT. *Cell Mol Immunol* **16**, 679–682 (2019).
258. Anderson, A. C., Joller, N. & Kuchroo, V. K. Lag-3, Tim-3, and TIGIT: Co-inhibitory Receptors with Specialized Functions in Immune Regulation. *Immunity* **44**, 989–1004 (2016).
259. Maruhashi, T. *et al.* Binding of LAG-3 to stable peptide-MHC class II limits T cell function and suppresses autoimmunity and anti-cancer immunity. *Immunity* **55**, 912–924 (2022).
260. Niu, M., Liu, Y., Yi, M., Jiao, D. & Wu, K. Biological Characteristics and Clinical Significance of Soluble PD-1/PD-L1 and Exosomal PD-L1 in Cancer. *Front Immunol* **13**, (2022).
261. Orme, J. J. *et al.* ADAM10 and ADAM17 cleave PD-L1 to mediate PD-(L)1 inhibitor resistance. *Oncoimmunology* **9**, (2020).
262. He, X. H., Liu, Y., Xu, L. H. & Zeng, Y. Y. Cloning and identification of two novel splice variants of human PD-L2. *Acta Biochim Biophys Sin* **36**, 284–289 (2004).

263. Chen, Y. *et al.* Development of a sandwich ELISA for evaluating soluble PD-L1 (CD274) in human sera of different ages as well as supernatants of PD-L1 + cell lines. *Cytokine* **56**, 231–238 (2011).
264. Li, Y. *et al.* Role of soluble programmed death-1 (sPD-1) and sPD-ligand 1 in patients with cystic echinococcosis. *Exp Ther Med* **11**, 251–256 (2016).
265. Dezutter-Dambuyant, C. *et al.* A novel regulation of PD-1 ligands on mesenchymal stromal cells through MMP-mediated proteolytic cleavage. *Oncoimmunology* **5**, (2016).
266. Choudhuri, S. & Garg, N. J. Trypanosoma cruzi induces the parp1/ap-1 pathway for upregulation of metalloproteinases and transforming growth factor β in macrophages: Role in cardiac fibroblast differentiation and fibrosis in chagas disease. *mBio* **11**, (2020).
267. Ferragut, F. *et al.* Expression of Inhibitory Receptors TIGIT, TIM-3, and LAG-3 on CD4+ T Cells from Patients with Different Clinical Forms of Chronic Chagas Disease. *The Journal of Immunology* **210**, 568–579 (2023).
268. Zhu, C. *et al.* The Tim-3 ligand galectin-9 negatively regulates T helper type 1 immunity. *Nat Immunol* **6**, 1245–1252 (2005).
269. Wada, J. & Kanwar, Y. S. Identification and characterization of galectin-9, a novel β -galactoside-binding mammalian lectin. *Journal of Biological Chemistry* **272**, 6078–6086 (1997).
270. Wada, J., Ota, K., Kumar, A., Wallner, E. I. & Kanwar, Y. S. Developmental regulation, expression, and apoptotic potential of galectin-9, a β -galactoside binding lectin. *Journal of Clinical Investigation* **99**, 2452–2461 (1997).
271. Enninga, E. A. L., Nevala, W. K., Holtan, S. G., Leontovich, A. A. & Markovic, S. N. Galectin-9 modulates immunity by promoting Th2/M2 differentiation and impacts survival in patients with metastatic melanoma. *Melanoma Res* **26**, 429–441 (2016).
272. Stempin, C. C., Dulgerian, L. R., Garrido, V. V. & Cerban, F. M. Arginase in parasitic infections: Macrophage activation, immunosuppression, and intracellular signals. *J Biomed Biotechnol* **2010**, (2010).
273. Yang, R. *et al.* Galectin-9 interacts with PD-1 and TIM-3 to regulate T cell death and is a target for cancer immunotherapy. *Nat Commun* **12**, (2021).

274. Cardoso, M. S., Reis-cunha, J. L., Bartholomeu, D. C., Fernandez, M. M. & Bartholomeu, D. C. Evasion of the Immune Response by *Trypanosoma cruzi* during Acute Infection. *Front Immunol* **6**, (2016).
275. Shimizu, Y. *et al.* Expression and localization of galectin-9 in the human uterodome. *Endocr J* **55**, 879–887 (2008).
276. Bozorgmehr, N. *et al.* Galectin-9, a player in cytokine release syndrome and a surrogate diagnostic biomarker in SARS-CoV-2 infection. *mBio* **12**, (2021).
277. Nebbia, G. *et al.* Upregulation of the Tim-3/Galectin-9 Pathway of T Cell Exhaustion in Chronic Hepatitis B Virus Infection. *PLoS One* **7**, (2012).
278. Pfefferkorn, E. R., Rebhun, S. & Eckel, M. Characterization of an indoleamine 2,3-dioxygenase induced by gamma-interferon in cultured human fibroblasts. *J Interferon Res* **6**, 267–279 (1986).
279. Sittig, S. P. *et al.* Human type 1 and type 2 conventional dendritic cells express indoleamine 2,3-dioxygenase 1 with functional effects on T cell priming. *Eur J Immunol* **51**, 1494–1504 (2021).
280. Yamamoto, S. & Hayaishi, O. Tryptophan Pyrrolase of Rabbit Intestine. *Journal of Biological Chemistry* **242**, 5260–5266 (1967).
281. Boulland, M. L. *et al.* Human IL4I1 is a secreted L-phenylalanine oxidase expressed by mature dendritic cells that inhibits T-lymphocyte proliferation. *Blood* **110**, 220–227 (2007).
282. Michalek, R. D. & Rathmell, J. C. The metabolic life and times of a T-cell. *Immunol Rev* **236**, 190–202 (2010).
283. Buck, M. D., O’Sullivan, D. & Pearce, E. L. T cell metabolism drives immunity. *Journal of Experimental Medicine* **212**, 1345–1360 (2015).
284. Li, X. L. *et al.* Mechanism and Localization of CD8 Regulatory T Cells in a Heart Transplant Model of Tolerance. *The Journal of Immunology* **185**, 823–833 (2010).
285. Terness, P. *et al.* Inhibition of allogeneic T cell proliferation by indoleamine 2,3-dioxygenase-expressing dendritic cells: Mediation of suppression by tryptophan metabolites. *Journal of Experimental Medicine* **196**, 447–457 (2002).

286. Fallarino, F. *et al.* T cell apoptosis by tryptophan catabolism. *Cell Death Differ* **9**, 1069–1077 (2002).
287. Sadik, A. *et al.* IL4I1 Is a Metabolic Immune Checkpoint that Activates the AHR and Promotes Tumor Progression. *Cell* **182**, 1252–1270 (2020).
288. Nguyen, N. T. *et al.* Aryl hydrocarbon receptor and kynurenine: Recent advances in autoimmune disease research. *Front Immunol* **5**, (2014).
289. Gutiérrez-Vázquez, C. & Quintana, F. J. Regulation of the Immune Response by the Aryl Hydrocarbon Receptor. *Immunity* **48**, 19–33 (2018).
290. Mezrich, J. D. *et al.* An Interaction between Kynurenine and the Aryl Hydrocarbon Receptor Can Generate Regulatory T Cells. *The Journal of Immunology* **185**, 3190–3198 (2010).
291. Liu, Y. *et al.* Tumor-Repopulating Cells Induce PD-1 Expression in CD8+ T Cells by Transferring Kynurenine and AhR Activation. *Cancer Cell* **33**, (2018).
292. Greene, L. I. *et al.* A role for tryptophan-2,3-dioxygenase in CD8 T-cell suppression and evidence of tryptophan catabolism in breast cancer patient plasma. *Molecular Cancer Research* **17**, 131–139 (2019).
293. Cerbán, F. M. *et al.* Signaling pathways that regulate *Trypanosoma cruzi* infection and immune response. *Biochim Biophys Acta Mol Basis Dis* **1866**, (2020).
294. Opperdoes, F. R., Butenko, A., Flegontov, P., Yurchenko, V. & Lukeš, J. Comparative Metabolism of Free-living Bodo saltans and Parasitic Trypanosomatids. *J Eukaryot Microbiol* **63**, 657–678 (2016).
295. Zuo, M. *et al.* IL4I1-catalyzed tryptophan metabolites mediate the anti-inflammatory function of cytokine-primed human muscle stem cells. *Cell Death Discov.* **1**, (2023).
296. Sheehy, M. E., McDermott, A. B., Furlan, S. N., Klenerman, P. & Nixon, D. F. A novel technique for the fluorometric assessment of T lymphocyte antigen specific lysis. *The Journal of Immunology Methods* **249**, 99–110 (2001).
297. Greene, L. I. *et al.* A role for tryptophan-2,3-dioxygenase in CD8 T-cell suppression and evidence of tryptophan catabolism in breast cancer patient plasma. *Molecular Cancer Research* **17**, 131–139 (2019).

298. Presset, M. *et al.* Identification of inhibitors of the immunosuppressive enzyme IL4I1. *Bioorg Chem* **94**, (2020).

Supplement

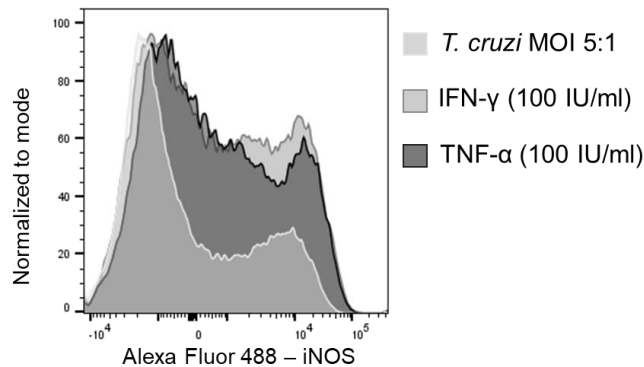


Figure 27: Histogram of iNOS expression in *T. cruzi*-infected, IFN- γ and TNF- α stimulated muscle cells. Differentiated primary human muscle cells were infected with *T. cruzi* (MOI 5:1), stimulated with IFN- γ and TNF- α and harvested after 48 h. Cells were stained intracellularly with an AF-488-conjugated iNOS antibody analysed by flow cytometry.

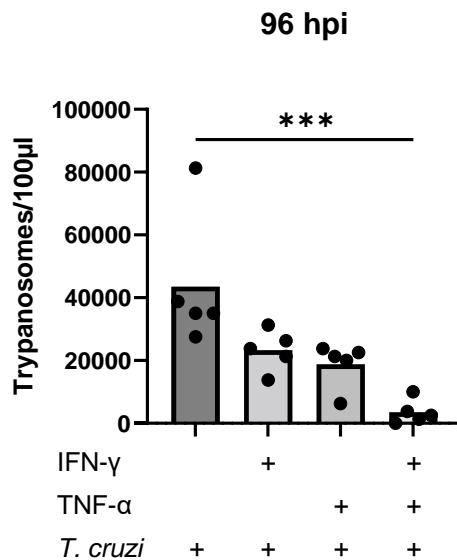


Figure 28: Lower amounts of *T. cruzi* trypomastigotes are released from muscle cells after stimulation with pro-inflammatory cytokines at 96 hpi. Differentiated primary human muscle cells were infected and stimulated with the cytokines IFN- γ (100 IU/ml) and TNF- α (100 IU/ml) and infected with *T. cruzi* (MOI 5:1). Medium was exchanged every day. After 96, the supernatant was obtained, and free and living Trypomastigotes were counted using a Neubauer cell chamber. Each point represents one technical replicate from one donor; the respective means are shown as bars. After testing for normal distribution, statistical significance was calculated the Friedman's test (for non-normal distribution): *** $p \leq 0.001$.

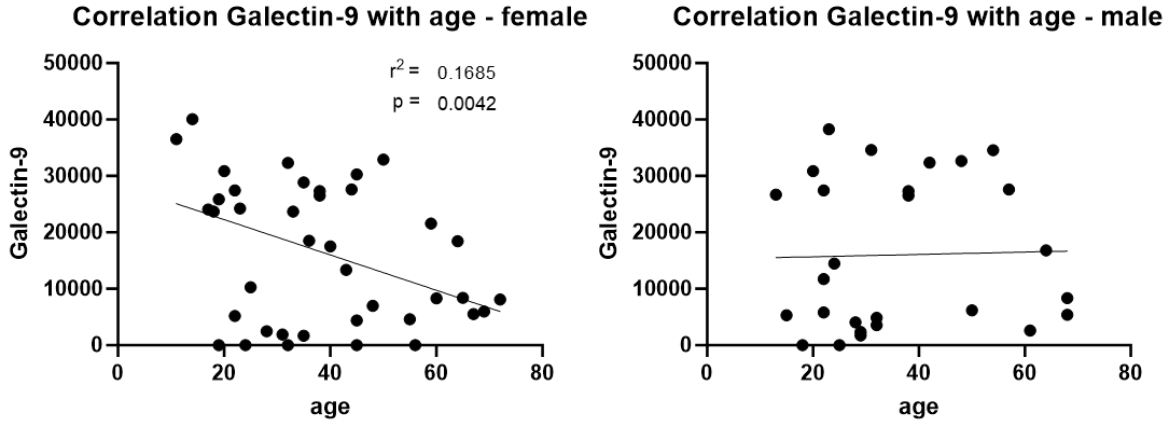


Figure 29: Negative correlation between serum galectin-9 concentration and age in female Chagas patients. Galectin-9 was analysed in the serum of patients in Columbia and analysed using a customised human LEGENDplex. Galectin-9 serum levels were plotted against the age of the patients for females and males. Linear regression was performed and a significant decline of Galectin-9 with age was seen in females.